(NASA-CR-150152) DEVELOPMENT OF THERMAL CONTROL METHODS FOR SPECIALIZED COMPONENTS AND SCIENTIFIC INSTRUMENTS AT VERY LOW TEMPERATURES (FOLLOW-ON) Final Report, 31 Mar. - 30 (Rockwell International Corp., G3/34

N77-15347
HC A06
MF A01
Unclas
59660

SD 76 SA 0230

Development of Thermal Control Methods for Specialized Components and Scientific Instruments at Very Low Temperatures (Follow-on)

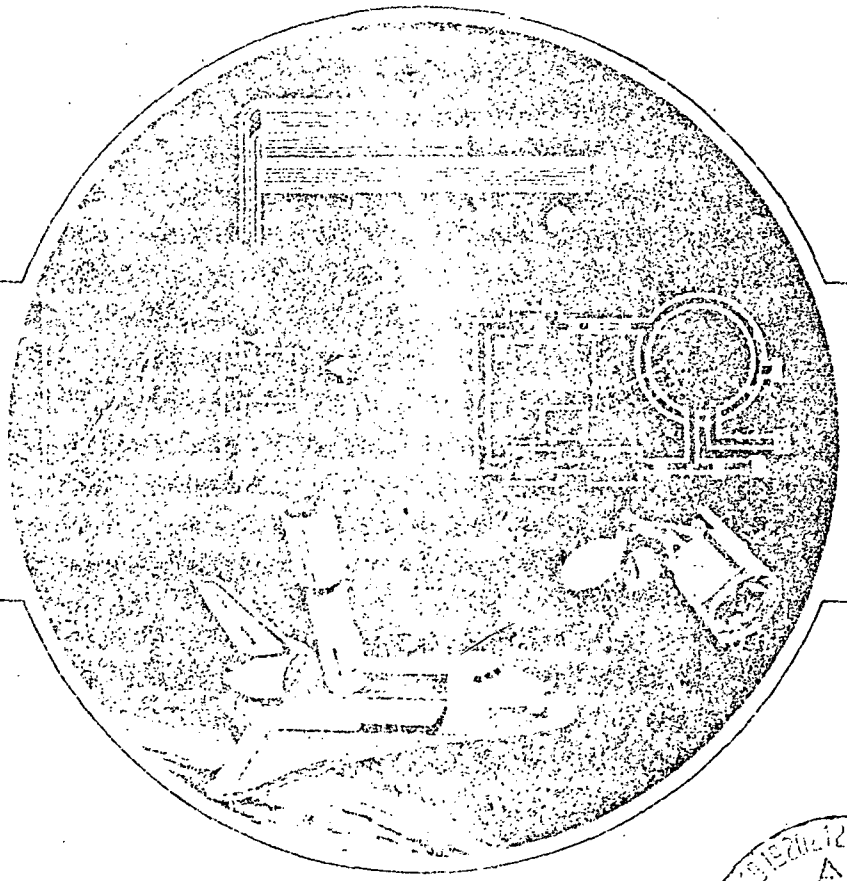

Rockwell International
Space Division

SD 76-SA-0230

DEVELOPMENT OF THERMAL CONTROL METHODS FOR SPECIALIZED COMPONENTS AND SCIENTIFIC INSTRUMENTS AT VERY LOW TEMPERATURES (FOLLOW-ON)

November 1976

FINAL REPORT

CONTRACT NAS8-31324
EXHIBIT B

Prepared by:

J. P. Wright
Study Manager
Aerothermo

D. E. Wilson
Aerothermo
Advanced Programs

Approved by:

for E. G. Cole
Director
Technology Programs

Rockwell International
Space Division

TECHNICAL REPORT INDEX ABSTRACT

ACCESSION NUMBER							DOCUMENT SECURITY CLASSIFICATION	
							UNCLASSIFIED	

TITLE OF DOCUMENT

DEVELOPMENT OF THERMAL CONTROL METHODS FOR SPECIALIZED COMPONENTS AND SCIENTIFIC INSTRUMENTS AT VERY LOW TEMPERATURES

LIMITATIONS (IF ANY)

AUTHOR(S)

J. P. WRIGHT, D. E. WILSON

CODE	ORIGINATING AGENCY AND OTHER SOURCES	DOCUMENT NUMBER
	SPACE DIVISION, ROCKWELL INTERNATIONAL	76-SA-0230

PUBLICATION DATE	CONTRACT NUMBER
NOVEMBER 1976	NAS8-31334

DESCRIPTIVE TERMS

LOW-TEMPERATURE COOLING CONCEPTS, MULTISTAGE RADIATOR OPTIMIZATION DIODE HEAT PIPE RADIATOR, PASSIVE COOLING CONCEPTS, RADIATOR FIN OPTIMIZATION

ABSTRACT

MANY PAYLOADS ARE CURRENTLY PROPOSED TO BE FLOWN BY THE SPACE SHUTTLE SYSTEM WHICH REQUIRE LONG-DURATION COOLING IN THE 3 TO 200°K TEMPERATURE RANGE. COMMON REQUIREMENTS ALSO EXIST FOR CERTAIN DOD PAYLOADS. THIS STUDY PERFORMS PARAMETRIC DESIGN AND OPTIMIZATION STUDIES FOR MULTISTAGE AND DIODE HEAT PIPE RADIATOR SYSTEMS DESIGNED TO OPERATE IN THIS TEMPERATURE RANGE. ALSO OPTIMIZED ARE GROUND TEST SYSTEMS FOR TWO LONG-LIFE (> 2 YEARS) PASSIVE THERMAL CONTROL CONCEPTS OPERATING UNDER SPECIFIED SPACE ENVIRONMENTAL CONDITIONS. THE GROUND TEST SYSTEMS EVALUATED WERE ULTIMATELY INTENDED TO EVOLVE INTO FLIGHT TEST QUALIFICATION PROTOTYPES FOR EARLY SHUTTLE FLIGHTS.

FOREWORD

This report is submitted by the Space Division of Rockwell International Corporation to the National Aeronautics and Space Administration, George C. Marshall Space Flight Center, in accordance with the requirements of the follow-on effort to Contract NAS8-31324. The work was administered by the Science and Engineering Directorate, Structures and Propulsion Laboratory, Engineering Analysis Division, Thermal Engineering Branch. Mr. Howard Trucks was the Contracting Officer's Representative. Contract NAS8-31324 authorized a study to develop low-temperature cooling system concepts for future Shuttle payloads. The follow-on effort authorized the design and evaluation of specific ground test systems intended for ultimate prototype testing in early Shuttle flights. The work was performed from March 31, 1976, through November 30, 1976. This report contains the results of the study for this period.

The study was performed under the direction of J. P. Wright, Study Manager. Technical assistance was provided by D. E. Wilson and R. L. Swanson of the Aerothermo Group.

CONTENTS

PAGE INTENTIONALLY BLANK

ILLUSTRATIONS

PAGE INTENTIONALLY BLANK

TABLES

SUMMARY

This report summarizes the results of the follow-on effort of Contract NAS8-31324, "Development of Thermal Control Methods for Specialized Components and Scientific Instruments at Very Low Temperatures", for the period March 31, 1976 through November 30, 1976. The objective of this effort was to generate parametric design and optimization data and to develop detailed ground test system designs for two advanced low-temperature heat pipe radiator concepts.

The study was composed of the following four tasks:

1. Parametric analysis and tradeoff study
2. Design definition phase
3. Ground test plan
4. Final report

MULTISTAGE RADIATOR STUDY

The multistage radiator concept utilizes intermediate radiator stages to intercept parasitic heat loads through insulation and supports in order to permit the outermost stage to reject heat at extremely low temperatures. Mathematical models were developed for one-, two-, and three-stage radiator systems to determine optimum stage areas and system performance as a function of such parameters as insulation effectiveness, cold stage temperature, and heat load to the cold and intermediate stages.

The study shows that multistage radiator systems can be optimized on the basis of weight or projected area, and that single-stage, two-stage, and three-stage radiators have distinct temperature ranges in which they are optimum depending on the insulation effectiveness. Cold stage temperatures as low as 15°K are theoretically possible with present technology levels for insulation emittance. The study shows that the cold stage heat rejection capacity for three-stage radiators is a strong function of insulation emittance in the analyzed range of 0.005 to 0.020 and drops off sharply at temperatures below about 30°K.

Optimum radiator geometry for a given temperature was found to be independent of the magnitude of the heat load; hence, the results can be scaled up or down for any size system. The addition of a heat load to the intermediate stage did not significantly affect cold stage heat rejection for heat loads up to 10 times the cold stage load. This is significant for sensor systems requiring additional cooling at intermediate temperatures.

A parametric analysis also was performed to determine optimum radiator fin geometry and heat pipe spacing as a function of temperature, m terial properties, and heat pipe weight. Results show that optimum fin geometry is significantly different at cryogenic temperatures than at ambient temperature. For example, below 50°K, optimum thickness for an aluminum radiator is less than 1 mil and the optimum heat pipe spacing is greater than 5 feet. For a deep space-facing radiator, the fin efficiency corresponding to the minimum-weight system was found to be 0.565 and is independent of both temperature and material properties for a rectangular fin of constant properties.

Based on the above results and those of the multistage radiator study, a ground test system was designed for a three-stage radiator with heat rejection requirements of 10 MW at 35°K on the cold stage and 100 MW at the second stage. The areas of the first, second, and third stages are 10.0, 7.5, and 3.5 square feet, respectively. Side and end shields were sized for a sun-synchronous low earth orbiting spacecraft with a local vertical attitude such as would be used for a low-temperature infrared sensor system. Three heat pipes are used to distribute heat over the individual stages. Working fluids were selected based on the predicted stage temperature—ethane for the first stage, oxygen for the second stage, and neon for the third stage.

A detailed thermal network was made to determine the performance of the ground test system. Based on the design heat loads, the predicted temperature for the third stage is 36.3°K. The system is shown in Figure 2-44.

DIODE HEAT PIPE RADIATOR STUDY

The diode radiator concept utilizes diode heat pipes to thermally disconnect a radiator from a low-temperature sensor during periods when the external environment does not permit heat rejection. The unique feature

of this concept is that it can provide low-temperature cooling in low earth orbits where radiator cooling was never before considered possible.

Feasibility studies of this type of system were performed during the earlier phase of this contract and are reported in Reference 1. Results indicated that temperatures as low as 175°K could be achieved even in subsolar earth orbits (worst case), and lower for higher altitude orbits. Additional transient analyses were performed during this study to determine the heat rejection capability and detector temperature excursion as a function of the thermal capacitance of the system. Both fixed capacitance plates and phase change thermal storage devices were analyzed. Results indicate that a phase change device would be required for geosynchronous orbits, whereas a fixed capacitance (e.g., aluminum block) would be adequate for lower orbits with shorter orbital periods.

A ground test system for a diode heat pipe radiator system was designed based on the results of the parametric analysis. The system was designed for a simulated detector heat load of 1 watt and a required operating temperature of 175°K. Environmental heat loads to the radiator were computed for a 100-n.mi. subsolar earth orbit as in the previous cases. The system consists of a simulated detector which is attached to a 3-lbm aluminum heat sink block, a diode heat pipe, a variable conductance heat pipe and reservoir, and the radiator. The system is supported off a mounting structure which simulates the spacecraft interface (300°K boundary) by low conductance supports.

The diode heat pipe is a 1/4-inch outside diameter stainless steel pipe with ethane as the working fluid. It has a forward conductance of 4.1 watts/°C and a reverse conductance of 0.002 watts/°C. The shutdown energy of the diode heat pipe is estimated to be 0.36 watt-hours.

The variable conductance heat pipe (VCHP) also uses ethane as the working fluid. The VCHP is thermally connected to the diode heat pipe with an aluminum coupling block secured with tension straps. The VCHP reservoir is designed for a reservoir-to-condenser volume ratio of 10:1. Argon is used as the control gas. The system is shown in Figure 3-8.

A detailed thermal model was developed with special subroutines to simulate the performance of the diode and variable conductance heat pipes. Results of the detailed thermal analysis show that the detector temperature is maintained within the range of 175 $\pm$ 3°K while the radiator varies between 145°K and 255°K.

CONCLUSIONS

Based on the detailed analysis results for the selected multistage and diode heat pipe radiator design configurations, it can be concluded that significant improvements in low-temperature cooling technology can be realized with current thermal control elements. Both of these systems are applicable to many classes of proposed future Shuttle payloads and offer perhaps the only solution for long life (>1 year) low-temperature cooling for space systems.

A ground test program is strongly recommended, in which breadboard systems would be fabricated and tested based on the designs presented. Following the ground test program, flight-qualified versions of these systems should be flown and tested on early Shuttle test flight opportunities. The system would then be qualified for use on NASA as well as DOD payloads.

1. INTRODUCTION

This report summarizes the results of exhibit B to Contract NAS8-31324, "Development of Thermal Control Systems for Specialized Components and Scientific Instruments at Very Low Temperatures". The long term goal which this study addresses is the development of a set of space qualified thermal control systems which can be applied to a variety of low temperature Shuttle payload instruments. The purpose of the first phase of the contract (Exhibit A) was to identify proposed future low temperature Shuttle payloads and their cooling requirements; and based on these requirements to define and develop cooling system concepts for various categories of cooling requirements. The results of the Exhibit A effort are summarized in Reference 1.

The present study was a follow-on to the original contract. It is aimed at the further development of two of the advanced cooling concepts described in Reference 1 - the multistage radiator concept, and the diode heat pipe radiator concept. The specific objectives of the current effort were to develop design performance sensitivity and optimization data for these two radiator systems, and based on these results, to design test configurations for each concept for subsequent development and ground testing. The ground test program was ultimately intended to evolve into a flight test qualification program where flight rated prototypes of these systems would be flown and tested on test beds for early Shuttle flights such as the Advanced Technology Laboratory (ATL) or Spacelab.

The multistage radiator system is described in Section 2. The multistage radiator concept offers a unique approach to the problem of rejecting large heat loads at very low temperatures. The concept involves the use of heat pipes and radiator staging to permit passive heat rejection at temperatures substantially lower than would have been considered possible even a few years ago. Perhaps the most significant feature of the multistage radiator system is that great improvements or quantum jumps in insulation technology are not required to reach temperatures as low as 30°K. In fact, the baseline design for the ground test system was sized and designed based on current technology

insulation performance values, possibly even conservative values compared to what has been achieved in many flight applications.

To support the multistage radiator optimization analyses, a separate analysis of radiator fin optimization was performed. The analysis resulted in expressions for optimum fin thickness and heat pipe spacing as a function of temperature. The results were revealing in that at extremely low temperatures, optimum fin thicknesses were less than 1 mil and optimum heat pipe spacings were 5, 10, or even 15 feet. These results played a significant role in weight-optimizing the individual stages for the selected design configuration.

The diode heat pipe radiator system is described in Section 3. Some parametric analyses were performed during the first phase of the study and are reported in Reference 1. Additional parametric studies were performed during the current effort to characterize the performance capability of the diode system based on transient thermal analyses for worst-case orbital thermal environments. The unique feature of the diode radiator system is that it can provide heat rejection passively even in low earth orbits where previously passive radiators were assumed to be incapable of rejecting heat except in the special case of sun-synchronous orbits. This is significant since there are a number of low-temperature spectrometers and radiometers proposed for earth resources and earth monitoring applications which require non-synchronous low earth orbits. The diode radiator system is ideal for short wavelength infrared sensors which operate at 175°K to 200°K. Cooling at even lower temperatures (possibly as low as 100°K) is possible for higher altitude earth orbits even under worst-case sun angle conditions. The diode radiator system brings together several recent advances in cryogenic, diode, and variable conductance heat pipe technology to yield a very promising long-life cooling system.

Conclusions derived from this study (Section 4) indicate that these two passive cooling concepts are not only feasible, but can provide significant advances in cooling system technology with existing or very-near-term hardware. The next step is to fabricate and test these two systems in a space environment to verify their predicted performance and to learn more about the transient overall system response characteristics.

2. MULTISTAGE HEAT PIPE RADIATOR SYSTEM

A parametric and design definition study was performed to determine radiator performance and optimum geometry for multistage radiators and to show the sensitivity of size, heat rejection capability, and minimum achievable temperature to the geometry and thermal properties of the system. A separate analysis was performed to determine optimum radiator fin geometry and heat pipe spacing as a function of temperature.

Based on the results of the parametric analyses, a 1-g test prototype of a three-stage radiator was designed and optimized. A detailed three-dimensional thermal network of the system was used to define further the design configuration and to predict the 1-g system performance.

MULTISTAGE RADIATOR ANALYSIS

The multistage radiator concept is shown schematically in Figure 2-1. The principle of performance is based on each radiator stage intercepting the parasitic heat load where it can be efficiently radiated to space by a surface whose area is inversely proportional to the fourth power of the absolute temperature. Each stage is thermally isolated by multilayer insulation and low conductivity support posts to minimize heat conduction. The heat intercepted is transported from within the layers by the skins and heat pipes thermally attached to each stage. These intermediate stages also can provide efficient thermal rejection at the different temperature levels of the optics, baffles, shell, focal plane, and electronics within a sensor system.

Analytical expressions were developed for the performance of one-, two-, and three-stage radiators as a function of the geometry, temperature, and thermal properties of the system for various stage heat loads. Loads to two radiator stages were considered for the two- and three-stage radiators with the warmer stage load defined in terms of the cold stage load to simplify analysis. The insulation effectiveness (which accounts for heat leakage through the supports, penetrations, and edge losses as well as heat flow through the insulation blanket) was expressed in terms of an effective

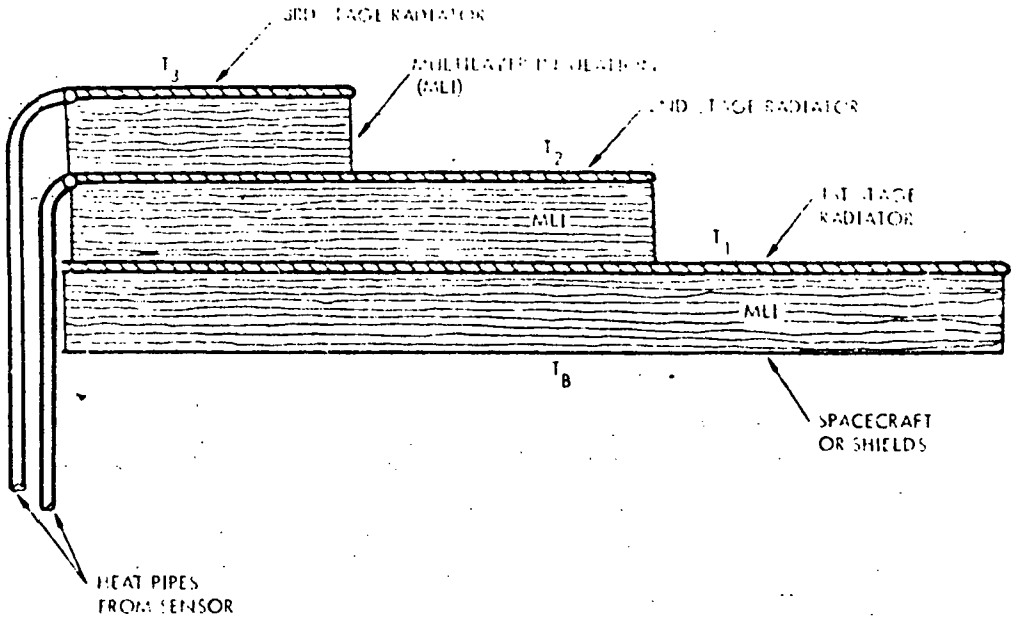

Figure 2-1. Multistage Heat Pipe Radiator Concept

insulation emittance, $\bar{\varepsilon}_{ins}$. Values of $\bar{\varepsilon}_{ins}$ ranging from 0.005 to 0.02 were assumed for this analysis.

Analytical Model

Figure 2-2 shows simplified schematics for one-, two-, and three-stage radiators. A generalized expression for the energy balance for the system is given by:

$$\dot{q}_B + \sum_{i=n-1}^{n} S_i = \sum_{i=1}^{n} \dot{q}_{i_{rej}} \qquad (1)$$

For an individual stage the energy balance is given by:

$$S_i + \dot{q}_{i-(i+1)} = \dot{q}_{(i+1)-(1+2)} + \dot{q}_{i_{rej}} \qquad (2)$$

By substitution of the appropriate terms from Figure 2-2 into Equations 1 and 2, the following expressions were derived for the cold stage temperature as a function of the individual stage areas:

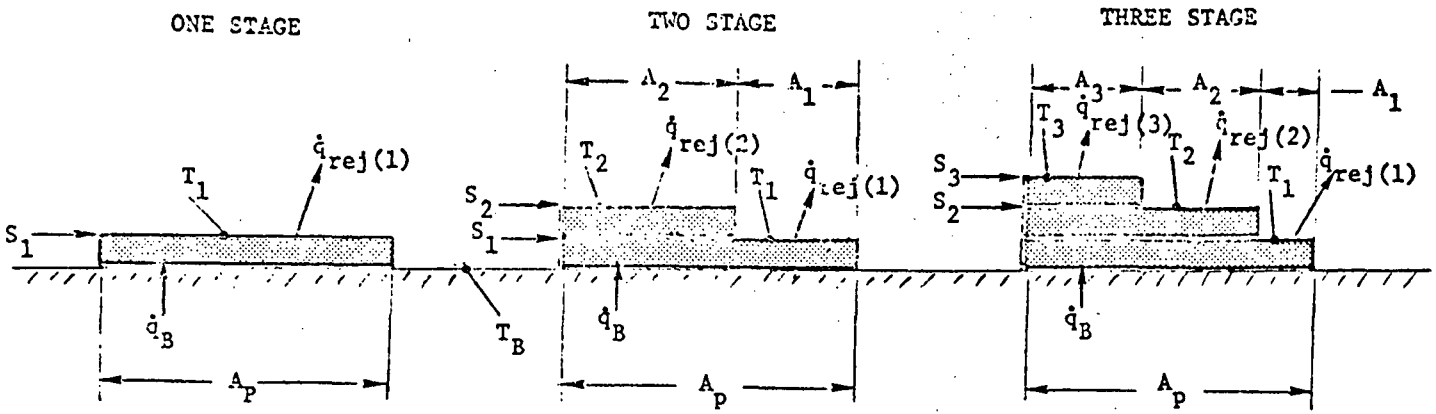

S_i	=	stage heat loads	T_B	=	boundary temperature
$\dot{q}_{rej(i)}$	=	stage heat rejection $[\sigma F_r \eta A_i T_i^4]$	α	=	stage heat load ratio $[S_i/S_{i-1}]$
A_i	=	exposed stage area	$\dot{q}_B$	=	parasitic heat leak $[\sigma F_c A_p (T_B^4 - T_1^4)]$
A_T	=	total stage area	F_r	=	ϵ_r, radiator surface emissivity
A_p	=	projected stage area (radiator base)	F_c	=	$\overline{\epsilon_{ins}}$, effective insulation emittance
T_i	=	stage temperature	η	=	radiator fin efficiency

Figure 2-2 Schematics and Analytical Models of One, Two and Three Stage Radiators

For a one-stage radiator-

$$T_1^4 = \frac{S_1 + cA_p T_B^4}{A_p (r + c)} \tag{3}$$

For a two-stage radiator-

$$T_2^4 = \frac{c^2 A_p T_B^4 - S_2 \left[r + c (1 + \alpha) - \frac{A_p}{A_2} (r + c) \right]}{A_p (r + c)^2 - r^2 A_2} \tag{4}$$

where

$A_1 = Ap - A_2$

For a three-stage radiator-

$$T_3^4 = \frac{A_p T_B^4 + S_3 \left\{ (1 + \alpha) + \frac{rA_2}{cA_3} + \frac{rA_1 + cA_p}{cA_3} \left[\frac{2 cA_3 + A_2 (c + r) + \alpha cA_3}{c (A_2 + A_3)} \right] \right\}}{(rA_1 + cA_p) \left[\frac{2cA_3 + A_2 (c + r)}{c(A_2 + A_3)} \left(\frac{r + c}{c} \right) - \frac{cA_3}{c(A_2 + A_3)} \right] + rA_2 \left(\frac{r + c}{c} \right) + rA3} \tag{5}$$

where

σ = Stephan Boltzman constant

$c = \sigma \bar{\varepsilon}_{ins}$

$r = \sigma \varepsilon_r$

These expressions can be optimized in terms of total weight or projected area, depending on which parameter is more crucial in a given application. This is done for the two- and three-stage radiators by expressing the individual stage areas in Equations 4 and 5 in terms of the total area of all stages, A_T (which is proportional to total system weight) or the projected area, A_p. The derivatives of the cold stage temperature or heat load with respect to area determine the optimum stage areas. The optimum areas produce the miminum cold stage temperature for given stage heat loads, or the maximum heat rejection for a given cold stage temperature. The cold stage coefficient of performance for each of these optimum configurations is defined as

$$COP_{\text{cold stage}} = \frac{S_{\text{cold stage}}}{r A_{\text{optimum}} T^4_{\text{cold stage}}} \tag{6}$$

where the area is the optimum value determined from solutions of the derivative expressions for A_I or A_p.

Weight Optimization

Figure 2-3 through 2-6 show weight-optimized COP values from Equation 6 versus cold stage temperature for radiators with a heat load on the cold stage only. Data are presented for one-, two-, and three-stage radiators for insulation emittance values of 0.005 through 0.02. The COP relates the cold stage heat rejection per unit of total area to that of an ideal one-stage radiator at the cold stage temperature with no parasitic (insulation) heat loads.

The curves in Figure 2-3 shows that on a weight basis, a single-stage radiator is the most efficient down to a temperature of approximately 95°K, below which two and three stages become more efficient. Below 95°K, the parasitic heat load to a one-stage radiator begins to approach the emissive power of the cold stage, and below about 85°K, the one-stage radiator is incapable of rejecting even the insulation heat load. The two-stage radiator is optimum from 95°K down to approximately 40°K, below which a three-stage radiator is optimum. Four- and five-stage radiators were not analyzed because a three-stage radiator would be optimum down to temperatures as low as 15°K. Furthermore, the analysis required for optimization would be extremely cumbersome.

The curves in Figure 2-4 through 2-6 show that the crossover points between optimum regimes for one-, two-, and three-stage radiators increase with increasing insulation emittance. Also, the COP is less for a given temperature and the minimum achievable temperature increases with increasing values of $\bar{\varepsilon}_{ins}$. Note that at 300°K, the COP reaches an asymtotic value in each case. This results from the assumption of a 300°K boundary temperature below the warmest stage. At 300°K, the COP for one-, two-, and three-stage radiators is 100, 50 and 33 1/3 percent, respectively.

Figure 2-7 shows the cold stage heat load per square foot of projected area as a function of cold stage temperature for one-, two-, and three-stage radiators based on a insulation emittance of 0.01. These data are compared to that for an ideal radiator (i.e., no parasitic heat load) and show that multi-

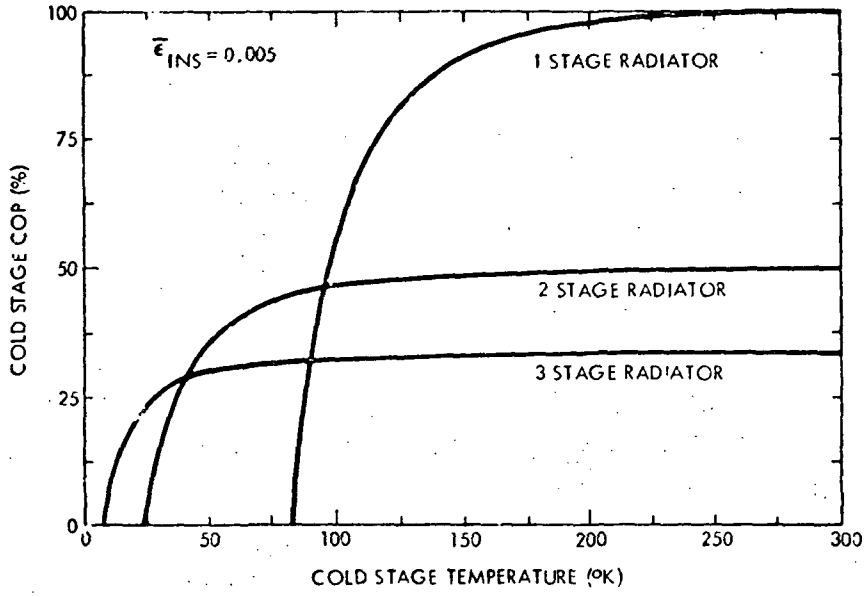

Figure 2-3. Weight Optimization Results ($\bar{\epsilon}_{ins}$ = 0.005)

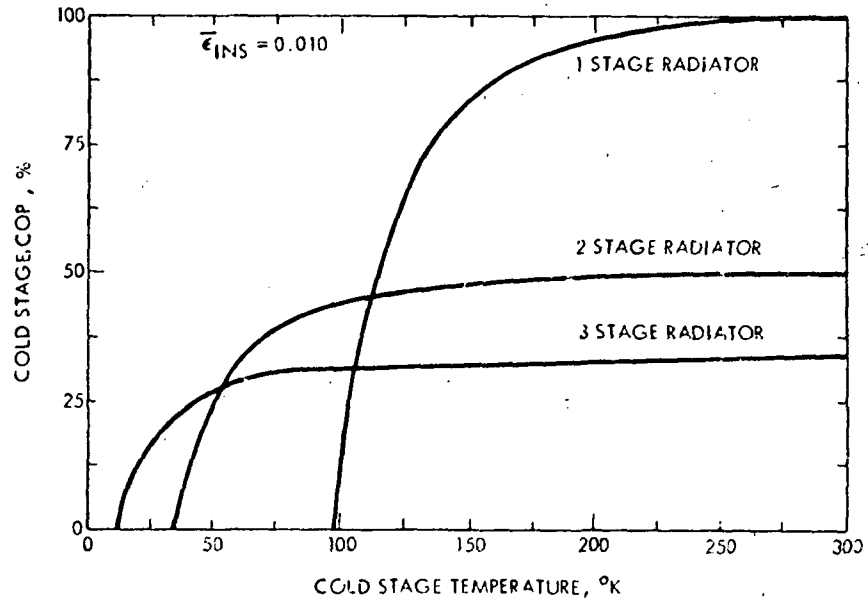

Figure 2-4. Weight Optimization Results ($\bar{\epsilon}_{ins}$ = 0.010)

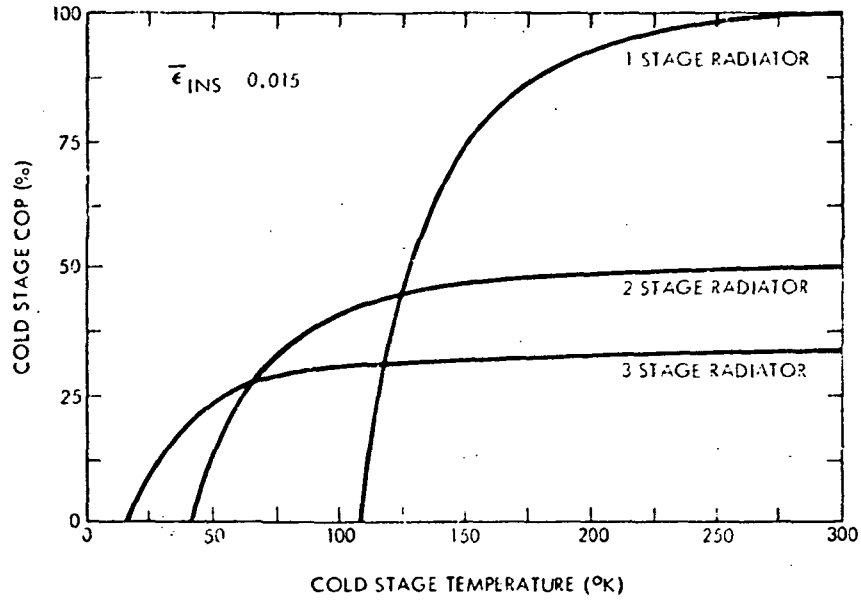

Figure 2-5. Weight Optimization Results ($\bar{\epsilon}_{ins}$ = 0.015)

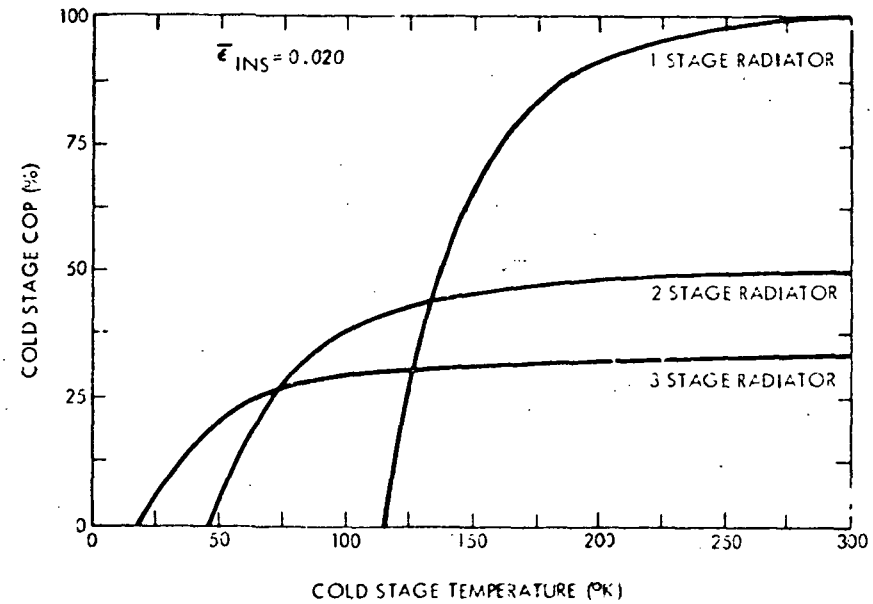

Figure 2-6. Weight Optimization Results ($\bar{\epsilon}_{ins}$ = 0.020)

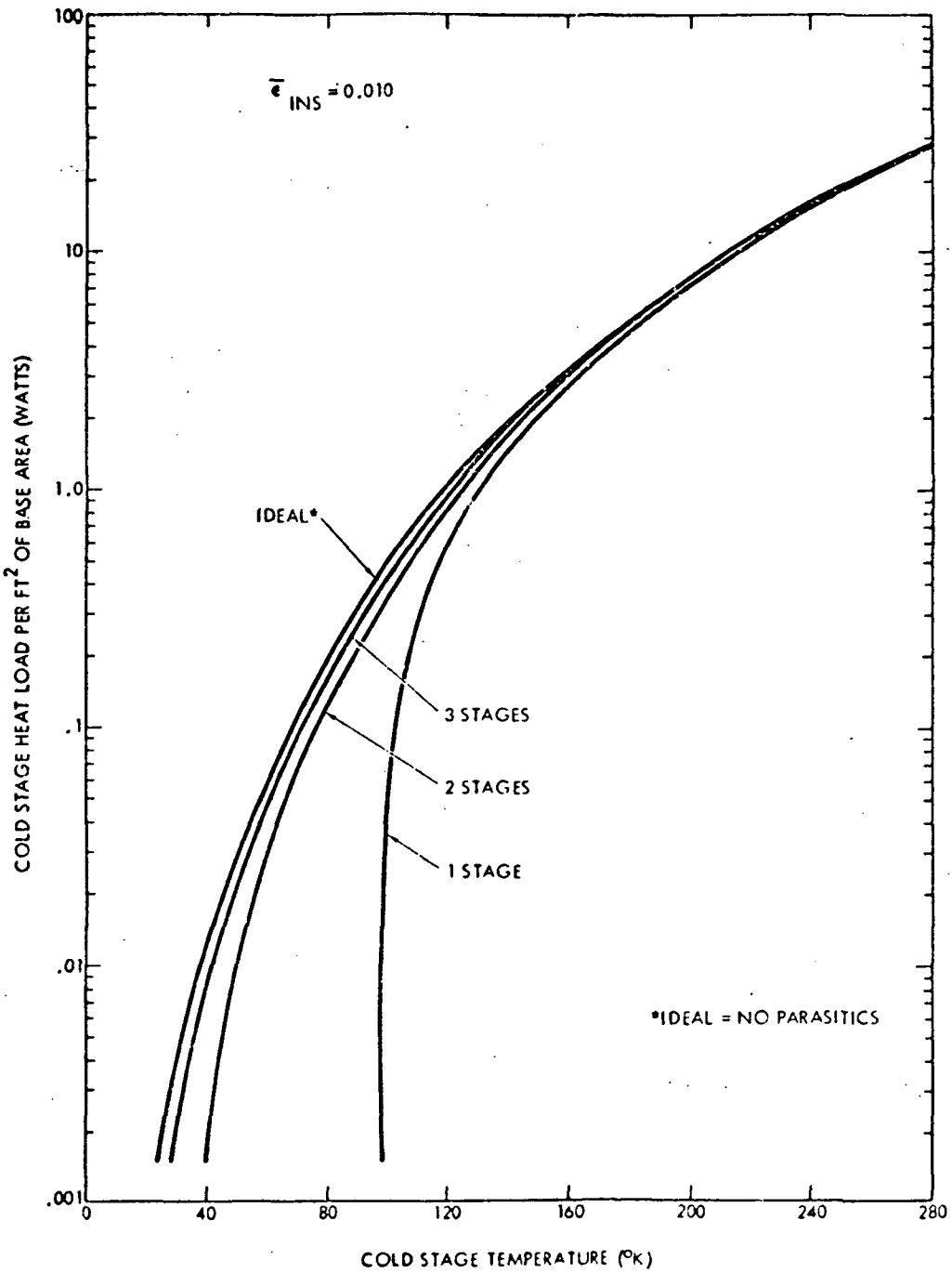

Figure 2-7. Cold Stage Heat Rejection Versus Temperature ($\bar{\epsilon}_{ins}$ = 0.010)

stage radiators more closely approach the ideal case by virtue of reducing the effects of parasitics with the lower stages. The impact of stage parasitics is further demonstrated in Figure 2-8 where the minimum temperature attainable (no stage loads) is plotted as a function of the insulation effective emittance. The slopes of these curves indicate that multistage radiators are less influenced by variation of $\bar{\varepsilon}_{ins}$ than a single-stage radiator. For example, the minimum attainable temperature increases by 33°K for a one-stage radiator and only 12°K for a three-stage radiator as the insulation effective emittance increases from 0.005 to 0.020. This is a significant result since ordinarily it would be expected that the sensitivity to insulation performance would increase with decreasing temperature.

The effects of adding heat loads to both of the outer two stages is shown in Figure 2-9, which gives cold stage COP versus cold stage temperature for radiators with an insulation effective emittance of 0.01. The two-stage radiator has loads to both the first and second stages; the three-stage radiator has heat loads to the second and third stages. The heat load on the warmer stage is expressed as an integral multiple of the cold stage load by use of the parameter α. A value of 10 for α would have a load 10 times that of the cold stage load on the stage immediately below. Figure 2-9 shows that as α increases, the cold stage COP is lowered as well as the temperature transition point where radiators with reduced stages become more efficient.

Figures 2-10 through 2-13 show optimum stage areas (per square foot of radiator base area) plotted as a function of cold stage temperature for α = 0, 5, 10, and 50, respectively. Optimum areas for the individual stages are expressed as a fraction of the projected area. The insulation emittance is 0.01 in all cases. The curves are terminated at the point where higher efficiencies are achieved with reduced stages.

Because the results are defined in terms of a one-square-foot projected area, the data in Figures 2-3 through 2-13 can be scaled up or down, depending on the magnitude of the desired heat load for a given application. For example, if a system had heat rejection requirements of 200 milliwatts at 40°K and 2 watts at 100°K to 150°K, the optimum geometry could easily be determined from Figures 2-3 through 2-13. If the somewhat conservative value for the insulation emittance of 0.01 is assumed, Figure 2-4 shows that a

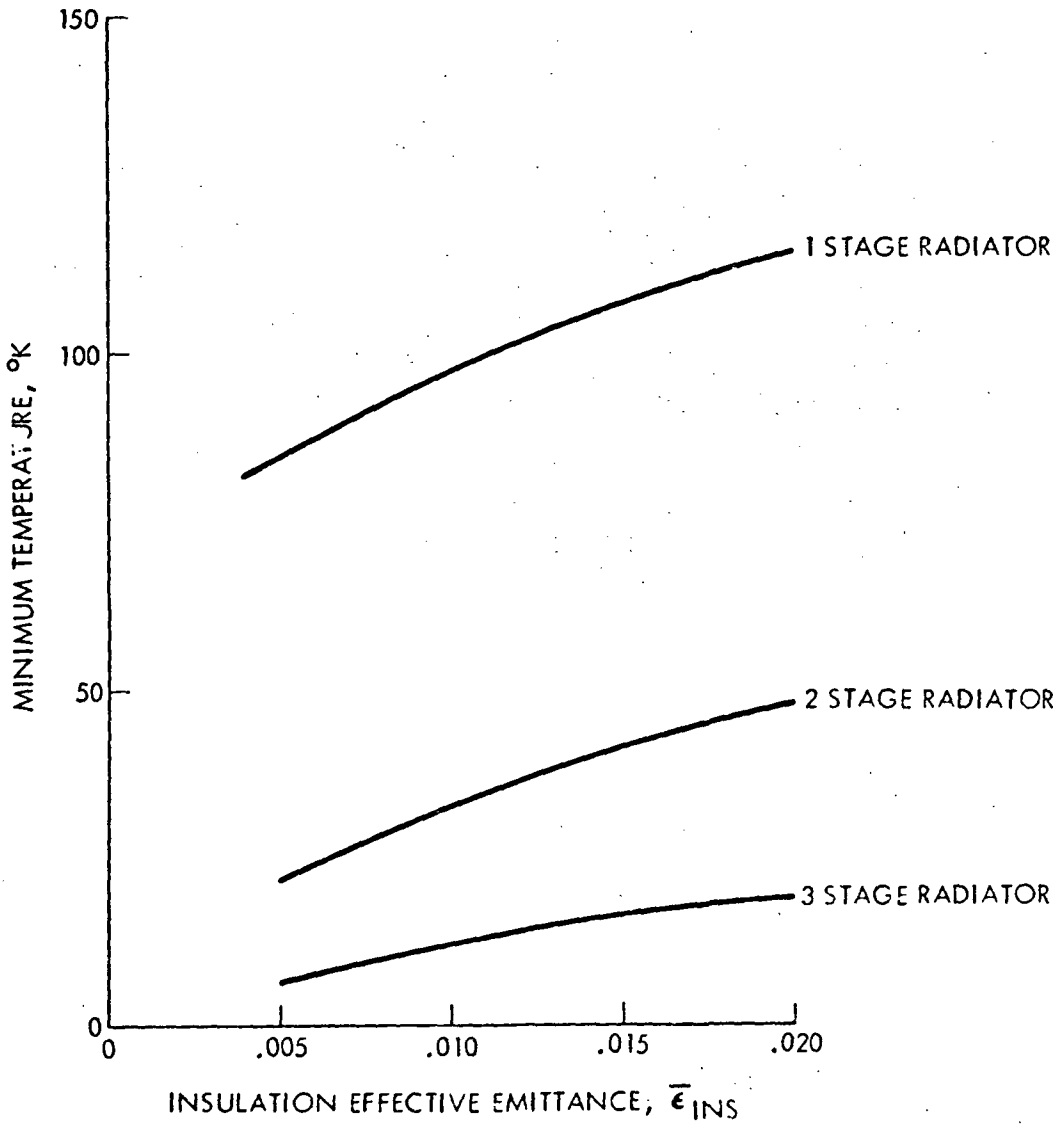

Figure 2-8 Minimum Cold Stage Temperature Versus Insulation Emittance

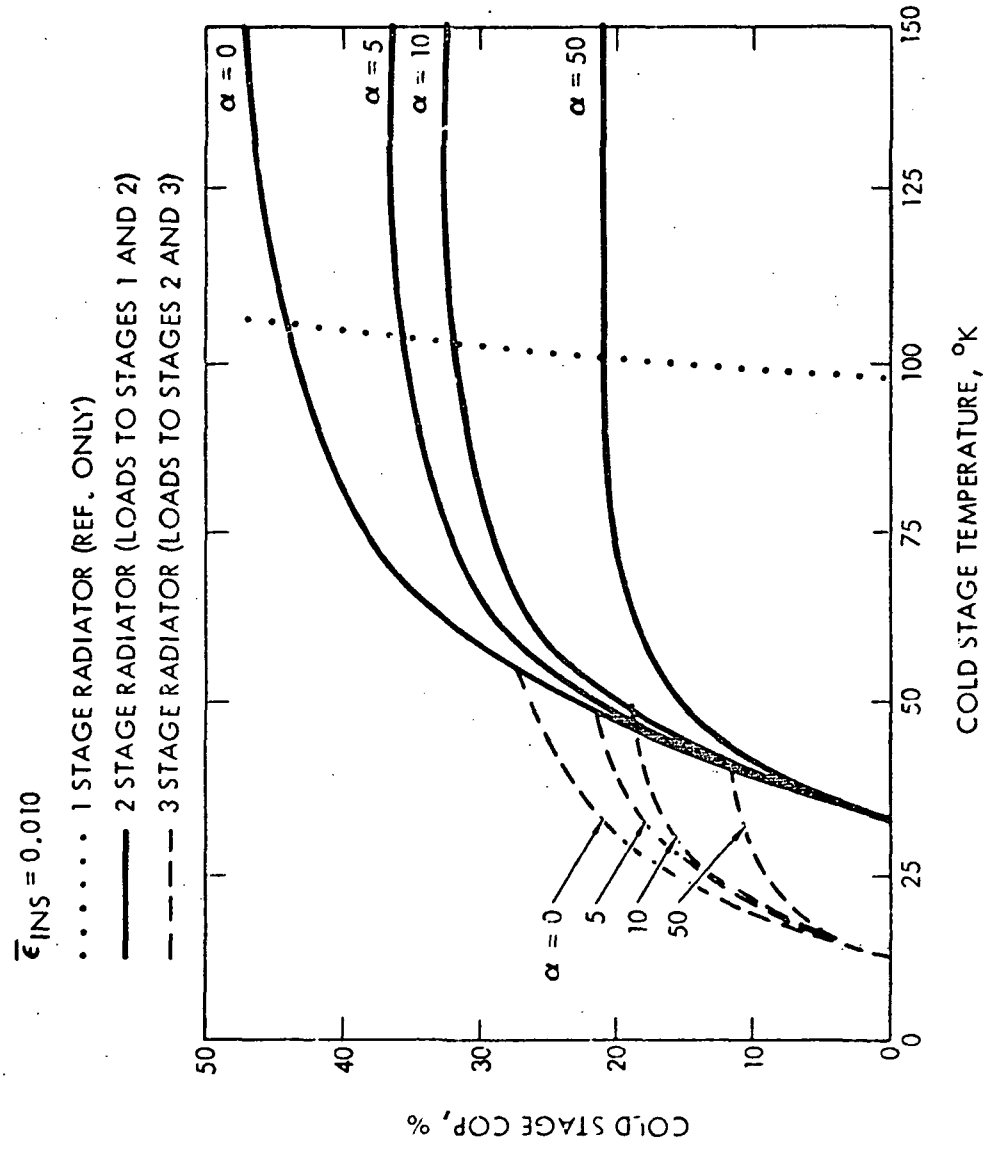

Figure 2-9. Weight Optimization Results for Heat Load to Two Stages ($\bar{\epsilon}_{ins}$ = 0.010)

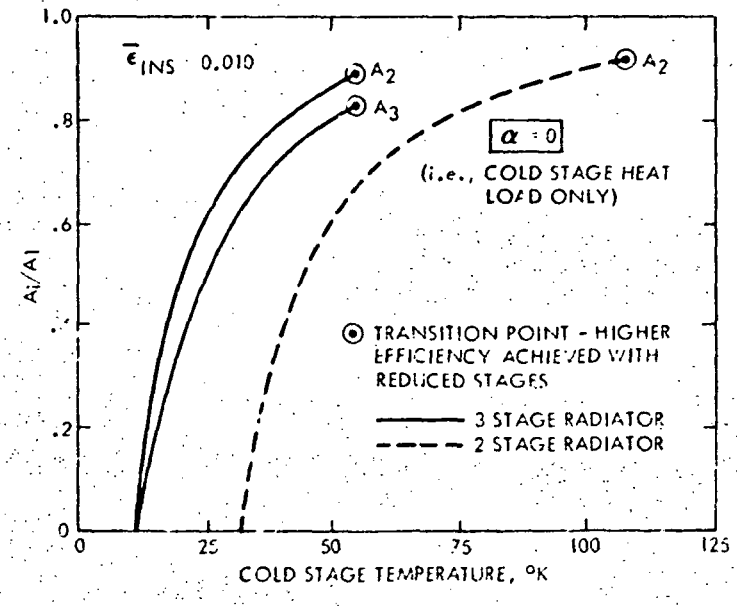

Figure 2-10. Optimum Stage Areas ($\bar{\epsilon}_{ins}$ = 0.01; α = 0)

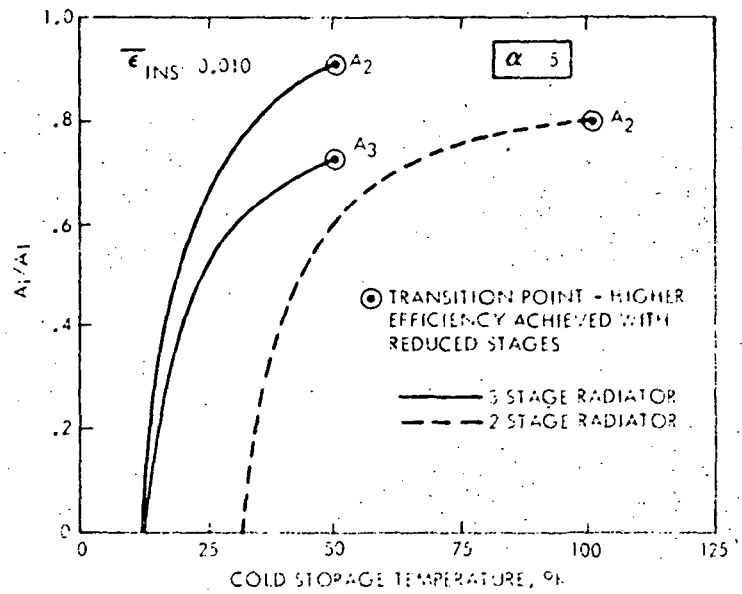

Figure 2-11. Optimum Stage Areas ($\bar{\epsilon}_{ins}$ = 0.01; α = 5)

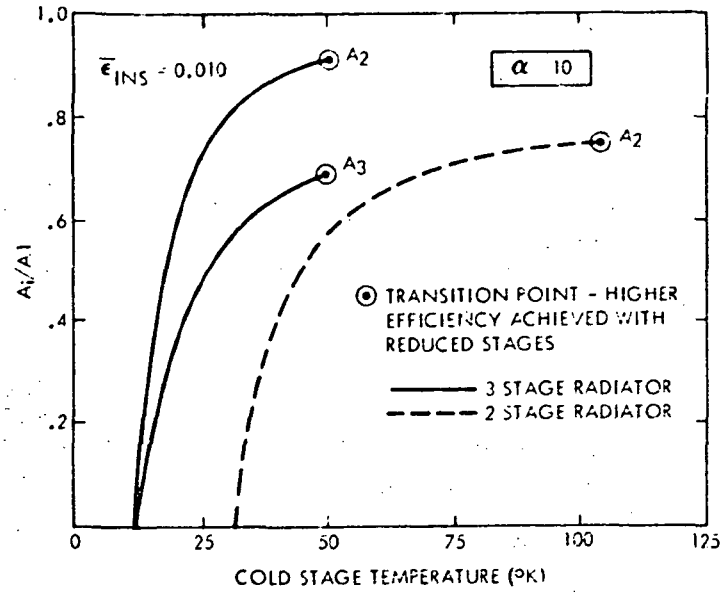

Figure 2-12. Optimum Stage Areas ($\bar{\epsilon}_{ins}$ = 0.01; α = 10)

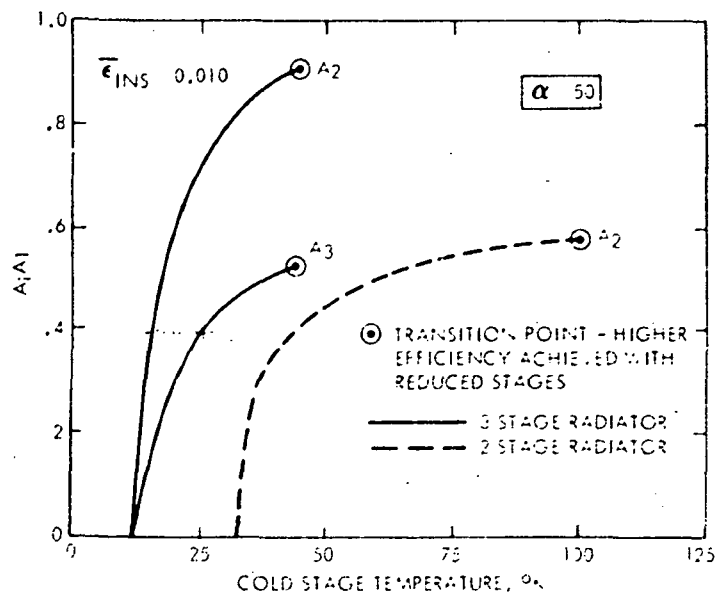

Figure 2-13. Optimum Stage Areas ($\bar{\epsilon}_{ins}$ = 0.01; α = 50)

three-stage radiator will be optimum on a weight basis. The two heat loads yield a value of $\alpha = 10$. On a unit area basis, from Equation 6 and Figure 2-9:

$$COP_3 = \frac{S_3}{A_T \sigma \varepsilon_r T_3^4} \tag{6}$$

where

$$A_T = \frac{A_1 + A_2 + A_3}{A_p}$$

From Figure 2-7:

$$\dot{q}_{ideal} = \sigma \varepsilon_r T_3^4 \tag{7}$$

therefore (per unit area)

$$S_3 = COP_3 A_T \dot{q}_{ideal} \tag{8}$$

For the specified lead, S_3', the area required is given by

$$A_p' = \frac{S_3'}{S_3)\ \text{unit area}} = \frac{S_3'}{COP_3 A_t \dot{q}_{ideal}} \tag{9}$$

where

$S_3' = 200 \times 10^{-3}$ watts (specified)

$COP_3 = 0.17$ (Figure 2-9 with $\alpha = 10$)

$\dot{q}_{ideal}' = 0.012$ watts (Figure 2-7)

$\frac{A_3}{A_p} = 0.65$ and $\frac{A_2}{A_p} = .9$ (Figure 2-10)

with $A_1 \equiv A_p$

This gives $A_p' = \frac{200 \times 10^{-3}}{0.17\ (1 + .9 + .65)\ 0.0.2)} = 38.45\ ft^2$

Therefore the required areas for each stage are:

$A_1 = 38.5\ ft^2$

$A_2 = 34.6\ ft^2$

$A_3 = 25.0\ ft^2$

RADIATOR FIN OPTIMIZATION

The weight optimization analysis for the multistage radiator was based on minimizing the sum of the areas of the three stages. This assumes in effect that the weight per square foot of the various stages is equal. For an optimized system, however, each stage will be a different thickness, depending on the stage temperature. An analysis was performed to determine the relationship of optimum radiator fin geometry as a function of temperature.

Optimization Analysis

The analysis assumes a radiator of rectangular profile (constant thickness) as shown in Figure 2-14. Heat is distributed over the length of the radiator by a heat pipe which runs the length of the radiator; hence the problem reduces to a two-dimensional case involving heat conduction and radiation. The radiator temperature is expressed in terms of the fin root

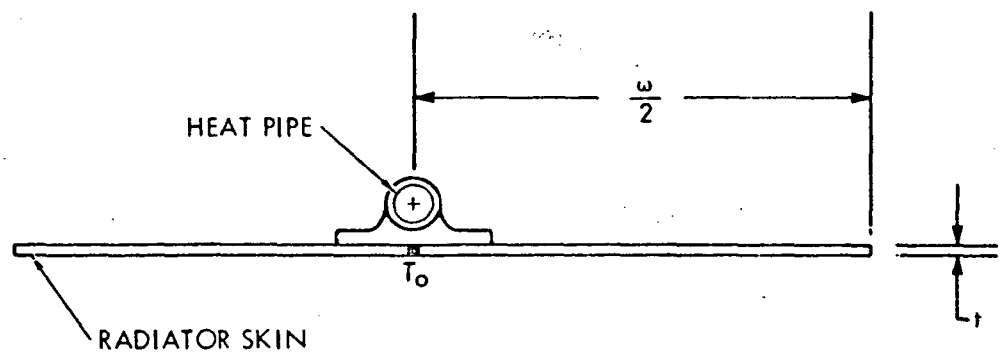

Figure 2-14 Radiator Fin Geometry

temperature, T_o, just below the heat pipe.

The general case of a radiating fin of rectangular profile is discussed and analyzed in Reference 2, which presents expressions for the temperature distribution and fin efficiency as a function of the fin geometry and properties.

The present analysis is concerned with the optimum geometry and weight of the radiator shown in Figure 2-14, including the weight of the heat pipe. The heat rejection capacity of the radiator shown in the figure is given by:

$$\left(\frac{q}{A}\right)_{rej} = \omega \sigma \varepsilon_R \eta_R (T_o^4 - T_s^4) \tag{10}$$

where

ε_R = radiator surface emittance

η_R = radiator fin efficiency

T_o = fin root temperature

T_s = effective sink temperature

The effective sink temperature is defined by the expression

$$T_s = \left[\frac{\Sigma q_{in}}{\sigma \varepsilon_R}\right]^{\frac{1}{4}} \tag{11}$$

The weight of the radiator per unit area is given by

$$W = \rho t \omega + \Omega \tag{12}$$

where

ρ = density of the radiator fin material

t = fin thickness

ω = total radiator width

Ω = weight per unit length of the heat pipe, insulation, and supports

To arrive at the optimum radiator, we wish to maximize the total heat rejection per total weight:

$$\frac{\dot{q}}{w} = \frac{\omega \sigma \varepsilon_R \eta_R (T_o^4 - T_s^4)}{\rho t \omega + \Omega} \tag{13}$$

Optimization of the radiator weight thus depends on maximizing the quantity

$$0 = \frac{\varepsilon_R \eta_R \omega}{\rho t \omega + \Omega} \tag{14}$$

where 0 is the optimization function.

From Reference 2, the fin efficiency, η_R, is expressed in terms of a dimensionless fin length, X, where

$$X = \frac{\omega}{2}\sqrt{\frac{\sigma \varepsilon_R T_o^3}{k t}} \tag{15}$$

and k is the thermal conductivity of the fin.

The optimum value of 0 exists for optimum values of ω and ε and the following conditions exist:

$$\frac{\partial 0}{\partial \omega} = 0 \tag{16}$$

$$\frac{\partial 0}{\partial t} = 0 \tag{17}$$

Solution of Equation 16 using Equations 14 and 15 yield the relationship for the optimum dimensionless fin length, X_o:

$$X_o = \left[\frac{\rho \omega^3 \sigma_R T_o^3}{2 K \Omega}\right]^{\frac{1}{2}} \tag{18}$$

Similarly, solution of Equation 17 yields

$$X_o = \frac{\Omega^2 \sigma \varepsilon_R T_o^3}{16 \rho^2 k t^3} \tag{19}$$

Equations 18 and 19 yield the following relationship between optimum thickness, t_o, and optimum radiation width, ω_o:

$$\omega_o = \frac{\Omega}{2 \rho t_o} \tag{20}$$

Substitution of Equation 20 into Equation 14 yields

$$0_c = \frac{2}{3} \frac{\epsilon_R}{\Omega} \eta_o \omega_o \tag{21}$$

where

η_o = fin efficiency corresponding to ω_o and t_o

Equation 21 was solved by assuming a polynominal power series expression for η_R in terms of X. Substitution and differentiation of 0_o with respect to ω_o yields the expression

$$\frac{\partial 0_o}{\partial \omega_o} = \frac{2}{3} \frac{\epsilon_R}{\Omega} \left[\frac{\rho \sigma \epsilon_R T_o^3}{2 k \Omega}\right]^{-3} X_o^{2/3} \eta(x_o) = o \tag{22}$$

The variable portion of Equation 22 is plotted in Figure 2-15. Selection yield an optimum value for X_o of 0.92 when $T_s = o$. It is interesting to note that this value is independant of Ω and is identical to that reported in Reference 2. The corresponding optimum efficiency is 0.565.

Substituting, we find that

$$\omega_o = \left[\frac{2 k \Omega X_o^2}{\rho \sigma \epsilon_R T_o^3}\right]^{\frac{1}{3}} \tag{23}$$

Values of ω_o and t_o are plotted for an aluminum radiator as a function of T_o in Figure 2-16. Figure 2-17 shows the value of the optimization function, 0_o, as a function of T_o.

The results of this analysis can be applied easily to single or multistage radiator systems. For a radiator with several heat pipes, the fin width is equal to one-half the heat pipe spacing. Detailed plots of the optimization function, 0, versus heat pipe spacing and fin thickness are shown in Figures 2-18 through 2-26 for temperatures of 300°K down to 20°K, based on a heat pipe

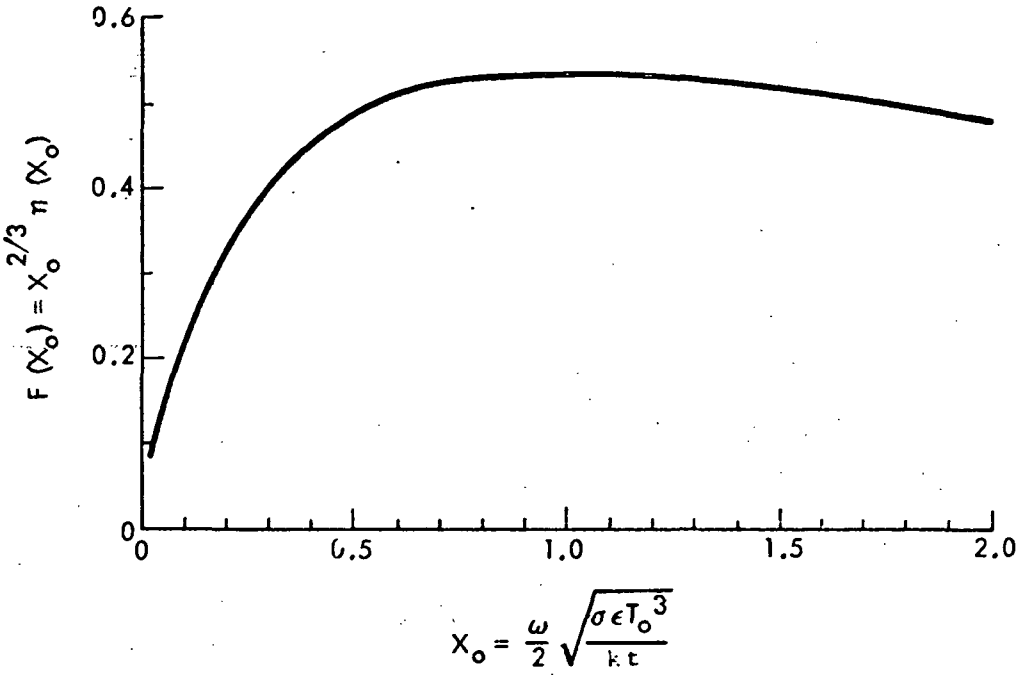

Figure 2-15 Radiator Optimization Function

weight of 0.3 lbm/ft. Lines of constant fin efficiency are indicated by the dotted lines. To show the effect of reducing the heat pipe weight, similar data are shown for a heat pipe weight of 0.1 lbm/ft in Figure 2-27 through 2-35.

The parametric fin optimization charts presented in Figures 2-16 through 2-35, together with the multistage radiator design data in Figures 2-3 through 2-13 provide a useful reference and design tool for designing and optimizing low temperature passive radiators over a wide range of temperatures and heat loads.

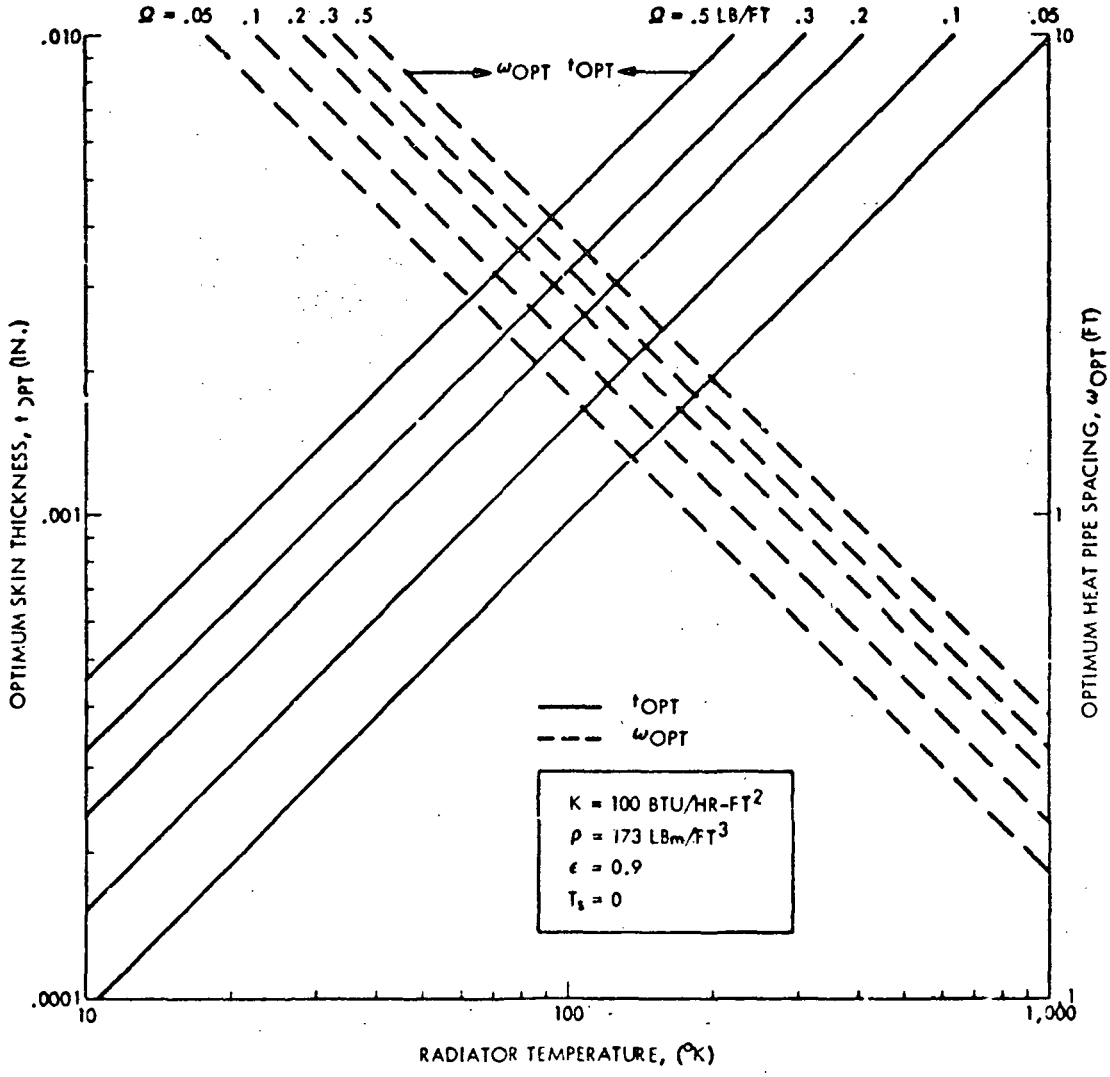

Figure 2-16 Optimum Radiator Width and Thickness vs. Temperatures

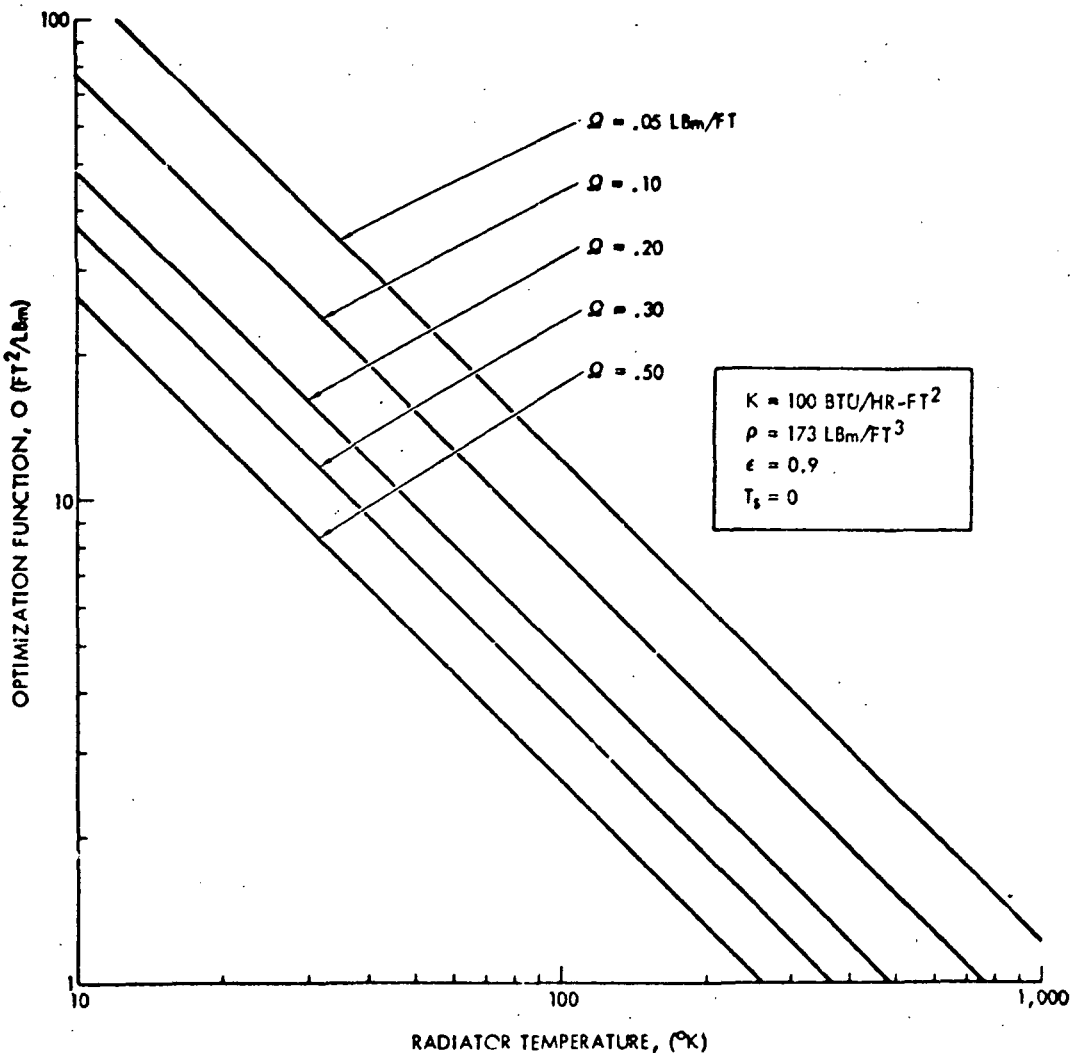

Figure 2-17 Optimization Function versus Temperatures

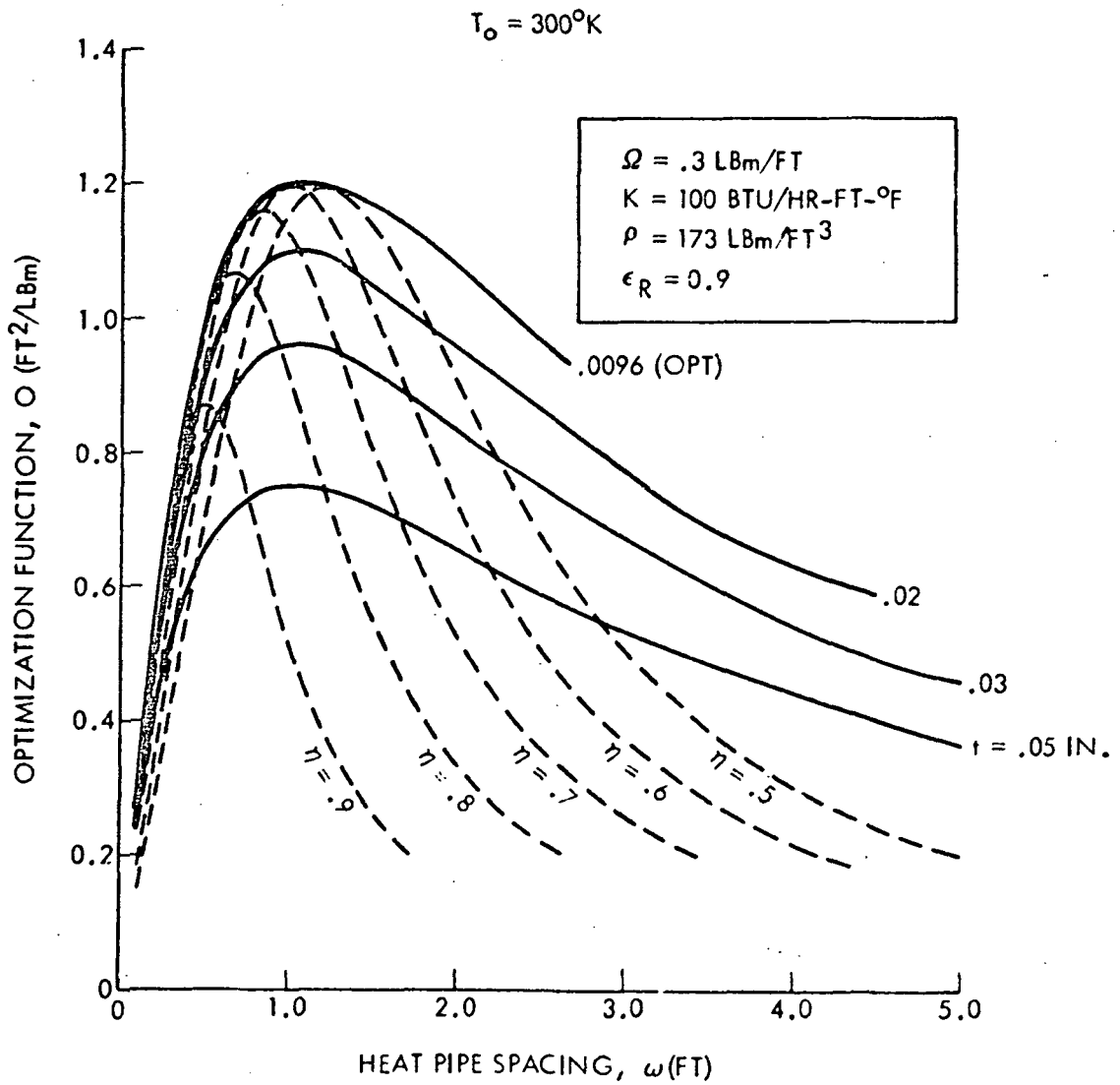

Figure 2-18 Radiator Optimization Function (Ω = 0.3 lb_m/ft, T_o = 300°K)

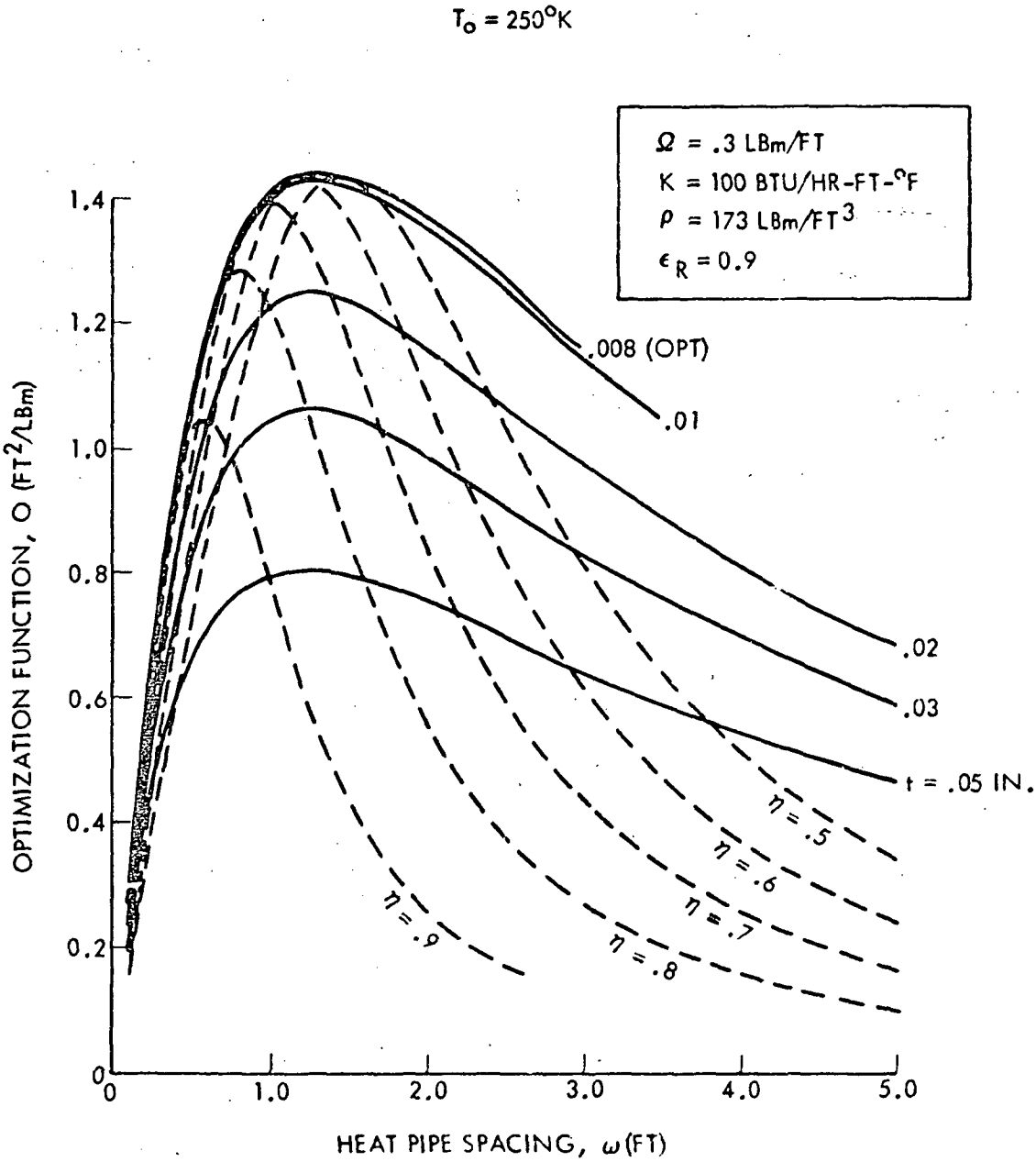

Figure 2-19 Radiator Optimization Function (Ω = 0.3 lb_m/ft, T_o = 250°K)

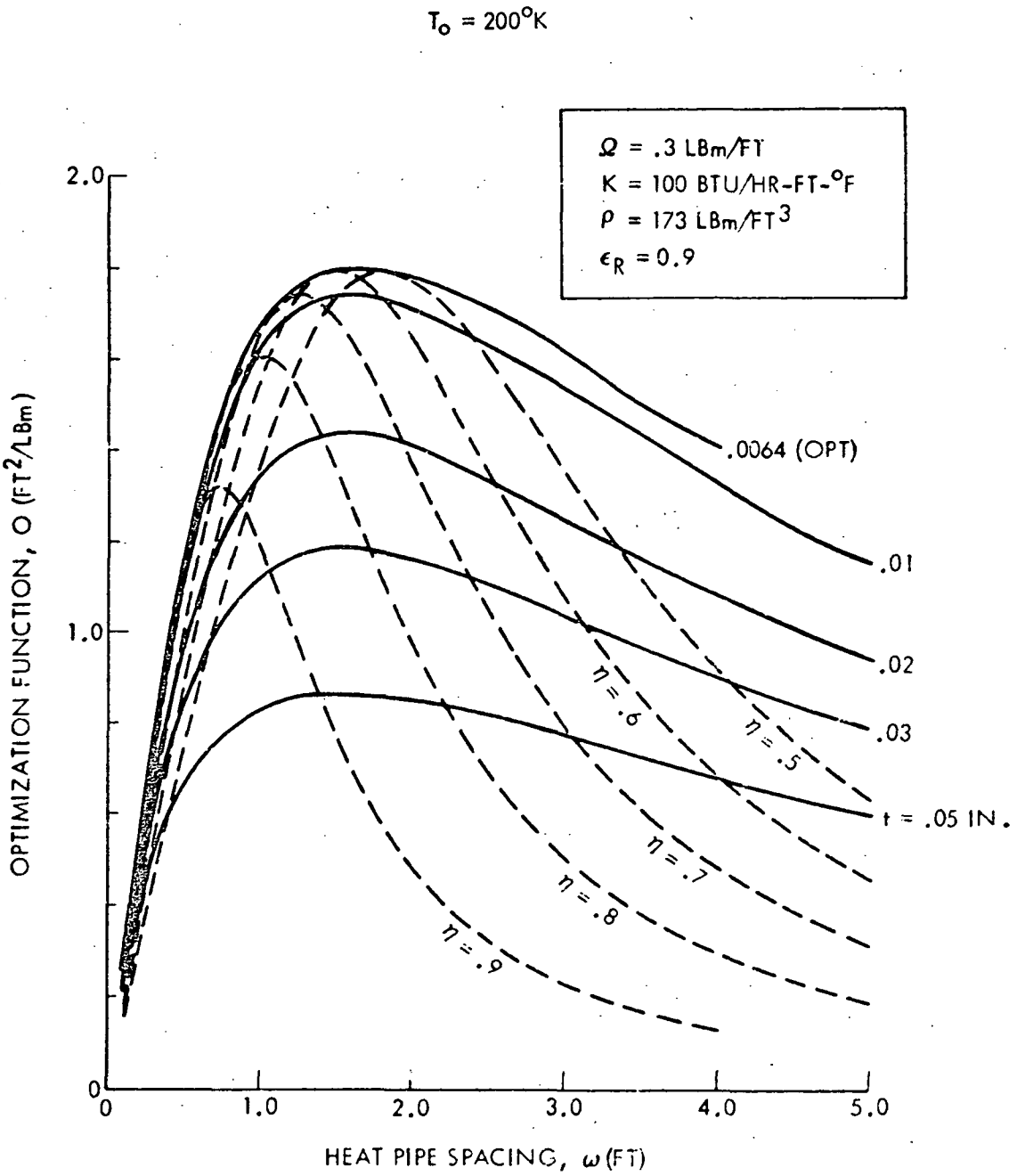

Figure 2-20 Radiator Optimization Function (Ω = 0.3 lb_m/ft, T_o = 200°K)

$T_o = 150^oK$

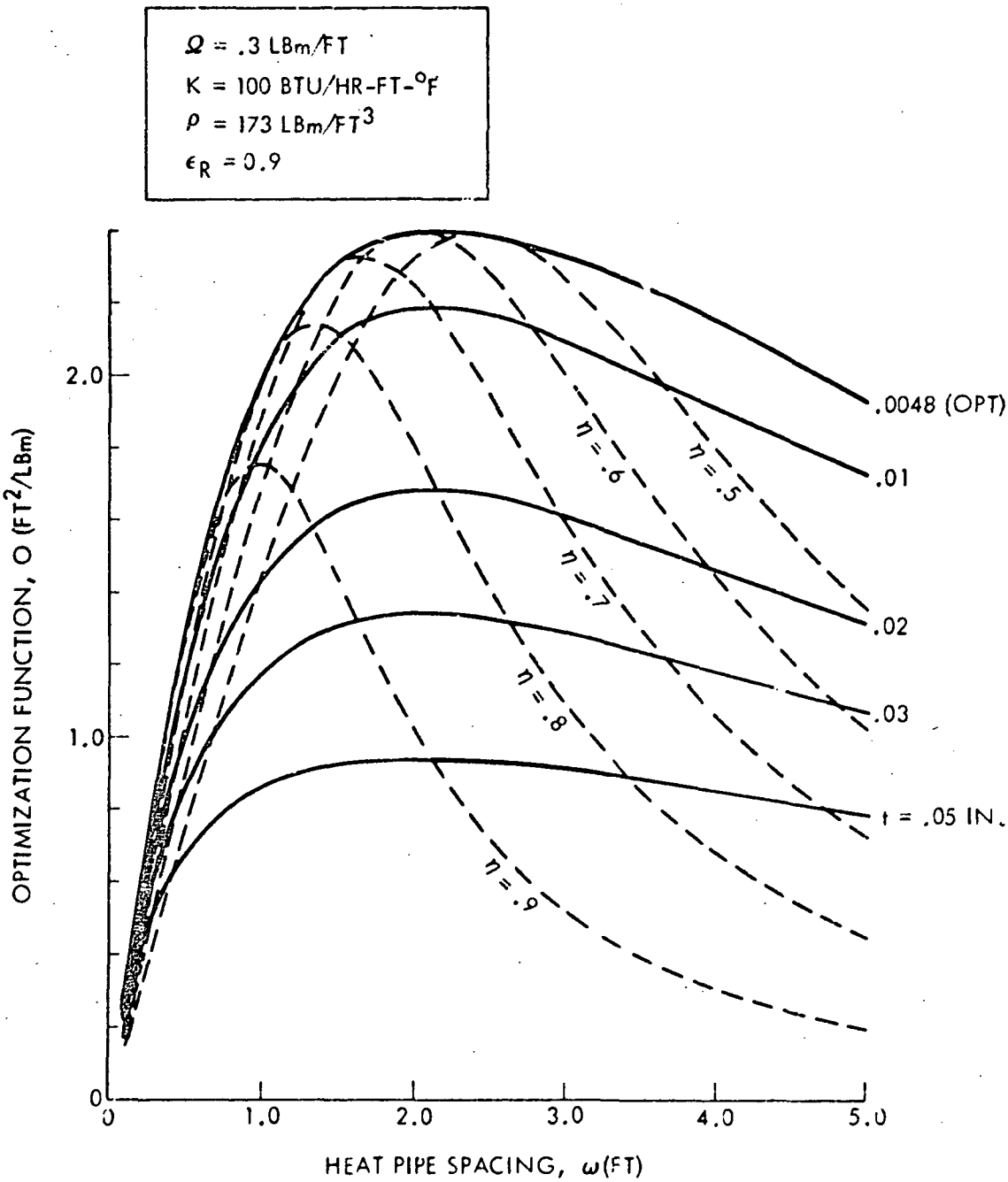

Figure 2-21 Radiator Optimization Function (Ω = 0.3 lb_m/ft, T_o = 150°K)

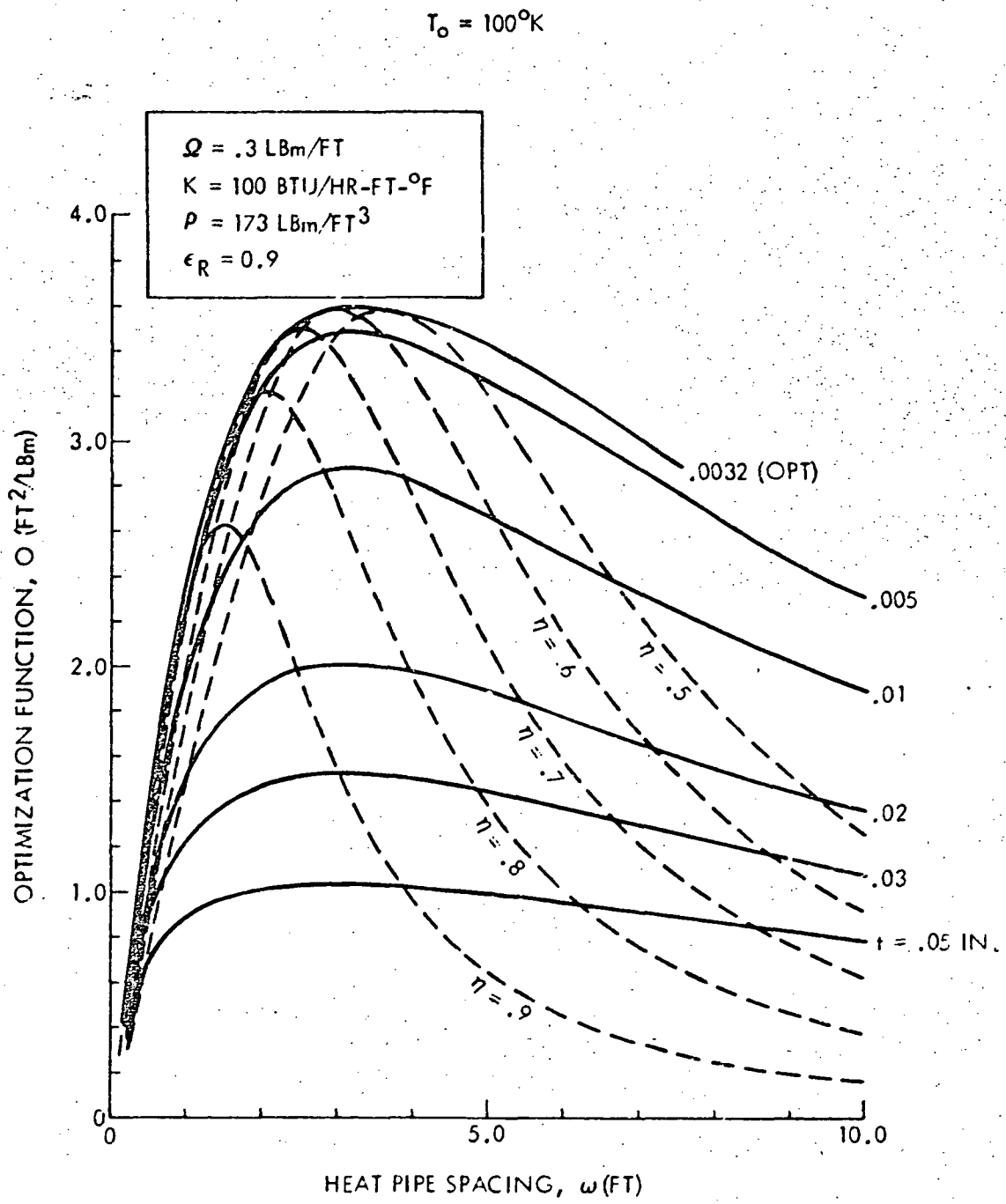

Figure 2-22 Radiator Optimization Function (Ω = 0.3 lb_m/ft, T_o = 100°K)

$T_o = 75^oK$

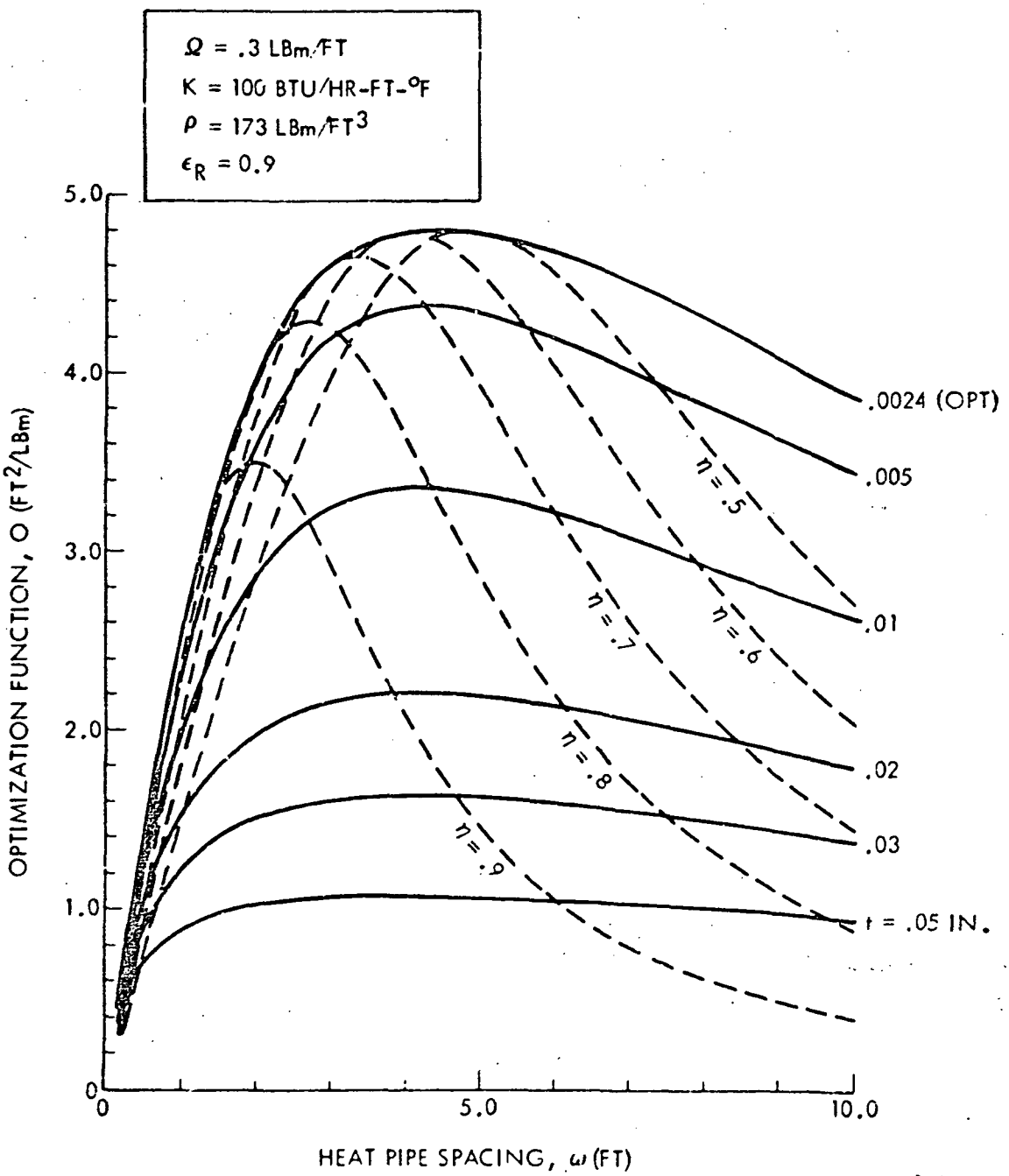

Figure 2-23 Radiator Optimization Function (Ω = 0.3 lb_m/ft, T_o = 75°K)

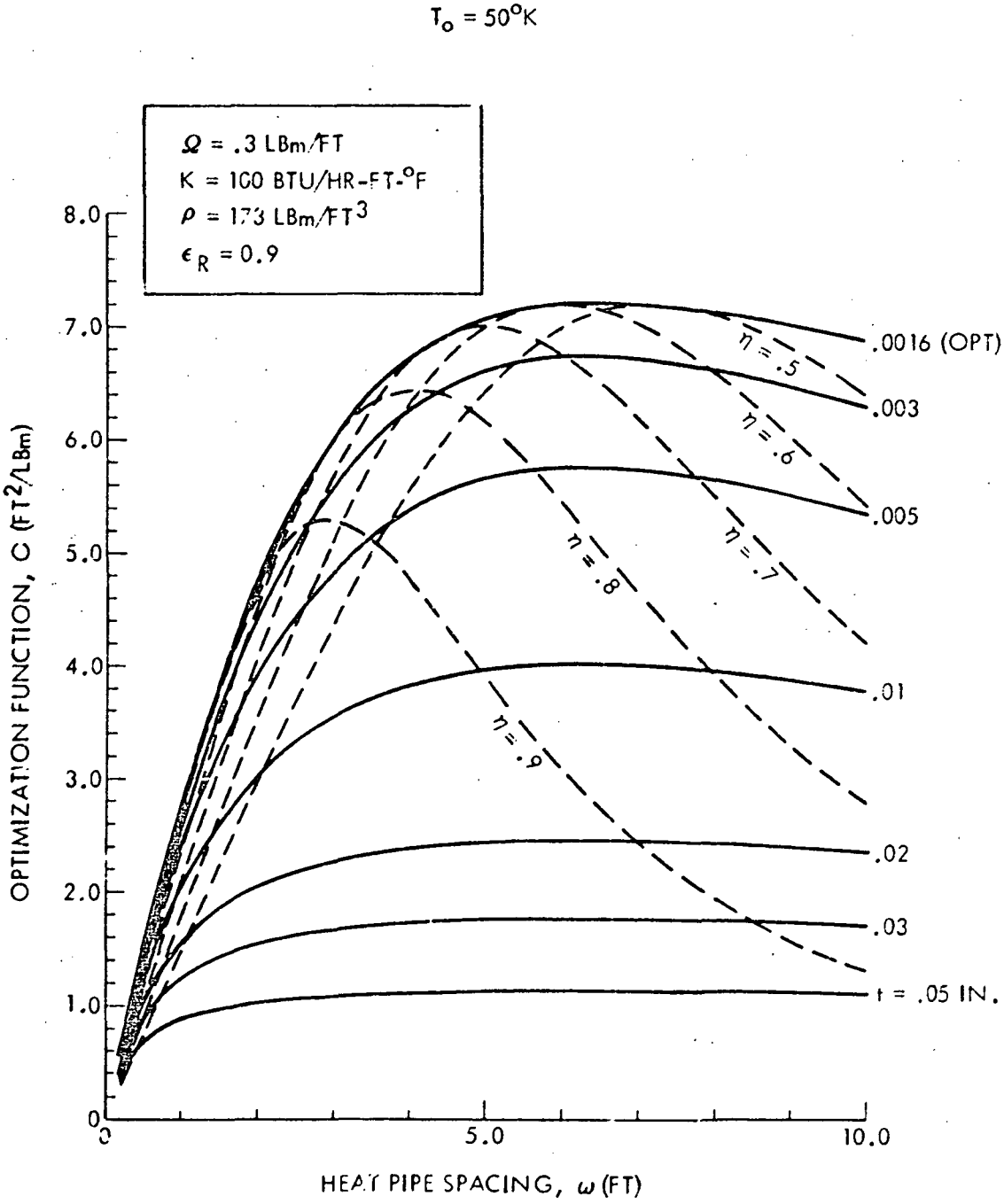

Figure 2-24 Radiator Optimization Function ($\mathcal{Q}$ = 0.3 lb_m/ft., T_o = 50°K)

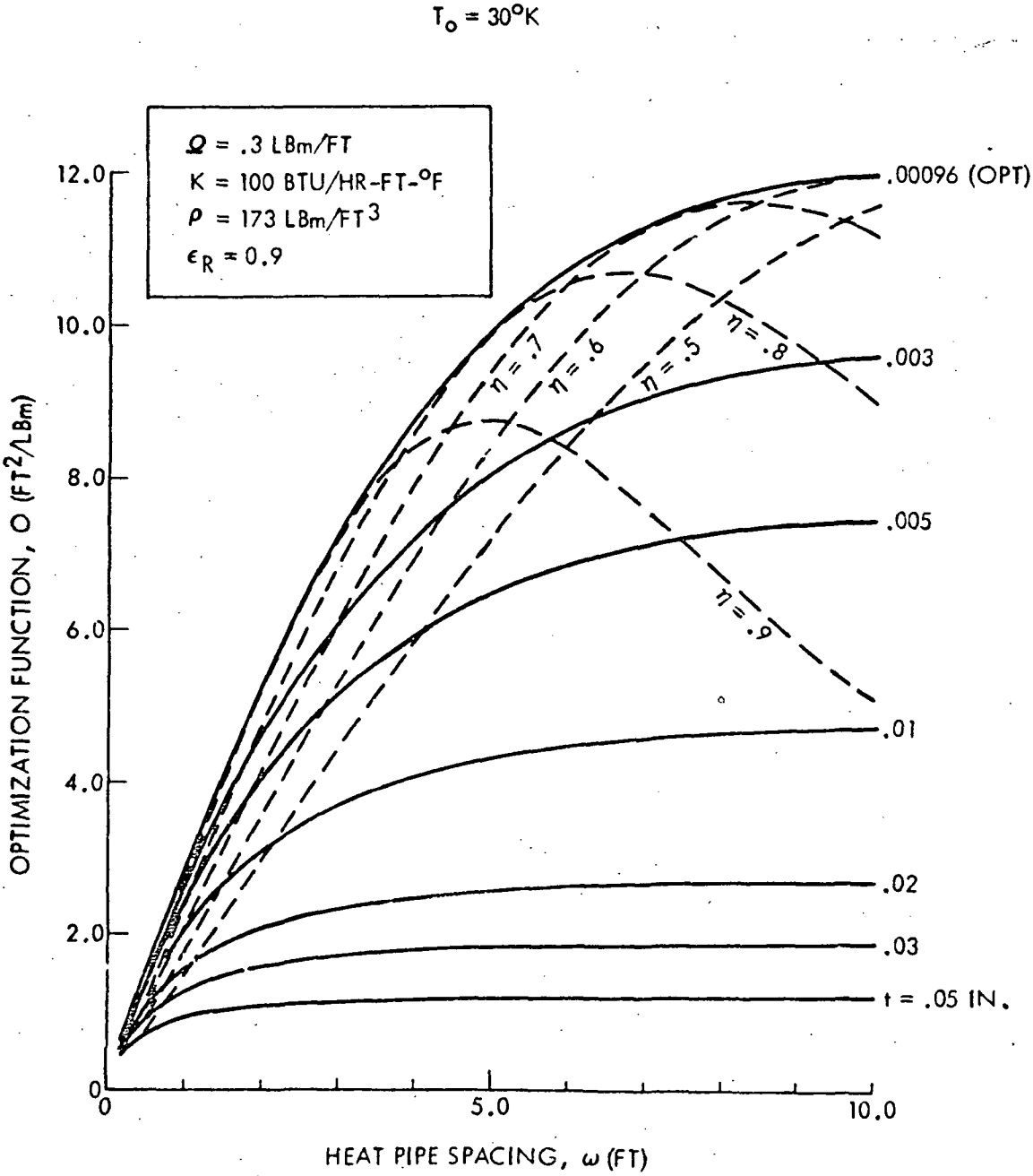

Figure 2-25 Radiator Optimization Function (Ω = 0.3 lb_m/ft, T_o = 30°K)

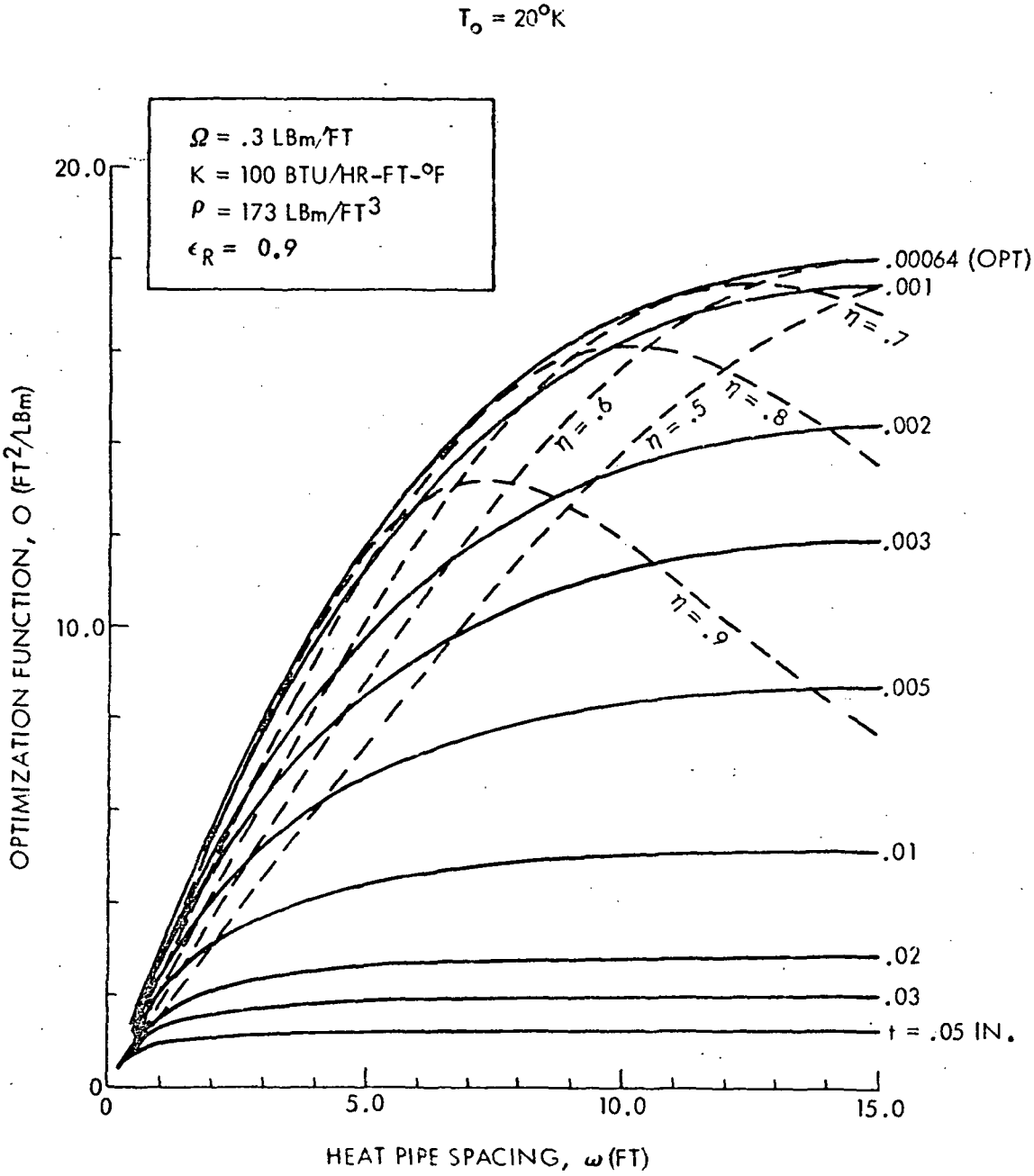

Figure 2-26 Radiator Optimization Function (Ω = 0.3 lb_m/ft, T_o = 20°K)

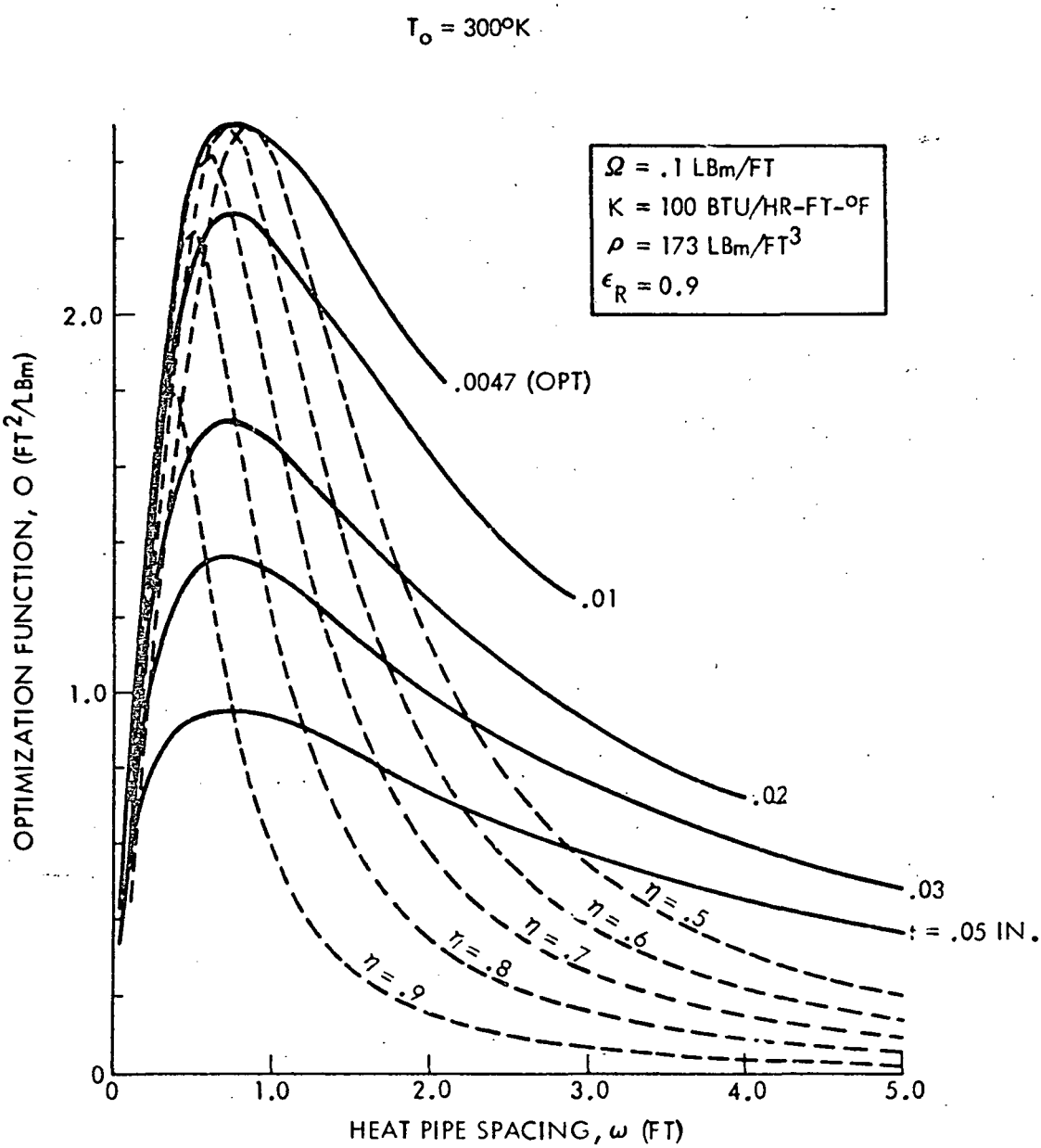

Figure 2-27 Radiator Optimization Function (Ω = 0.1 lb_m/ft, T_o = 300°K)

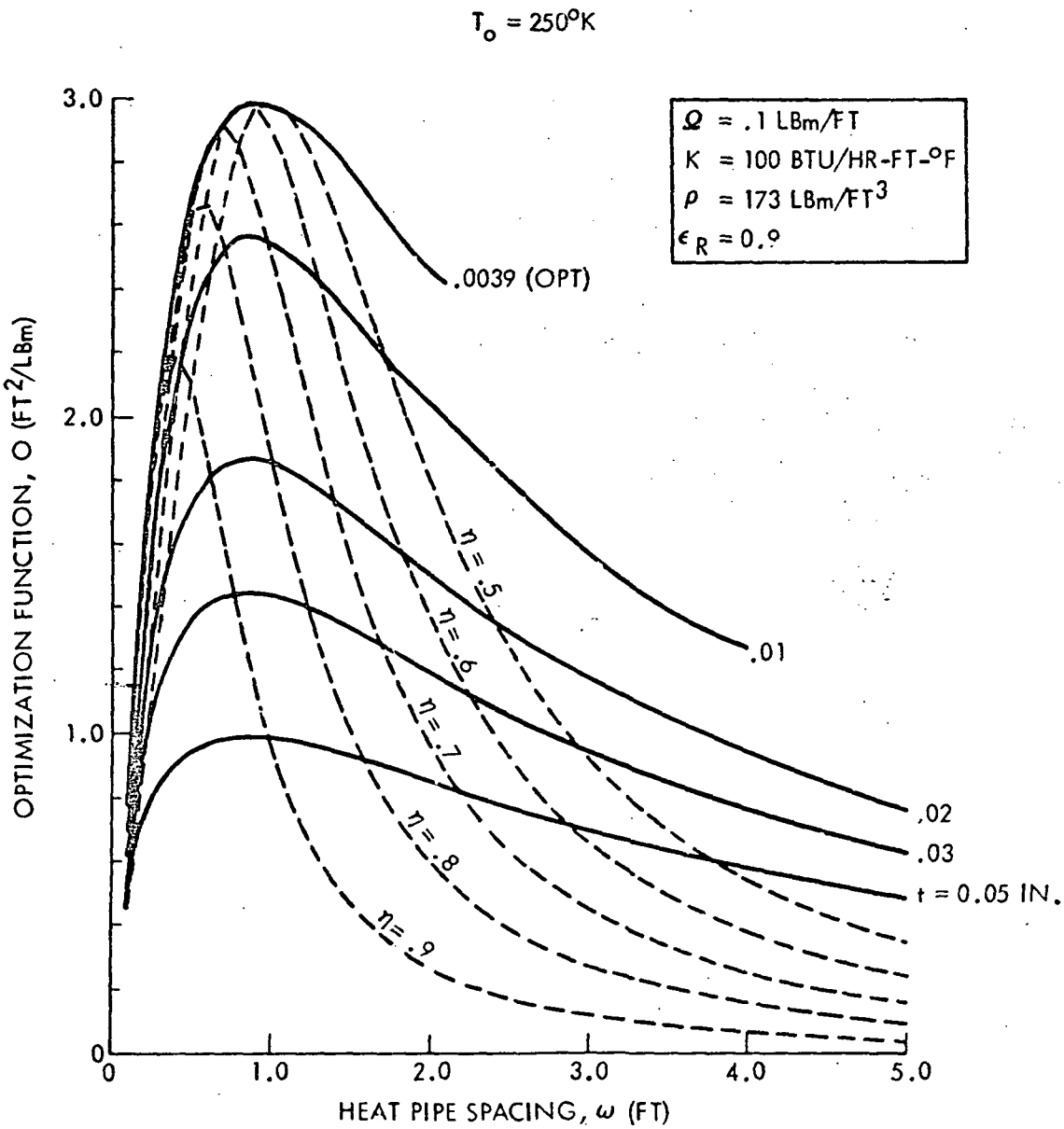

Figure 2-28 Radiator Optimization Function (Ω = 0.1 lb_m/ft, T_o = 250°K)

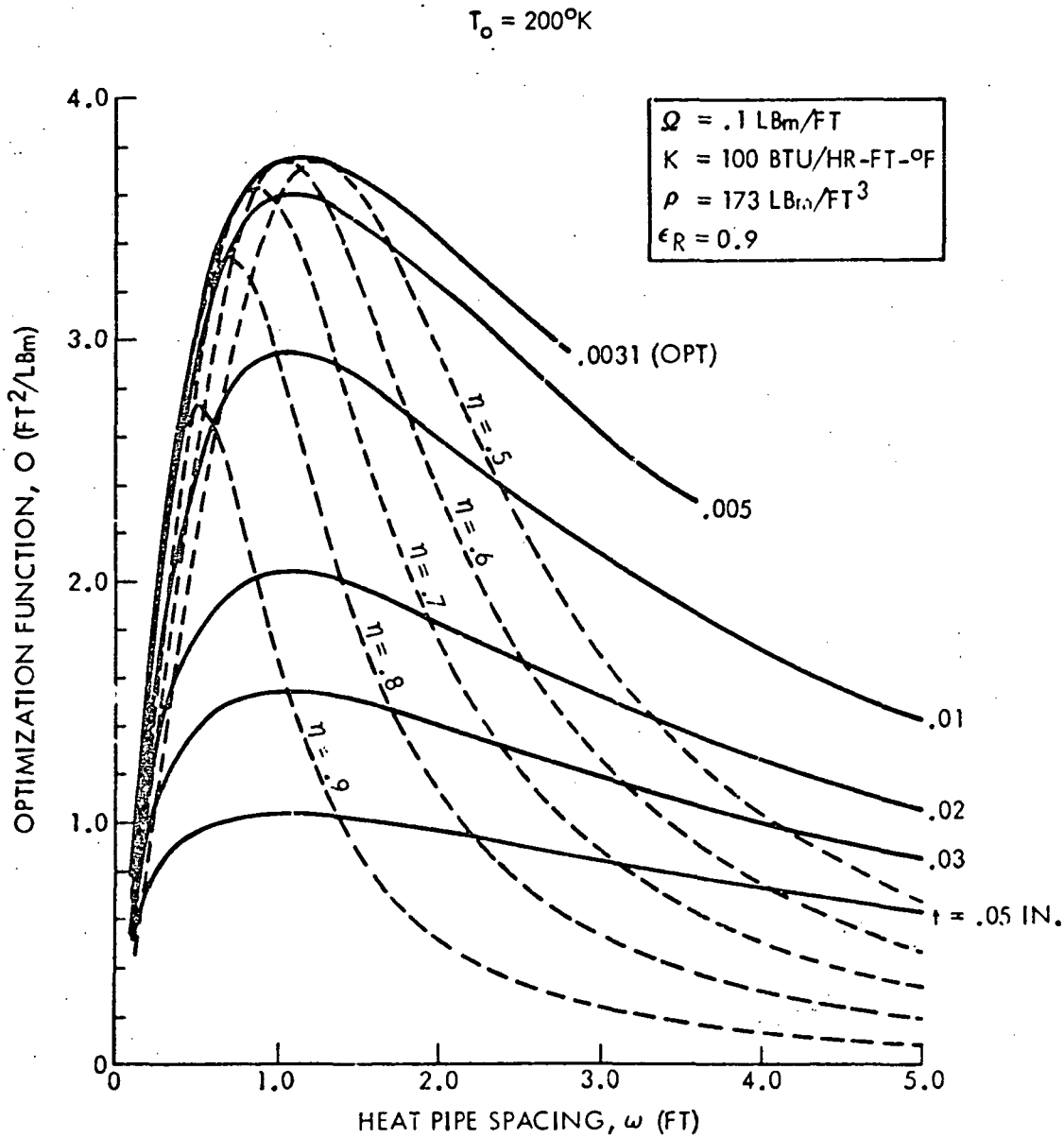

Figure 2-29 Radiator Optimization Function (Ω = 0.1 lb_m/ft, T_o = 200°K)

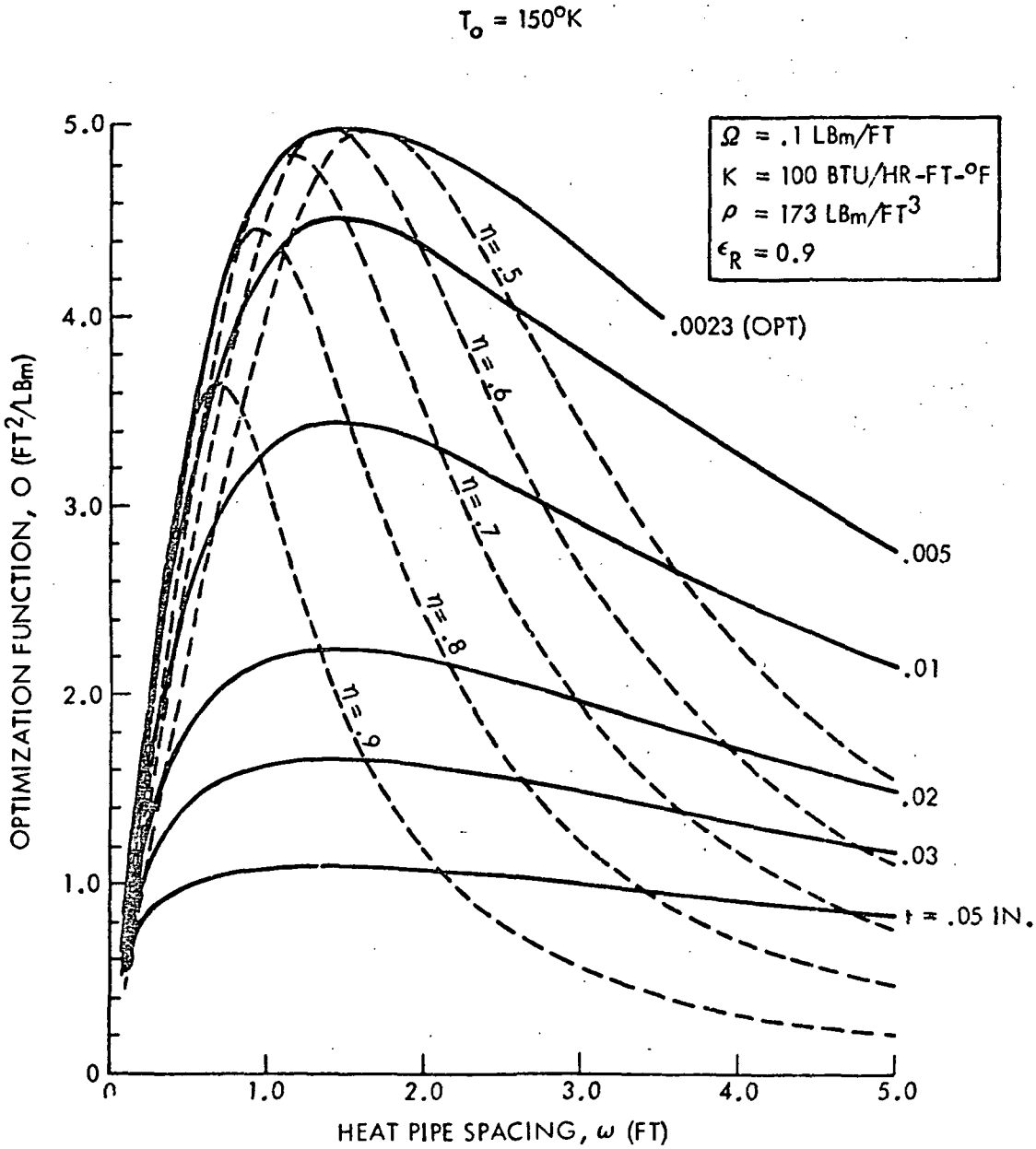

Figure 2-30 Radiator Optimization Function (Ω = 0.1 lb_m/ft, T_o = 150°K)

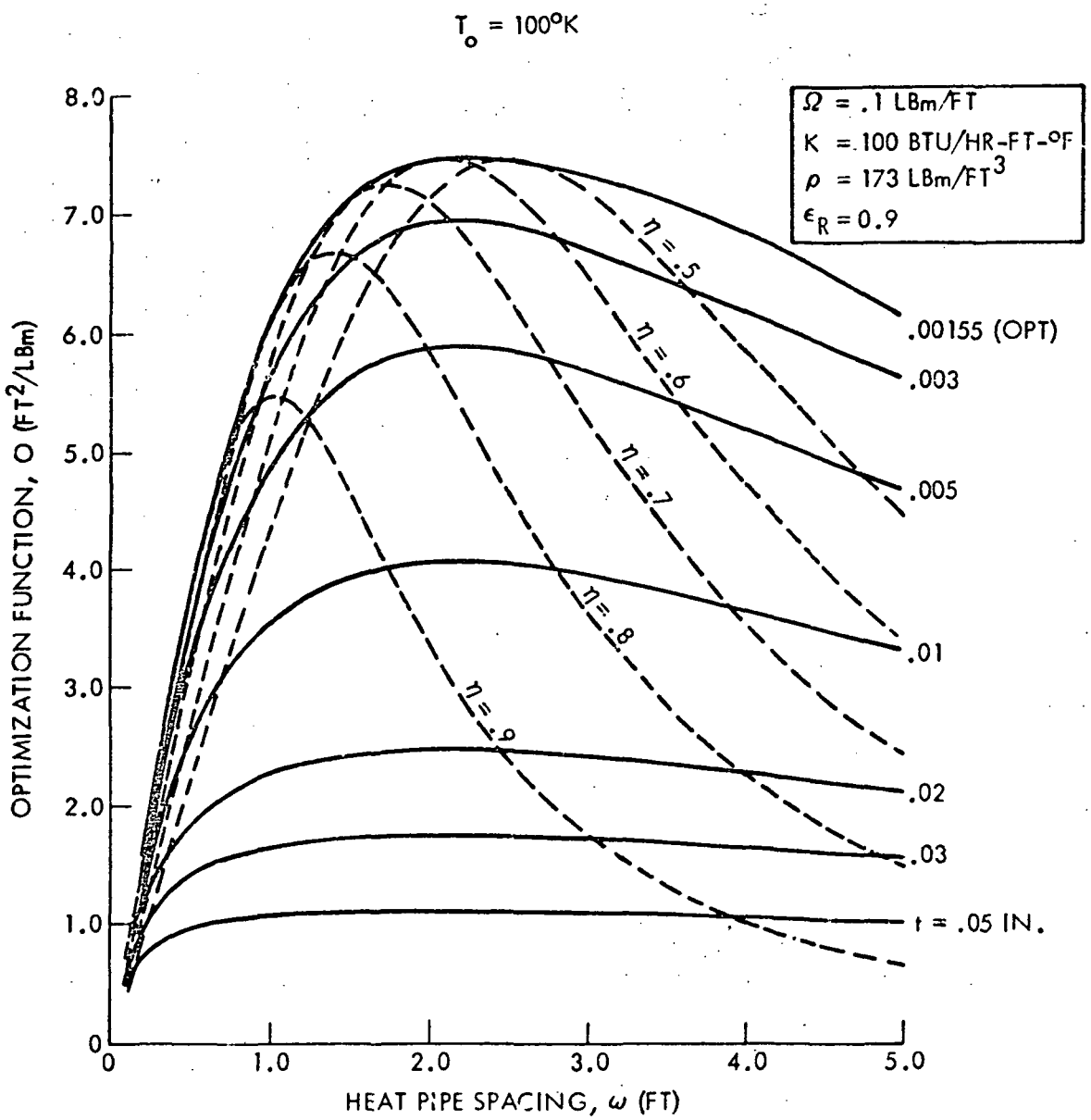

Figure 2-31 Radiator Optimization Function (Ω = 0.1 lb_m/ft, T_o = 100°K)

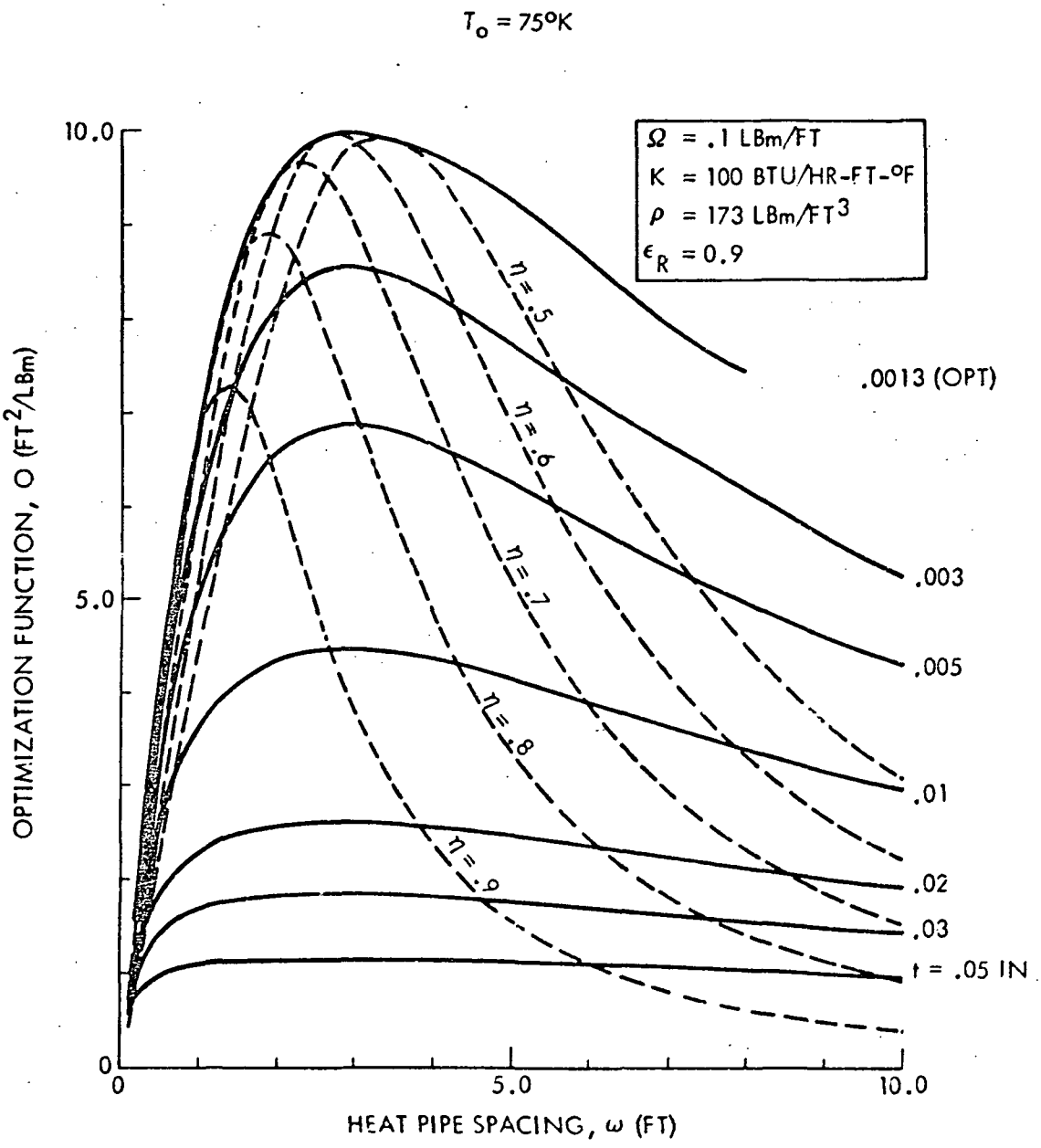

Figure 2-32 Radiator Optimization Function (Ω = 0.1 lb_m/ft, T_o = 75°K)

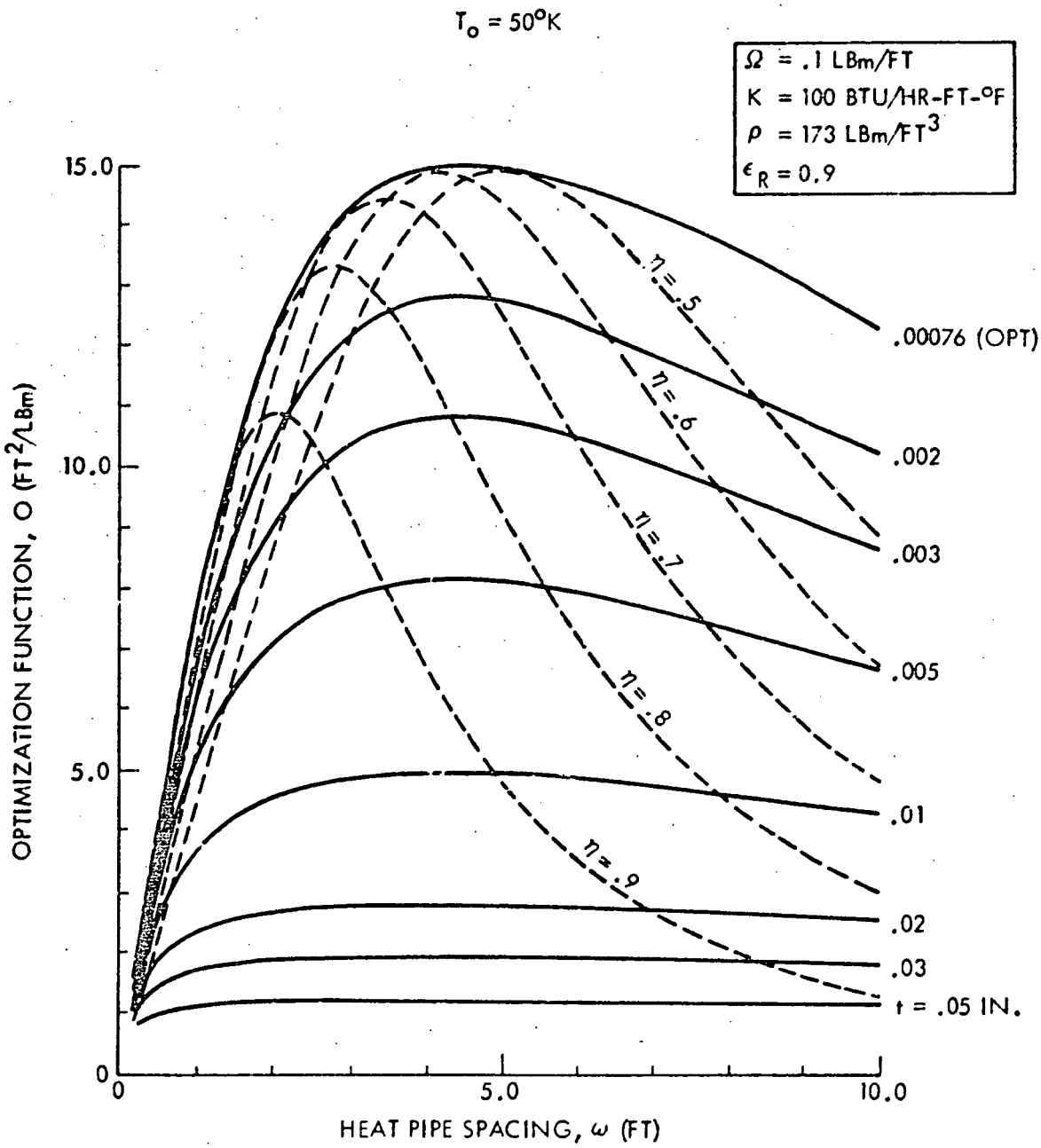

Figure 2-33 Radiator Optimization Function (Ω = 0.1 lb_m/ft, T_o = 50°K)

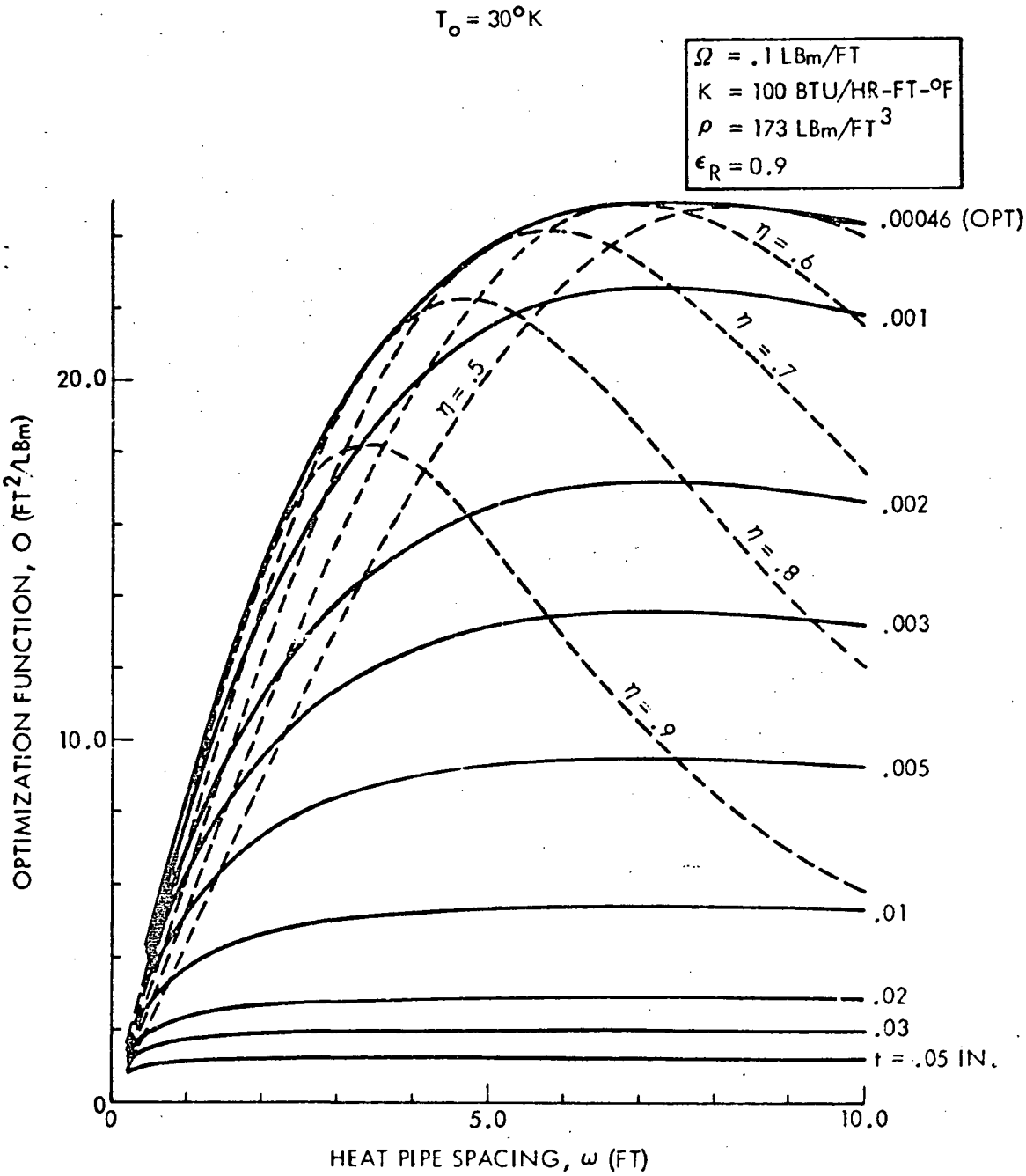

Figure 2-34 Radiator Optimization Function (Ω = 0.1 lb_m/ft, T_o = 30°K)

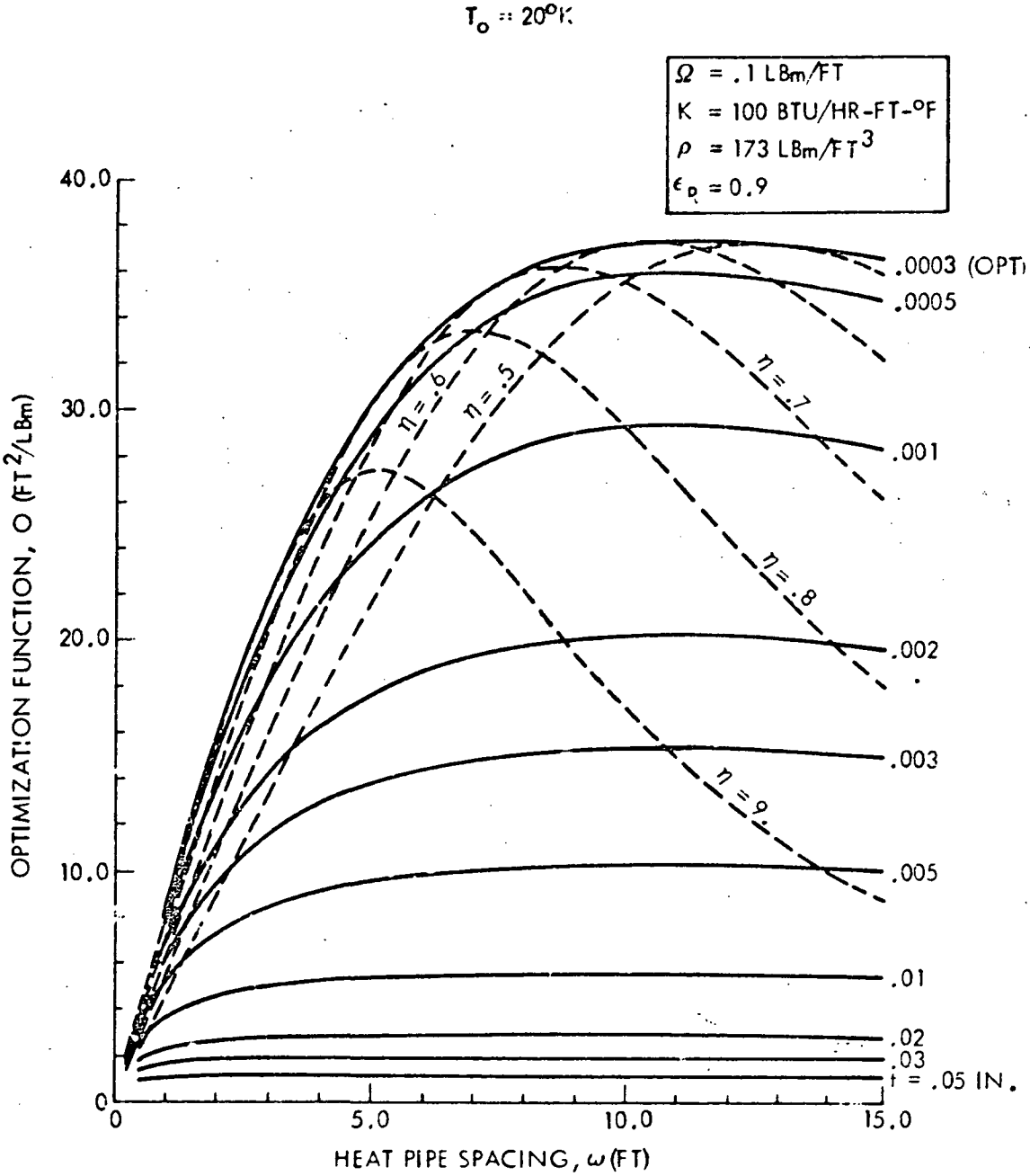

Figure 2-35 Radiator Optimization Function (Ω = 0.1 lb_m/ft, T_o = 20°K)

GROUND TEST SYSTEM DEFINITION

A 1-g test prototype of a three-stage heat pipe radiator was designed based on the results of the preceding parametric analyses. Design requirements for the system were defined based on the following considerations:

1. Projected cooling requirements for future LWIR sensor payloads.
2. Extension of the state of the art.
3. Practical size for 1-g testing.
4. Heat pipe working fluids.

Projected payload cooling requirements for future low-temperature payloads were summarized in the final report for Exhibit A, Reference 1. Based on a technical review of these conditions with the NASA COR, the following requirements were established as design goals:

Cold stage temperature - 35°K

Cold stage heat load - 10 mw

Intermediate stage heat load - 100 mw

The 35°K design goal was felt to be practical for a three-stage radiator and is believed to be attainable with current insulation technology. Furthermore, the 40°K to 60°K temperature range would preclude the use of a heat pipe system due to working fluid limitations.

A preliminary design value of 0.015 for the insulation effective emittance was selected for the initial baseline design studies; values of 0.010 and 0.015 were evaluated in the detailed design analysis. Both of these values are considered conservative when compared to the actual measured value of the flight-qualified system built for the RM-20B radiator which had an effective emittance of 0.008 (Reference 3).

The ground test system was optimized for a minimum projected area as opposed to minimum overall weight. This was done to minimize the overall system envelope for testing. Furthermore, results of the fin optimization studies show that the outer two stages will have very thin skins compared to the first stage, so that an area-optimized configuration would likely be the more valid.

The optimum areas were determined to be 4.73, 3.67, and 2.25 square feet for the first, second, and third stages, respectively (based on $\varepsilon_{ins} = 0.015$). The 0.015 insulation emittance value was assumed initially to account for additional parasitic heat loads which might ultimately arise from the heat pipes and the test fixture.

Design Sensitivity Analysis

Additional parametric analyses were performed to determine the sensitivity of the performance of the baseline design to variations in geometry, heat loads, or assumed insulation properties. Figure 2-36 shows the sensitivity of cold stage heat rejection capability at constant temperature to insulation emittance. At 35°K, the performance is a very strong function of ε_{ins}; the heat rejection capability (α=10) vanishes at $\varepsilon_{ins} = 0.019$. The sensitivity of cold stage temperature at a constant 10-mw load is shown in Figure 2-37. For an ε_{ins} of 0.010, the cold stage temperature is reduced only by 2.5°K.

Sensitivity of third-stage heat load and temperature to stage load ratio (α) is shown in Figures 2-38 and 2-39. When $\alpha = 0$, the heat rejection capability at 35°K is 13.5 mw, and the third stage temperature at a 10-mw load is 33.4°K.

Figures 2-40 and 2-41 show the minimum projected area requirements of three-stage radiators as a function of cold stage temperature and ε_{ins} for $\alpha = 10$ and $\alpha = 0$, respectively. All cases are for third-stage loads of 10 mw. These figures show the expected rapid increase (4th-power function) in area requirements with reduced temperature. In addition, the figures show that between 25°K and 35°K, the area requirement increases by an order of magnitude for $\varepsilon_{ins} = 0.02$ while by only a factc of two for $\varepsilon_{ins} = 0.01$.

Finally, Figure 2-42 shows the sensitivity of the heat rejection capability as a function of third-stage temperature for stage load ratios of

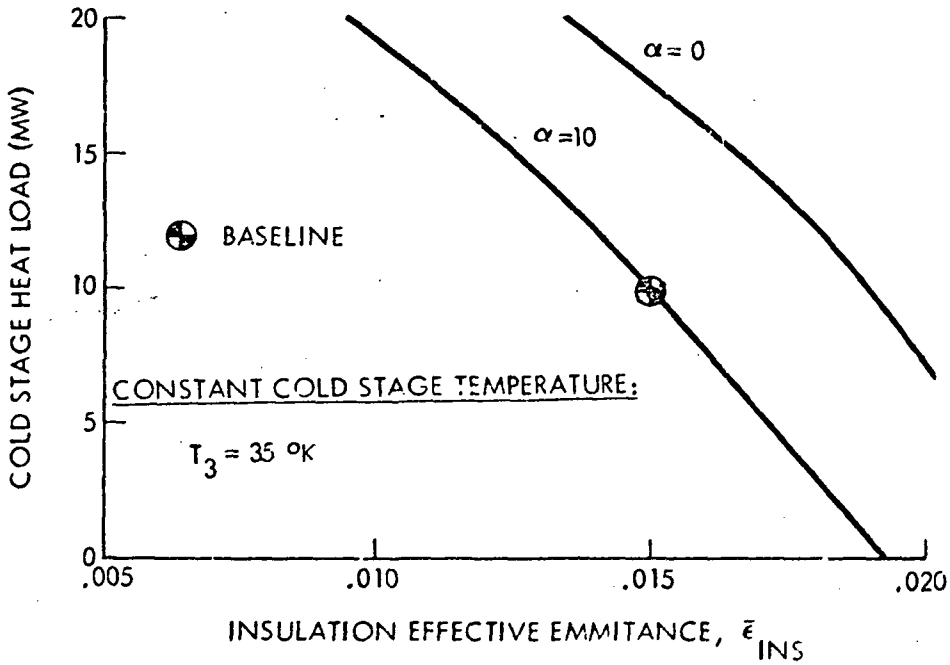

Figure 2-36 Cold Stage Rejection Capability vs. $\bar{\epsilon}_{ins}$

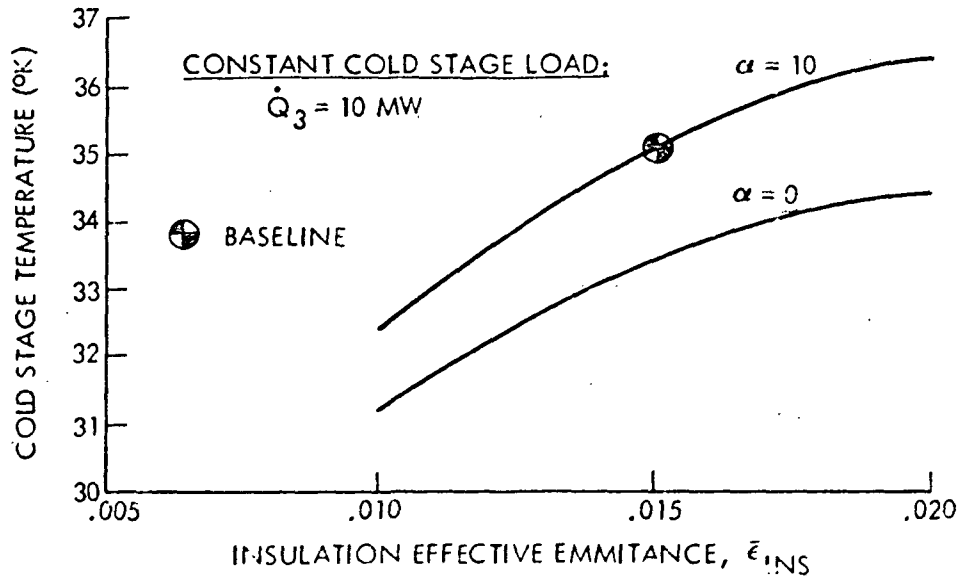

Figure 2-37 Cold Stage Temperature vs. $\bar{\epsilon}_{ins}$

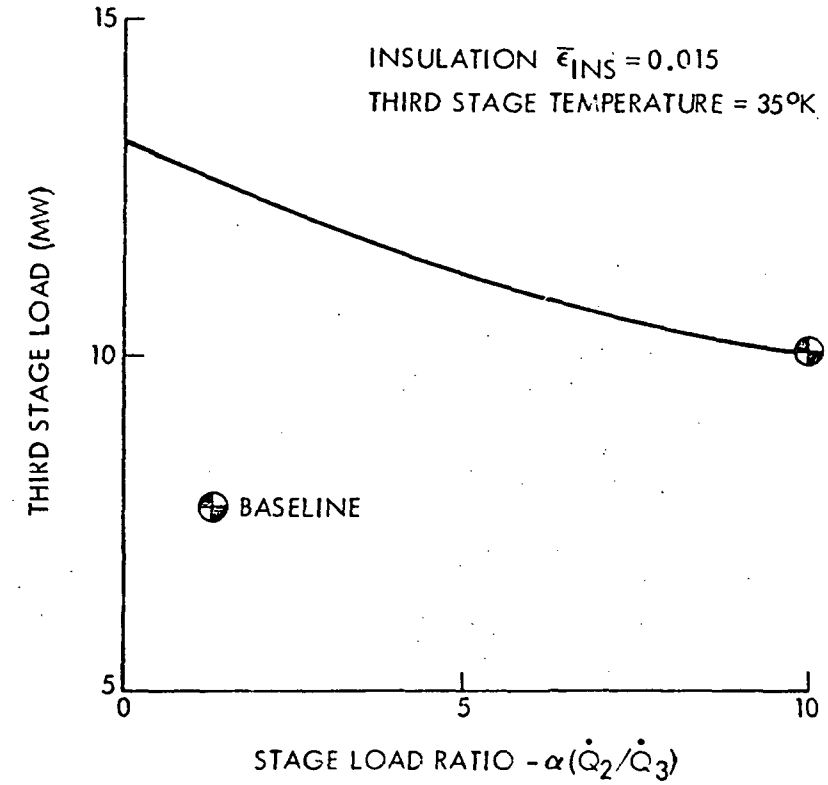

Figure 2-38 Third Stage Heat Load vs. α

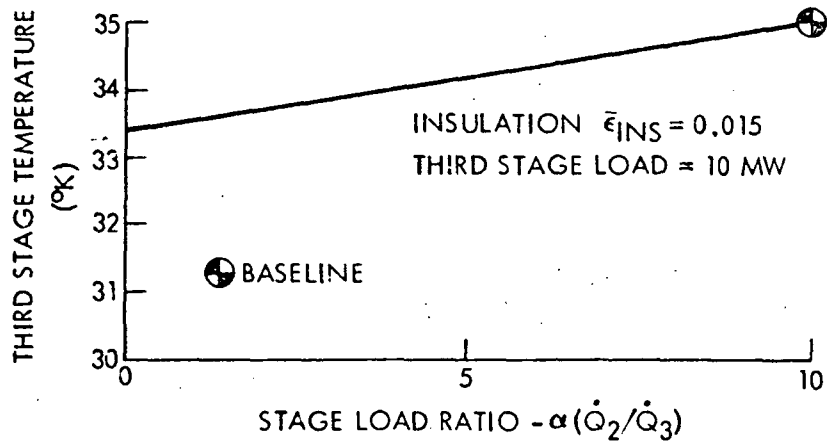

Figure 2-39 Third Stage Temperature vs. α

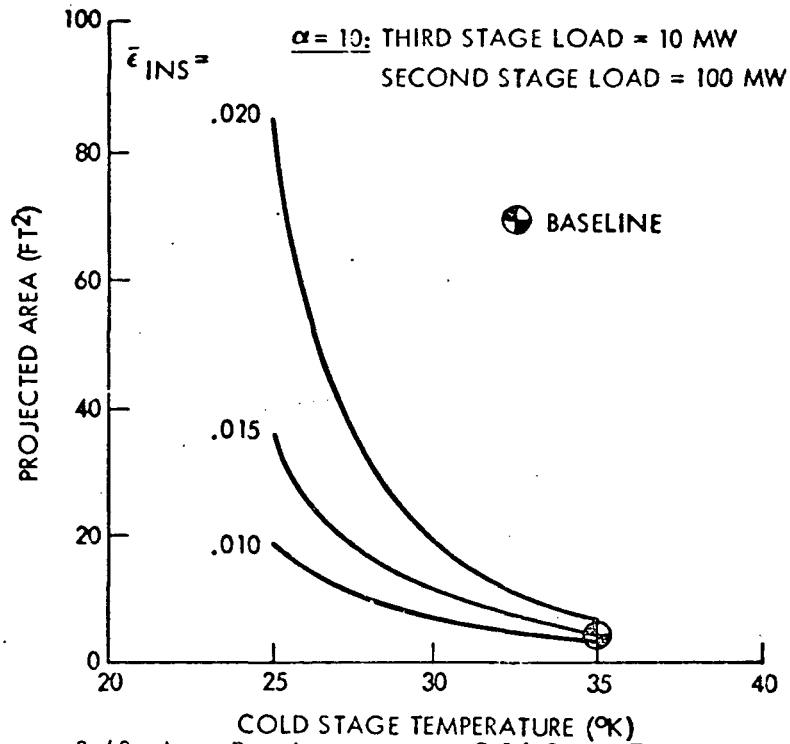

Figure 2-40 Area Requirements vs. Cold Stage Temperature (α = 10)

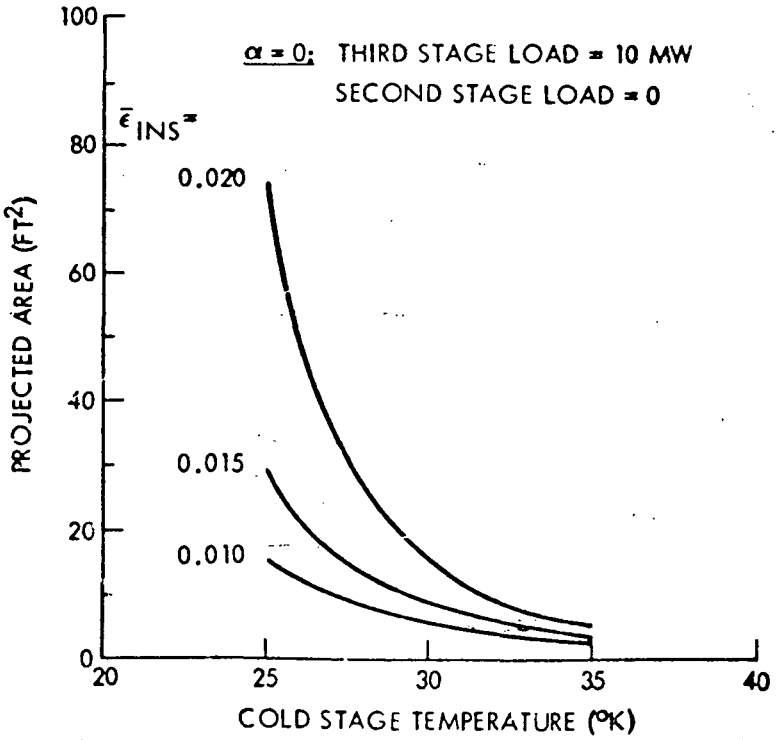

Figure 2-41 Area Requirements vs. Cold Stage Temperature (α = 0)

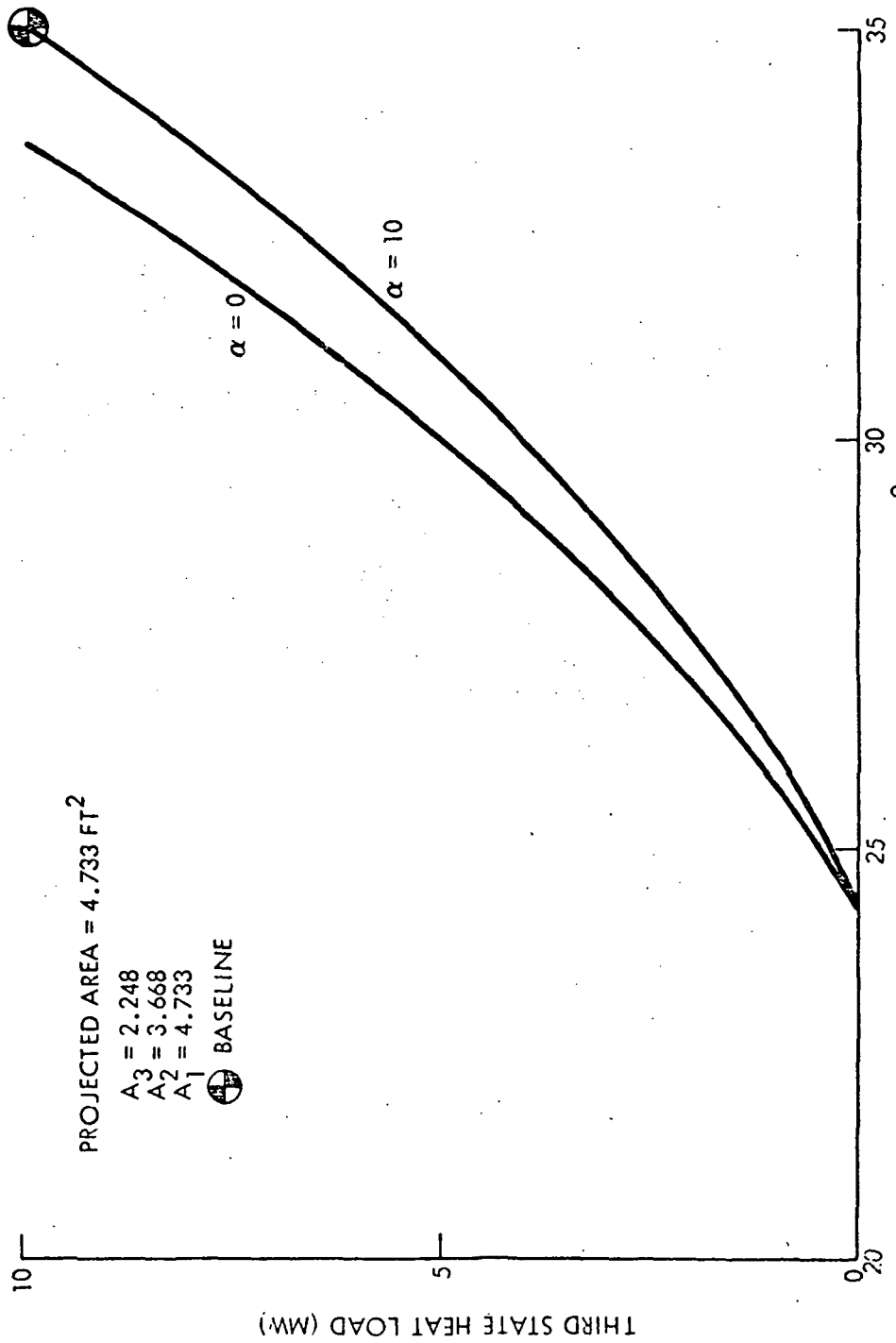

Figure 2-42 Heat Rejection Capability vs. Third Stage Temperature

0 and 10. The minimum achievable temperature with no loads on the radiator is 24.5°K. The performance data in Figure 2-42 are for the baseline design where the area requirements are determined with a perfect view to space from all external radiator surfaces. In most actual installations, however, the radiator will be partially exposed to the effects of shielding used to prevent direct solar energy impingement on the radiator surfaces while in orbit. Because of this, the stage areas must be increased to accommodate these additional loads.

Design Configuration

The detailed design configuration for the three-stage radiator was selected based on the results of the design sensitivity studies. Shielding requirements were established based on a 400-nautical-mile sun-synchronous orbit (Figure 2-43). Shielding requirements were analyzed during the first phase of this study and are reported in Reference 1.

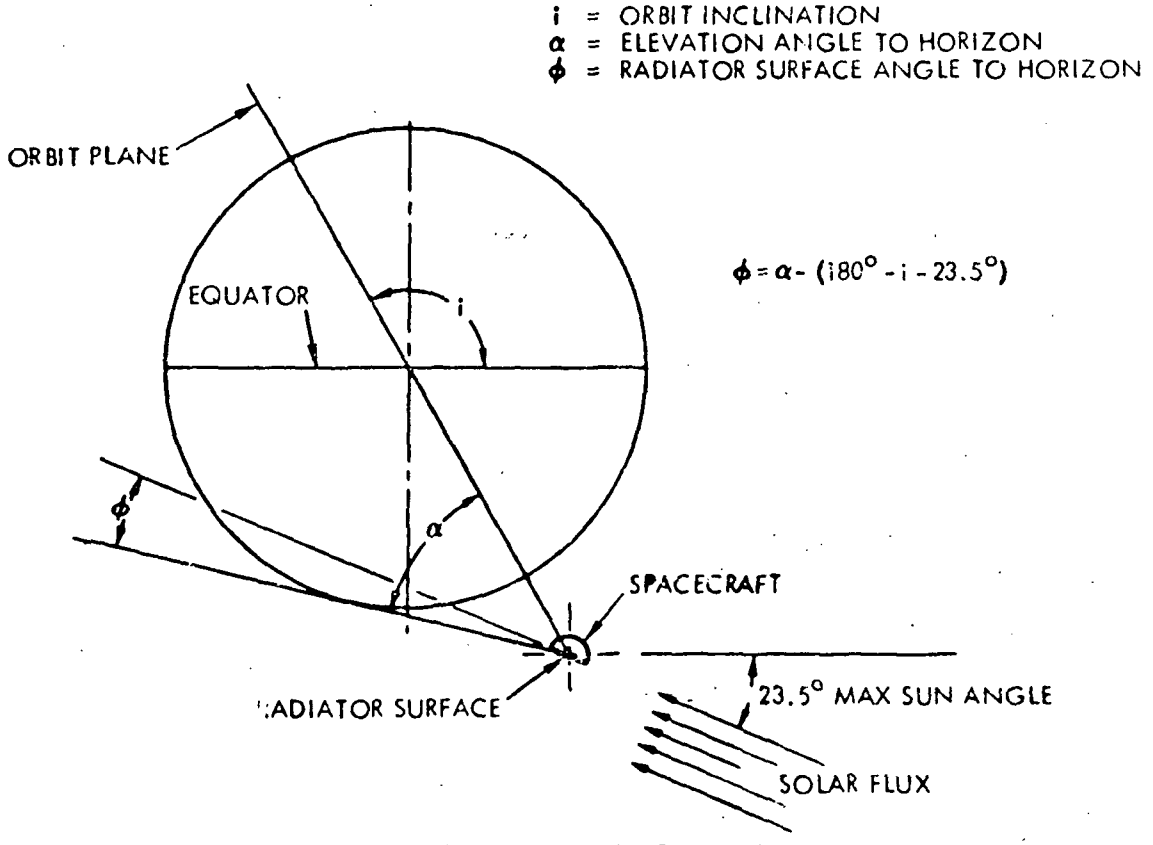

Figure 2-43 Orbital Configuration on Shielding Requirements

Table 2-1 summarizes the basic radiator design values. Because of the additional heat loads from the sun shield, the actual stage areas were scaled upward from these for the baseline design (Figure 2-42). The 5-degree sun shield requirement (Table 2-1) is defined in Figure 5-46 of the Phase I study final report (Reference 1). The final radiator design is shown in drawing Figure 2-44. The sun shields to the rear of the basic radiator were formed by extending the first- and second-stage radiator surfaces along an incline of 50 degrees to a height of approximately 7 inches. Along the sides, the sun shield was formed by the addition of side panel shields fabricated in a manner similar to a single radiator stage. The side panels also are at an angle of 50 degrees. The tilt angle was based on an analysis of the shield view factor to space and equilibrium temperature as a function of shield angle. The 50-degree angle was selected to reduce the shield temperature below 120°K to minimize parasitics to the cold radiator stage.

Table 2-1. Radiator Design Values

Parameter		Design Value
ε_{ins}	Insulation effective emittance	0.01
η	Radiator fin efficiency	0.9
ε_r	Radiator (and shield) emissivity	0.9
T_3	Cold stage temperature (design goal)	35°K
S_3	Cold stage heat load (design goal)	10 mw
α	Second-stage heat load ratio	10
T_B	Radiator boundary (sub-structure) temperature	300°K
	Sun shield angle (400-n.mi. sun-synchronous orbit)	5°
A_1	First-stage area	10.0 ft^2
A_2	Second-stage area	7.5 ft^2
A_3	Third-stage area	3.5 ft^2

The heat pipes from the individual stages are clustered together along the side of the radiator. The heat pipe going to the third stage is surrounded by insulation, around which there is a cylindrical guard which is thermally shorted to the second-stage heat pipe. In like manner, the insulation around the second-stage heat pipe is guarded by a clindrical shield which connects to the first-stage heat pipe. The heat pipes are staged in this manner to reduce the parasitic heat loads to the heat pipes from the 300°K environment.

The heat pipes going to the individual stages were sized based on the design heat loads, the parasitics through insulation and supports, and transient cooldown loads. The heat pipes are 1/4-inch inside diameter and are bonded to the individual radiator skins. The working fluids for the heat pipes are neon (third stage), oxygen (second stage), and ethane (first stage).

The radiator skin thicknesses were selected based on the results of the parametric radiator fin study, and are designed for an overall fin efficiency of 0.9. The skin thicknesses for the first, second, and third stages are 0.02, 0.003, and 0.001 inch respectively. Note that at these temperatures the required thicknesses for 90-percent efficiency are substantially less than for conventional ambient temperature radiators. The 1-mil skin on the third stage also is neccessary to reduce the transient cooldown time during testing. For example, with a 40-mil skin, the time required to cool from 300°K to 35°K with a 24.5°K equilibrium temperature is over 10 hours.

Analysis Results

The configuration shown in Figure 2-44 was analyzed in detail using the Rockwell thermal analyzer computer program (Reference 4) with detailed inputs for the thermal radiation network generated with the Martin Marietta thermal radiation analysis (TRASYS) program (Reference 5). The thermal network used for the computer model is shown in Figure 2-45. Insulation effective emittance values (ε_{ins}) of 0.015 and 0.010 were used in the analysis. Table 2-2 presents the results from the detailed analysis for both cases. The results are for a third-stage load of 10 mw and a second-stage load of 100 mw.

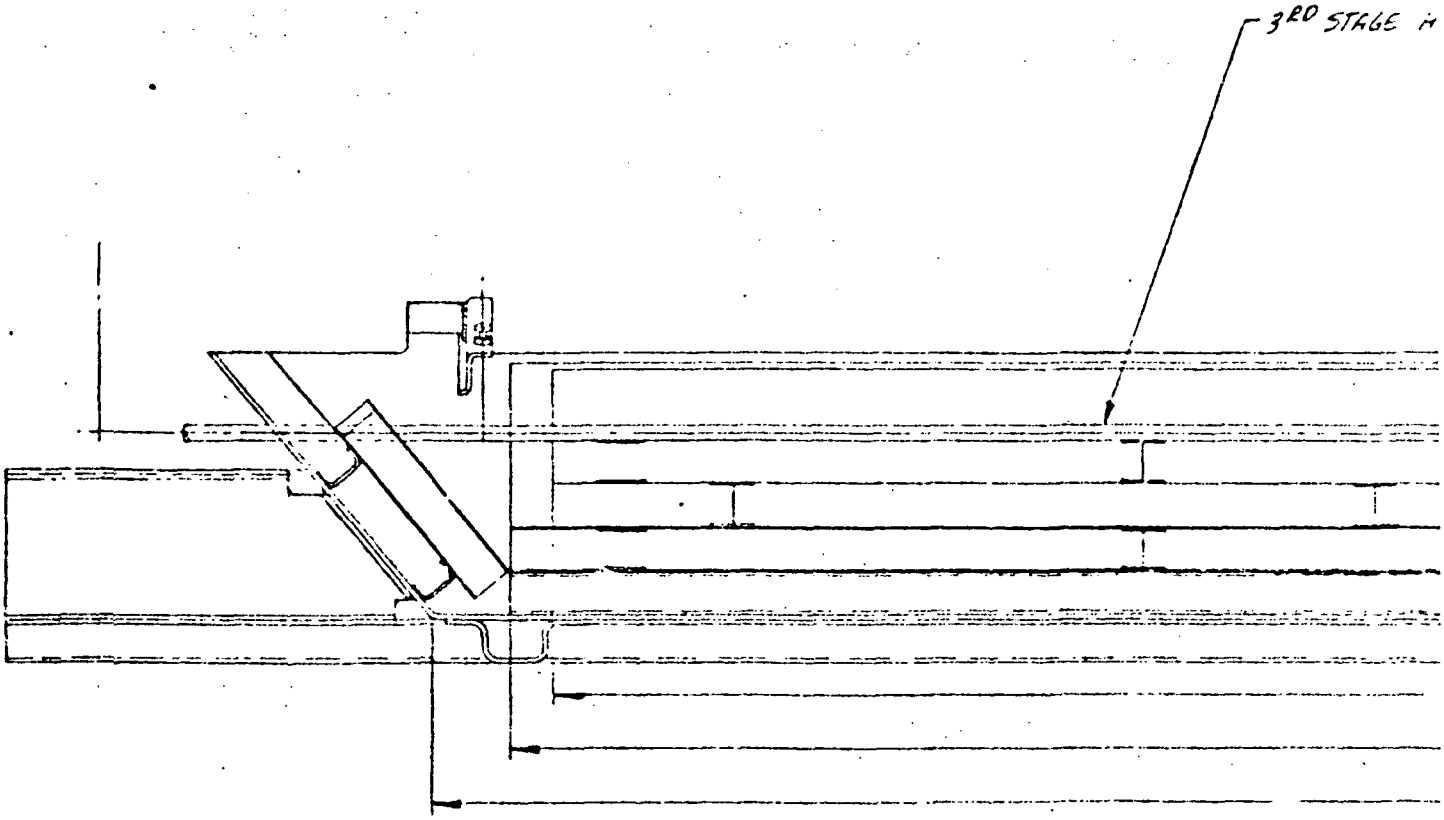

OLDOUT FRAME 1

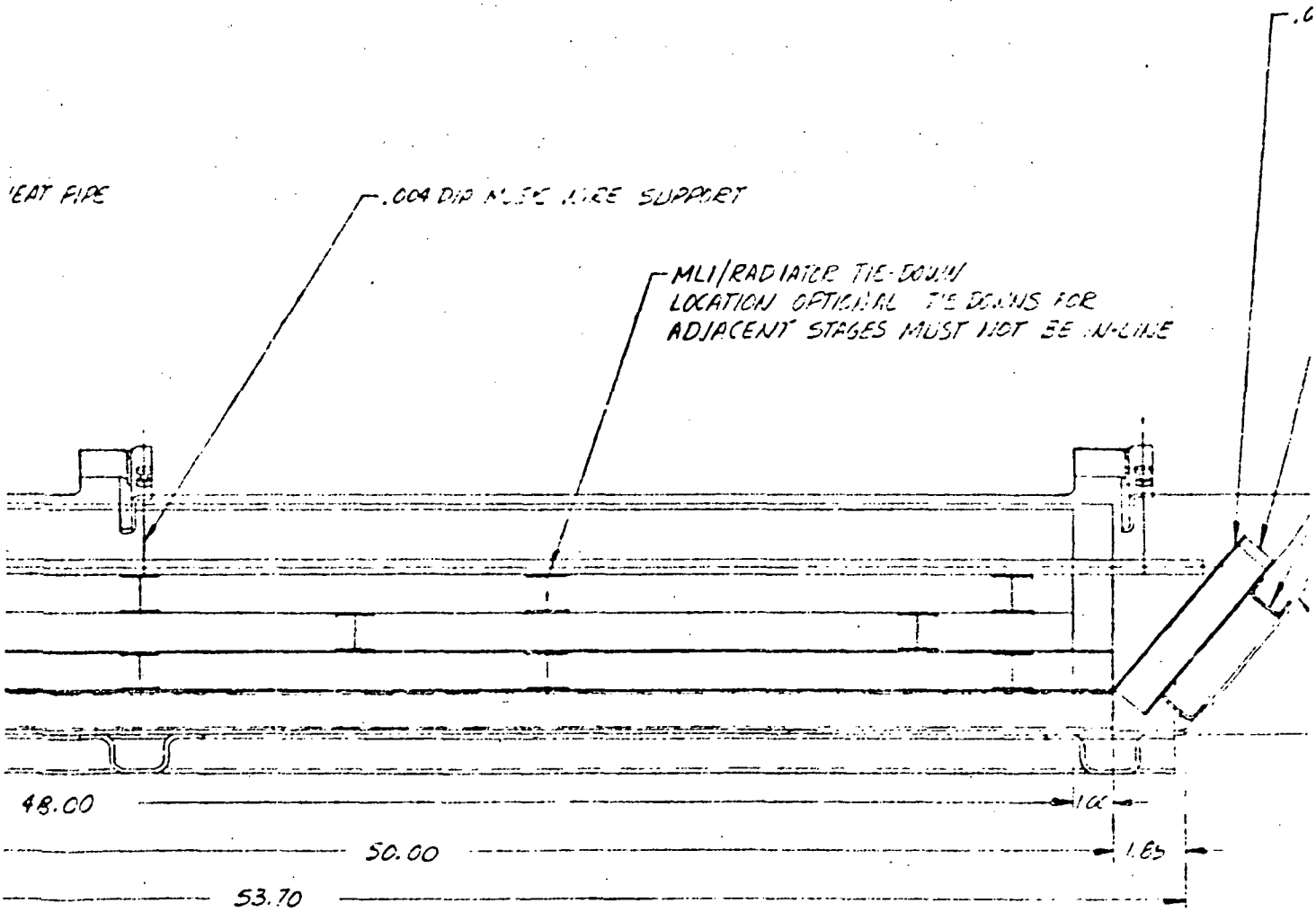

SECTION C-C
SCALE 1/2

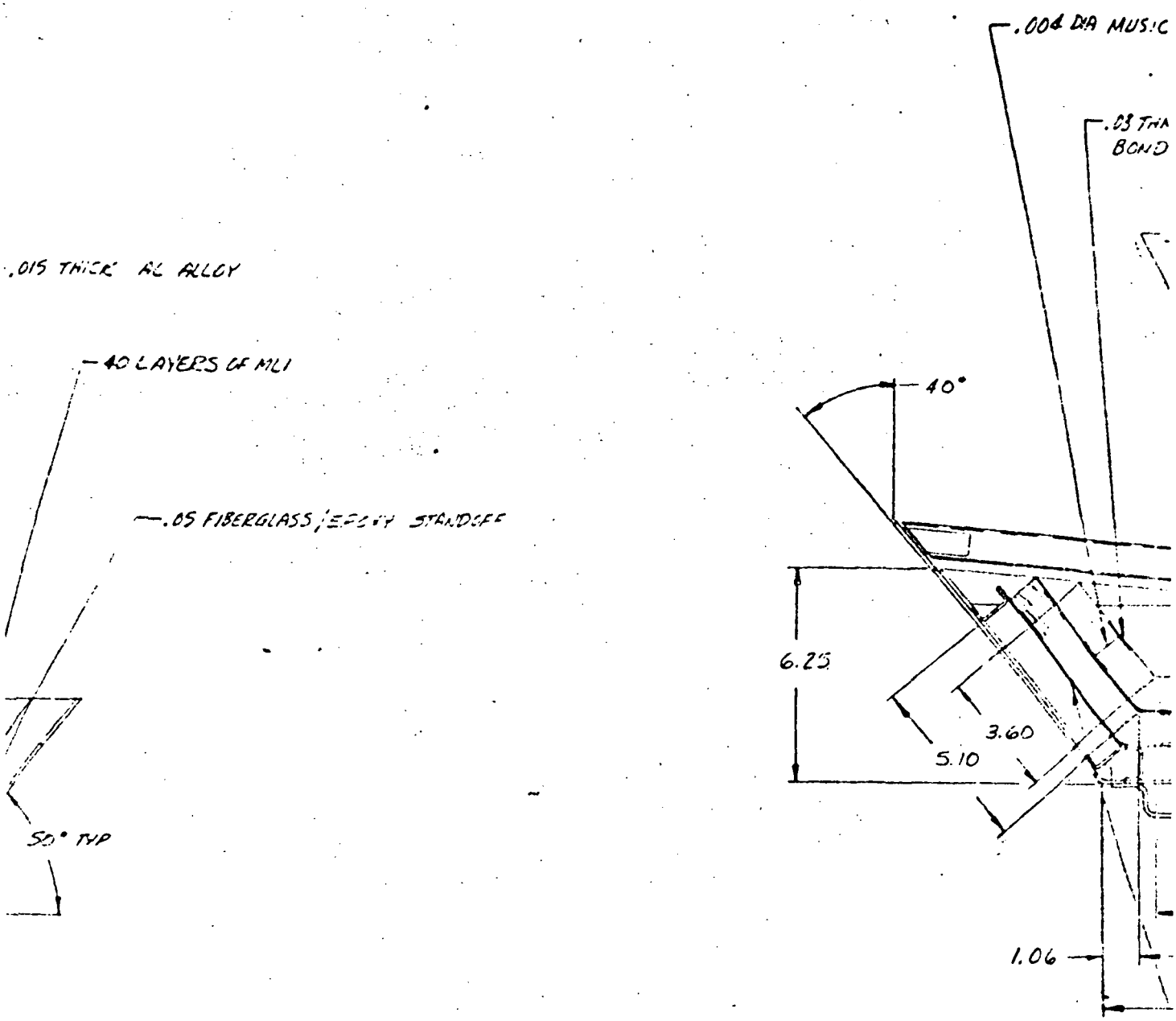

OLDOUT FRAME

: WIRE TIE

CK FIBERGLASS/EPOXY BUTTON
) TO RADIATOR

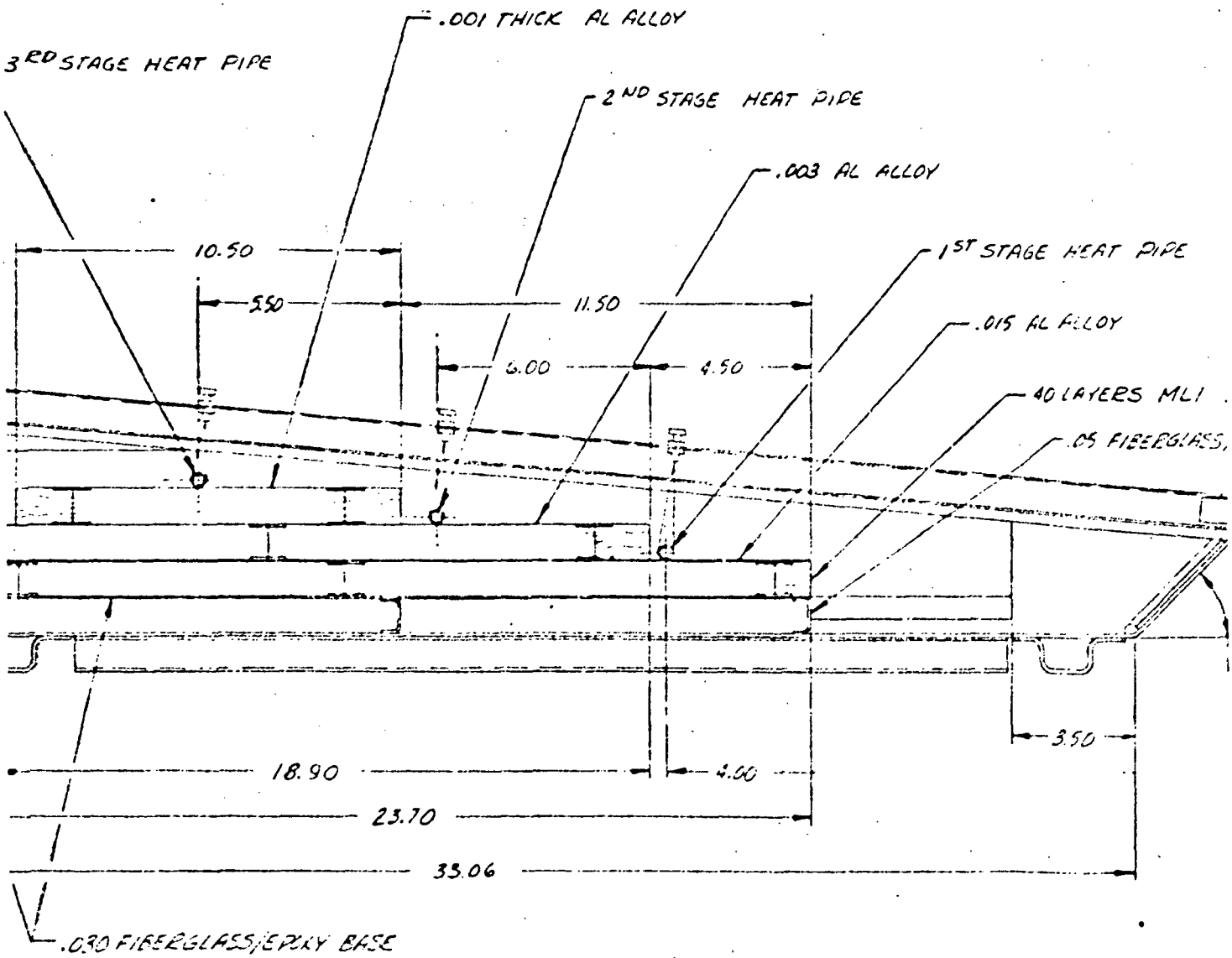

SECTION B-B
SCALE 1/2
ROTATED 90° CCW.

FOLDOUT FRAME 1

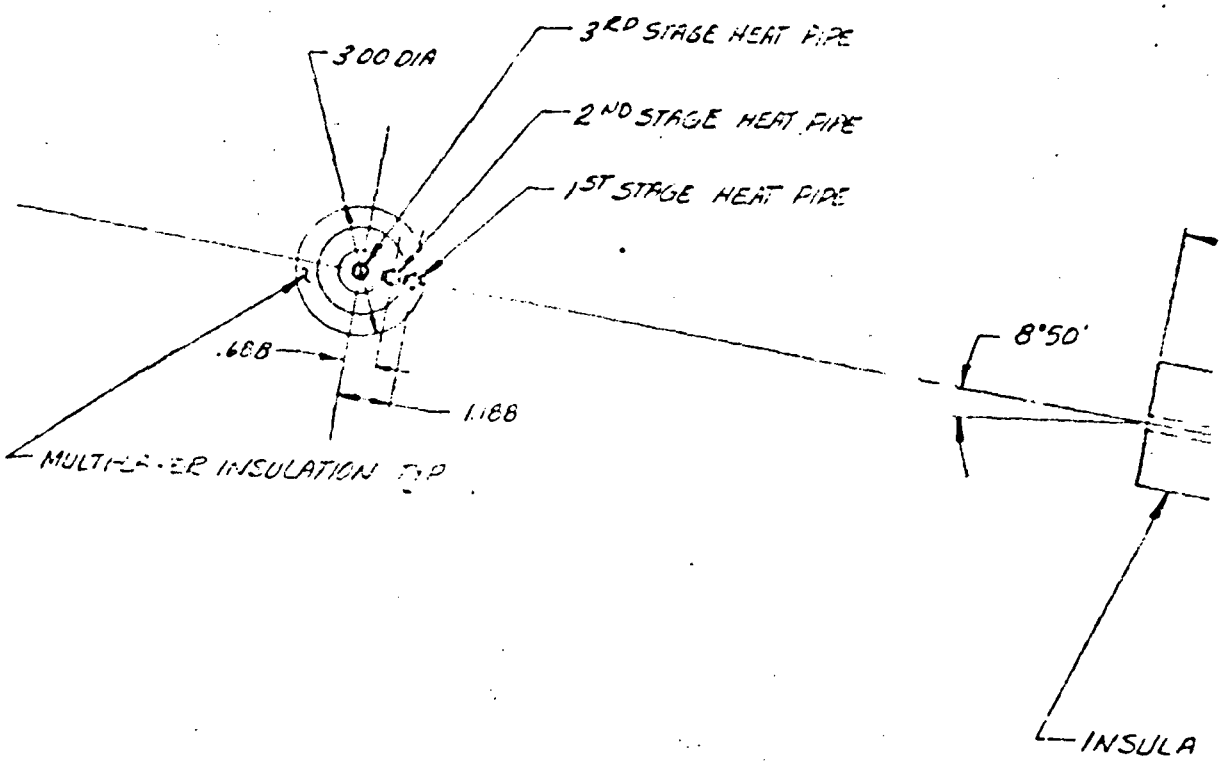

PLACES

45°

OUTLINE FRAME

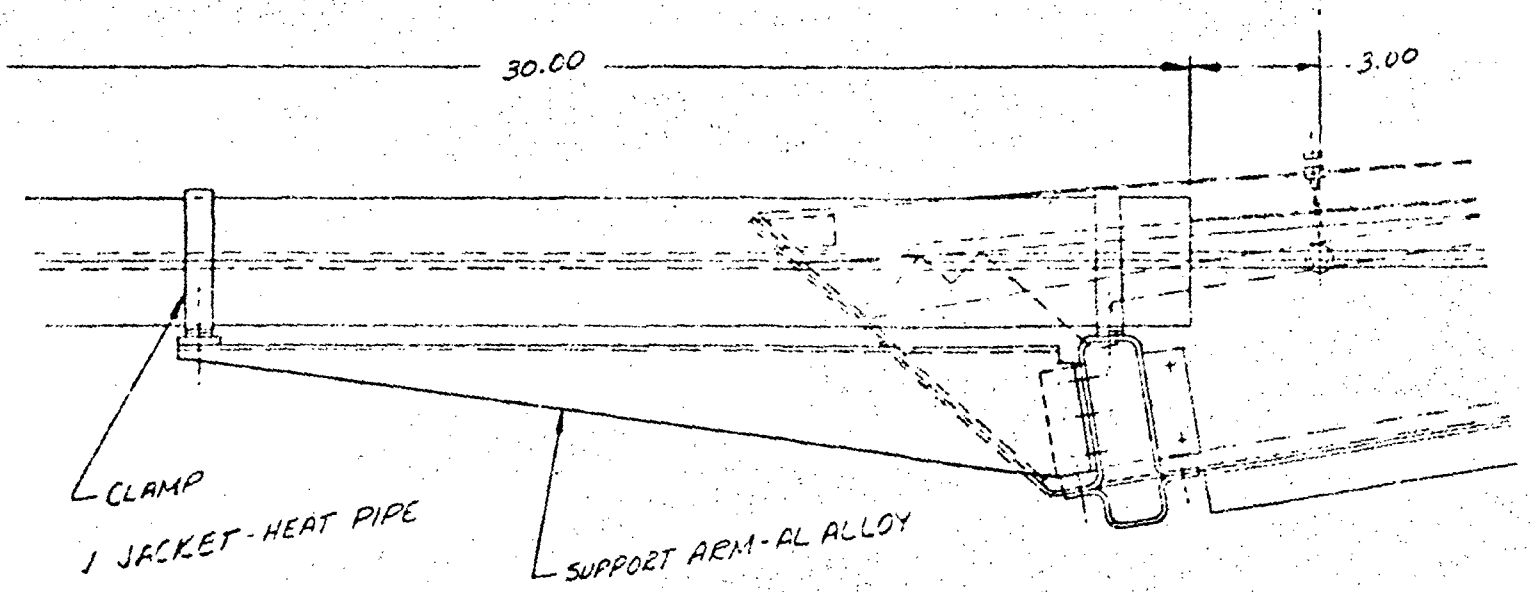

BOOM FRAME

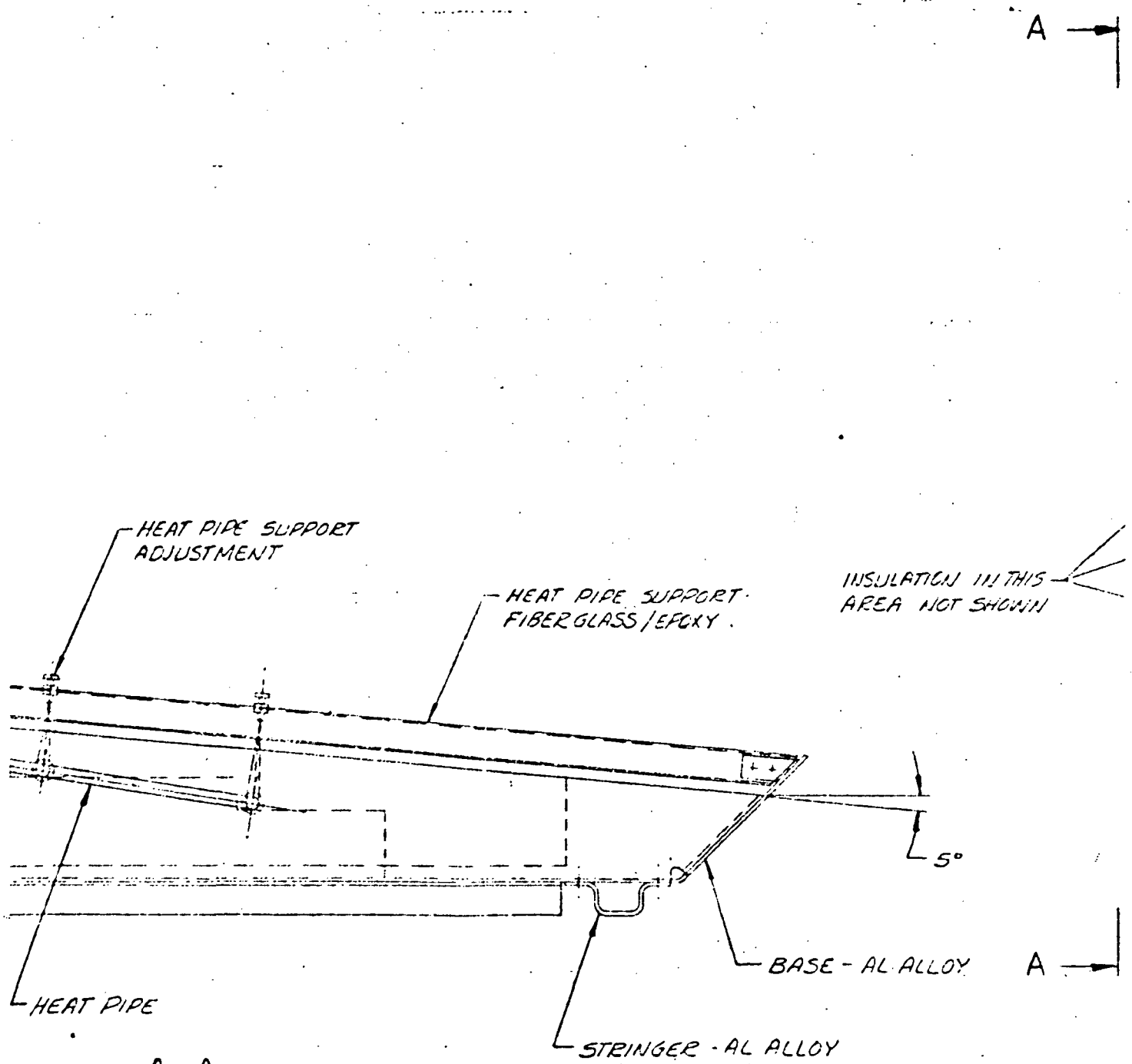

VIEW A-A
SCALE 1/2
'ROTATED 90° CCW

DOUT FRAME 7

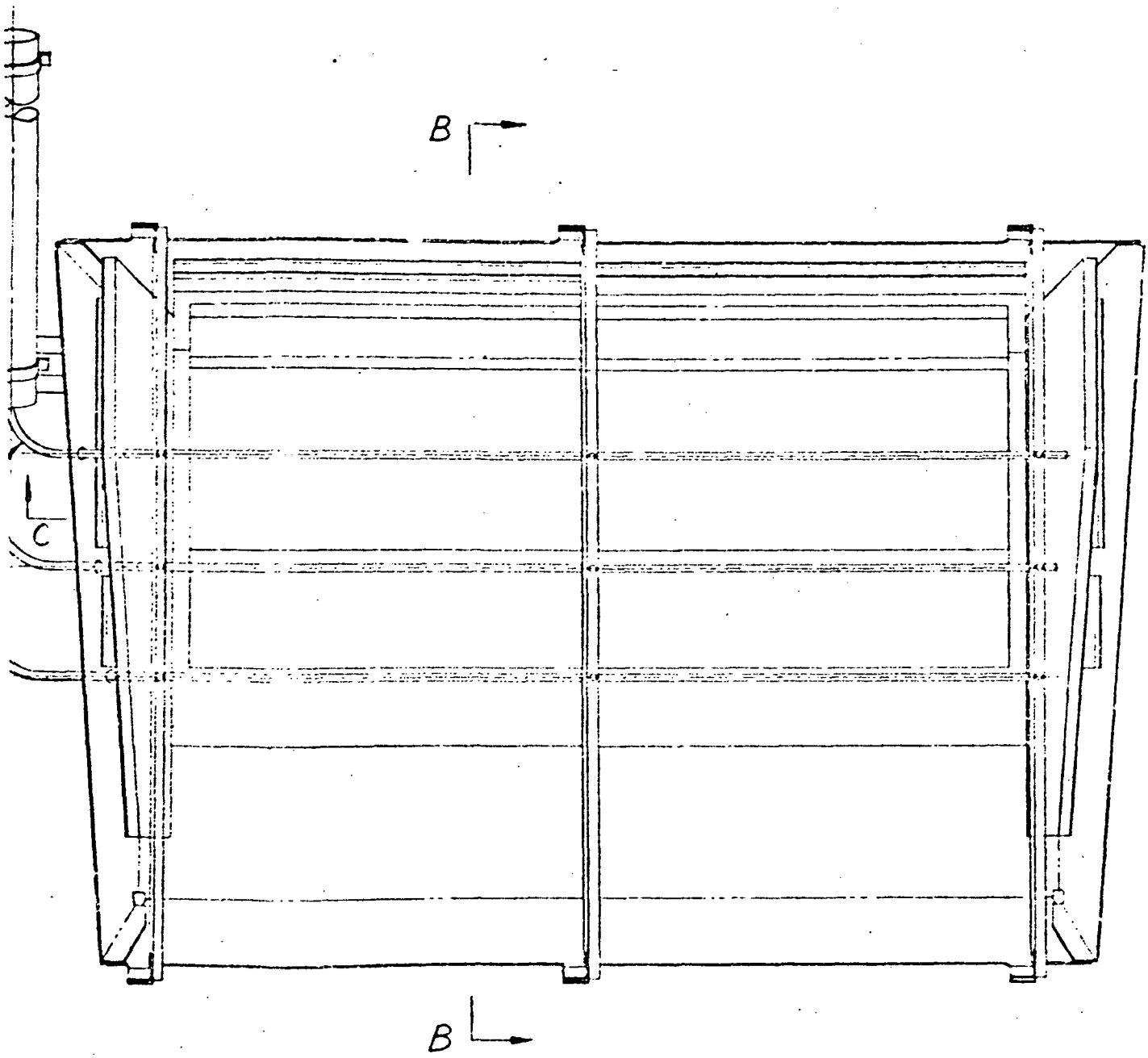

SCALE 1/4

Figure 2-44. Layout - Three-Stage Radiator

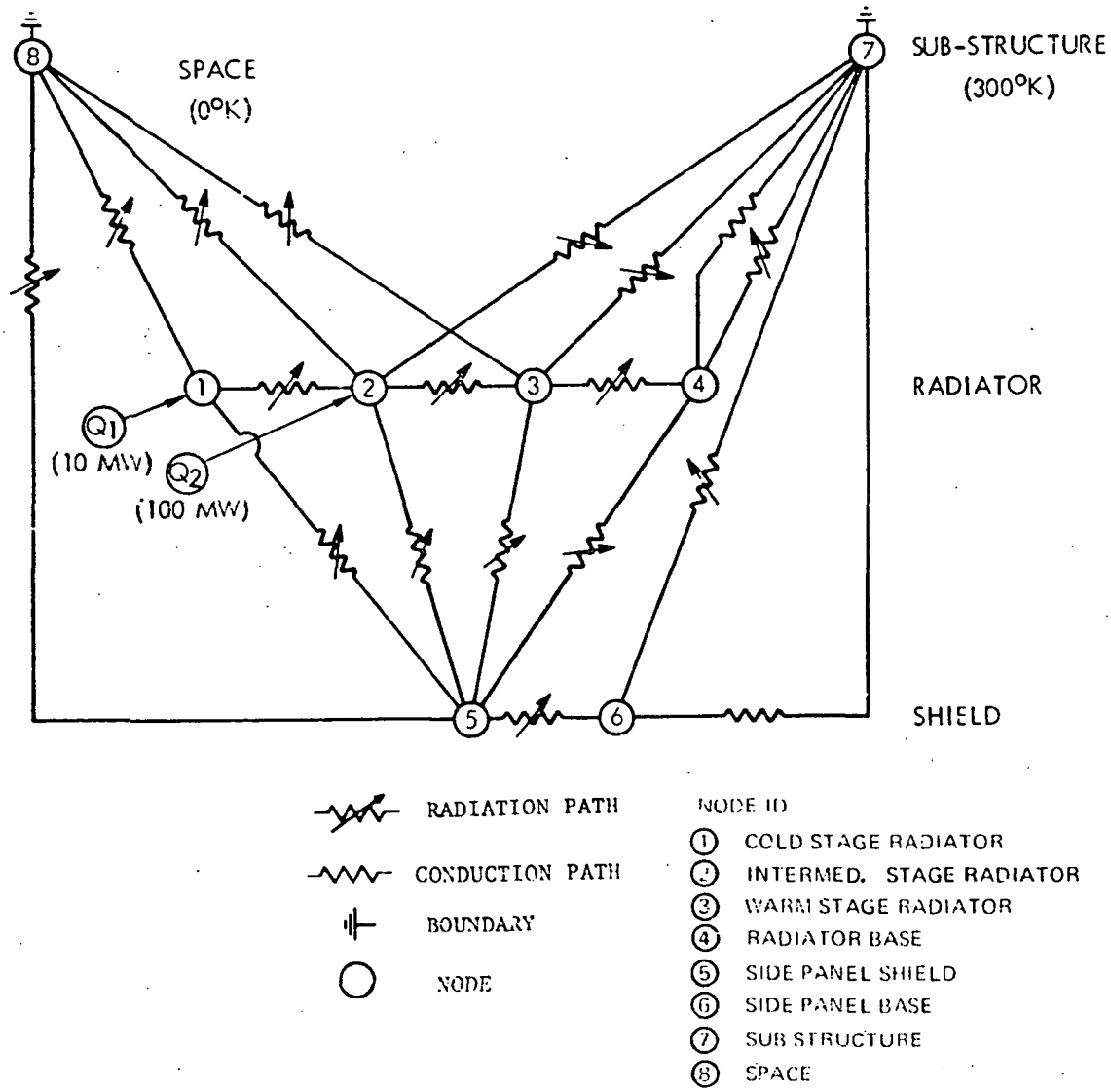

Figure 2-45 Three-Stage Radiator Thermal Network

Table 2-2. Preliminary Design Configuration
Computer Analysis Summary

Location	Temperature (°K)	
	$\varepsilon_{ins} = 0.015$	$\varepsilon_{ins} = 0.010$
Third-stage radiator	39.3	36.3
Second-stage radiator	85.2	78.6
First-stage radiator	180.7	176.5
Radiator base	283.8	287.8
Side panel shields	124.6	119.2
Sub-structure (boundary)	300	300

Test Setup

The 1-g test setup for the radiator assembly is shown in Figure 2-46. The heat pipes are held in a level orientation by long steel strands off an overhead beam to minimize the heat short. The proposed setup would employ a liquid helium shroud to simulate the space sink. The helium shroud would be shielded by a nitrogen shroud to minimize boiloff. The radiator structure is oriented so as to maintain the individual stage heat pipes horizontal to simulate zero-g performance. Heaters are attached to the heat pipes to provide the required heat loads to the second and third stages.

The geometric view of the radiator to the helium shroud will be the same as the view to space for the actual radiator installation. The shroud temperature becomes the "space" sink temperature during testing. Figure 2-47 shows the cold stage temperature as a function of the helium shroud sink temperature. The figure shows that for shroud temperatures below approximately 20°K, there is less than 1°K elevation in cold stage temperature over that of true space. To conserve liquid helium during testing, the shroud will be maintained at 20 ± 5°K. The steady-state heat load into the helium shroud is expected to be less than 10 watts. The liquid nitrogen shroud will be used to precool the radiator prior to introducing liquid helium into the helium shroud.

Hardware Development Items

With the possible exception of the cryogenic heat pipes, the required

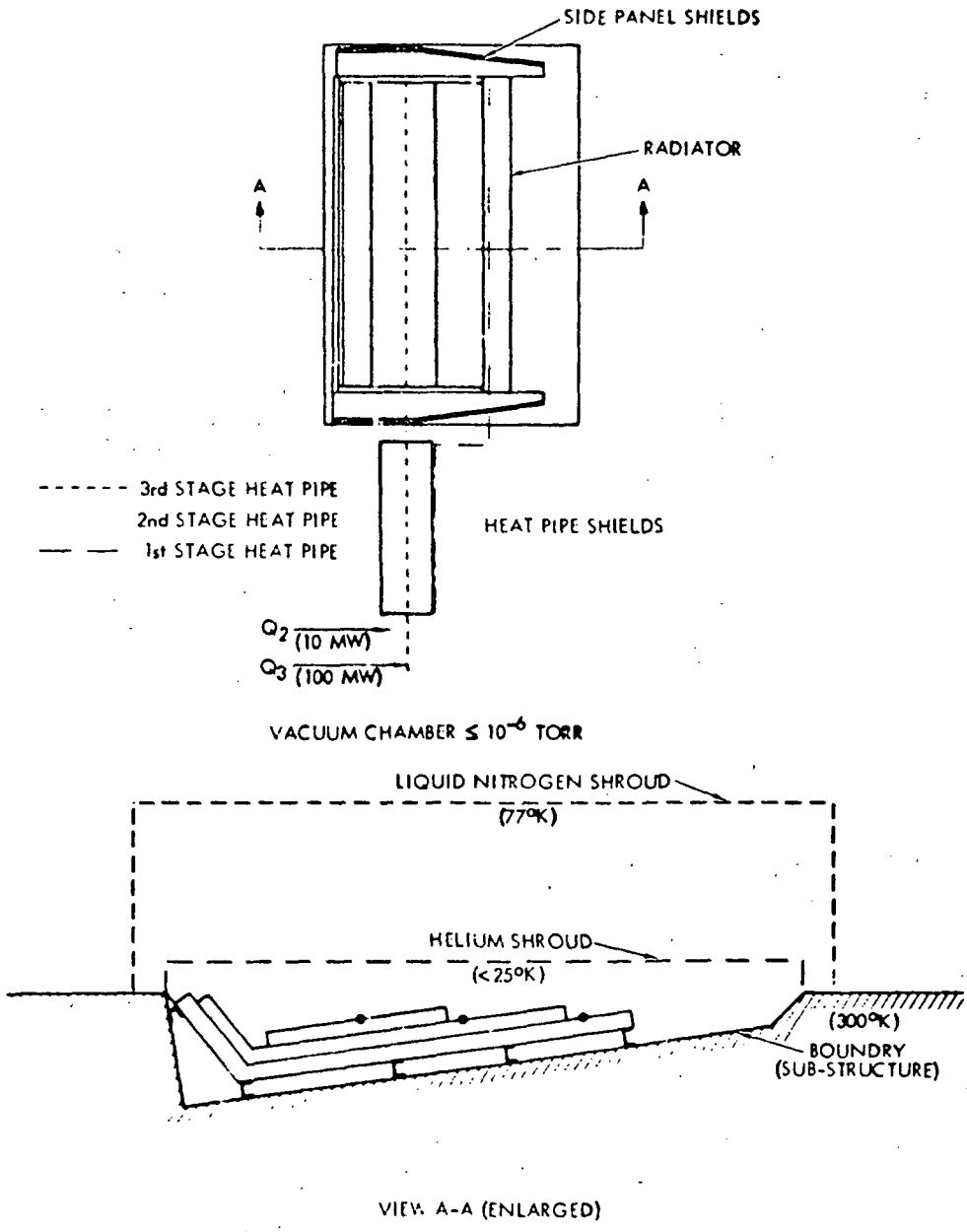

Figure 2-46 Schematic - Three-Stage Radiator Test Set-Up

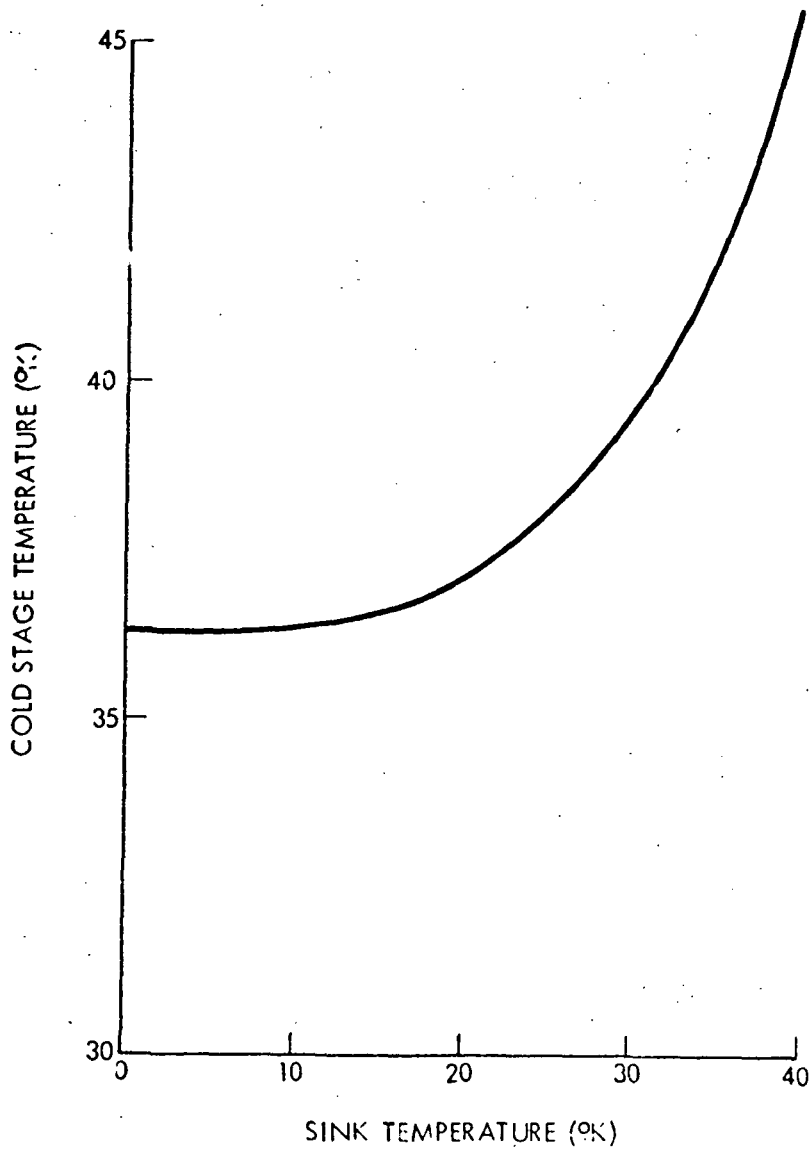

Figure 2-47 Effect of Sink Temperature on Radiator System Performance

hardware for this system is considered to be existing technology. High-performance insulation, low-conductance supports, thermal shields, thermal coatings, etc., have all been flown on various spacecraft. Thermal control coatings are and have been in a continuing state of development for use on very long space missions. This particular concept does not require flexible, diode or variable conductance heat pipes and rigid cryogenic heat pipes may be considered at least partially developed.

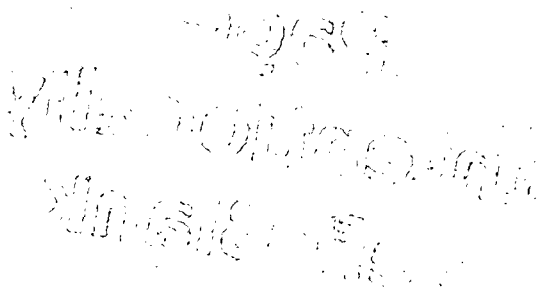

Page
Intentionally
Left Blank

3. DIODE HEAT PIPE RADIATOR DEVELOPMENT

The diode ratiator concept uses diode heat pipes to thermally disconnect a radiator from the sensor during periods when the external environment does not permit heat rejecti n. A concept which uses two radiators, each thermally connected to a sensor focal plane via diode heat pipes, is shown in Figure 3-1. In this case, the sun periodically illuminates each radiator. The diode heat pipe allows heat to be rejected from the large space-facing radiator and at the same time shuts off the radiator which is illuminated by the sun. The heat pipes turn on and off cyclically to provide constant heat rejection from the focal plane. The system is completely passive and has no moving parts.

The unique feature of the diode heat pipe radiator system is that it can provide low-temperature cooling in orbits where radiative cooling was never before considered. For non-sun-synchronous low earth orbits, conventional radiative coolers cannot be used since the orbit will eventually precess to a condition in which the radiator is illuminated by the sun. Cryogenically cooled detectors may be employed on payloads AS-01-A (Large Space Telescope), HE-01-A (Large X-Ray Telescope Facility), HE-11-A (Large High Energy Observatory-D), and SO-02-A (Large Solar Observatory). All of these are in low earth orbits (350-500 km) with inclinations of nominally 28 degrees. Mission durations are two to three years. The diode heat pipe radiator can be used to provide cooling as low as 150 to 175°K. A diode heat pipe radiator also could be used in conjunction with a cryostat to extend the life of the cryogen by reducing the parasitic heat load. The diode heat pipe radiator is used to cool the shroud around the cryogen dewar to reduce the parasitic heat leak from the environment. Using this system, the parasitic heat leak can be reduced by a factor of four or more, thus extending the useful life of the cooler. This approach also could be applied to helium-cooled payloads such as HE-09-A (Large High Energy Observatory-B) which uses a helium-cooled magnetometer and has a two-year life requirement. Another potential application is the Lunar Orbiter Satellite (payload No. LU-01-A) which has an IR scanning radiometer and flies in a 92.6-km lunar orbit. The radiators, each connected to the IR sensor via diode heat pipes, could provide a continuous heat rejection capability.

PAGE INTENTIONALLY BLANK

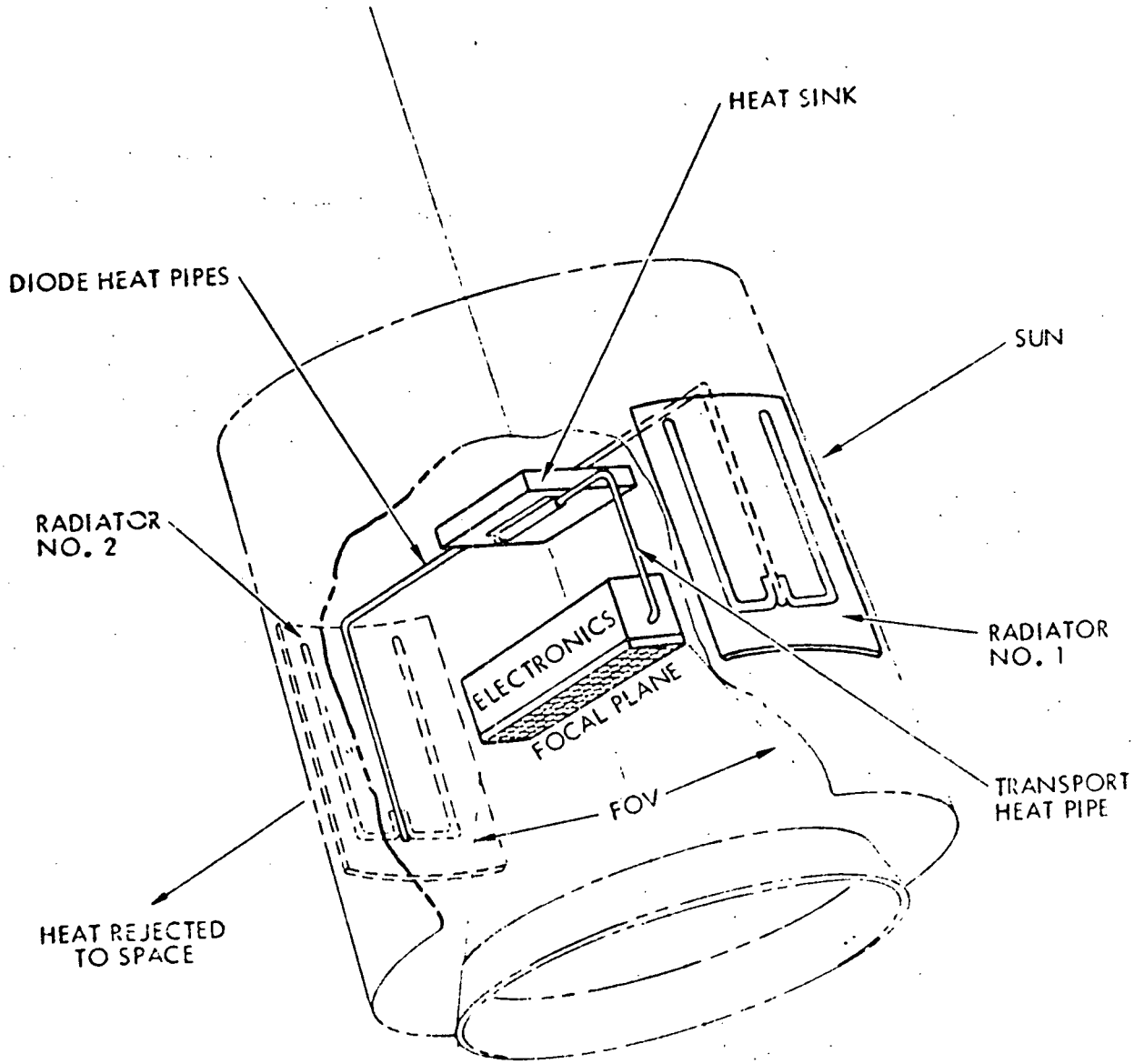

Figure 3-1 Diode Heat Pipe Radiator Concept

The objective of the current study was to design a one-g test system which would incorporate all of the elements of a diode radiator system suitable for future space applications. The selected design was based on the results of the previous study as well as additional transient parametric analyses that were performed during the present study. The following sections discuss the analytical models and parametric analyses and describe the selected design configuration and predicted system performance under simulated orbital heating conditions.

PARAMETRIC ANALYSIS

A transient thermal analysis was performed during the first phase of the study for a three-radiator system in a 100-n.mi. subsolar earth orbit (worst case). The thermal model is shown in Figure 3-2. Parametric cases were run for varous values of detector temperatures and radiator weight per square foot. Results of the study, shown in Figure 3-3, indicate heat rejection at temperature as low as 185°K for a 1.5-hour orbit and as low as 150°K or lower for a 24-hour (geosynchronous) orbit.

For all of the initial analyses, the detector was fixed at a constant temperature and was represented as an infinite capacitance node. However, to simulate the temperature control capabilities of the diode system, it was necessary to modify the thermal model (Figure 3-4) and permit the detector temperature to float with respect to the radiator temperature. This required assigning a capacitance value to the detector node. With the detector node now being driven by the radiator (which varies between 173.5 and 206°K during the eclipse and sun-lit periods of the simulated orbit), the temperature excursion of the detector node is approximately 14°K. Figure 3-5 shows the temperature response of the detector and radiator nodes for a 5.0-square-foot radiator and a 0.33-watt heat load.

Heat Storage Devices

To limit the temperature change of the detector, a heat storage device was proposed as an addition to the thermal model. Two devices were considered: a phase change material (PCM) and an aluminum heat sink. N-Hexane was selected for the PCM device since it has a low melt temperature of 178°K, which is close to the control temperature of 175°K. It also has a large value for the heat of

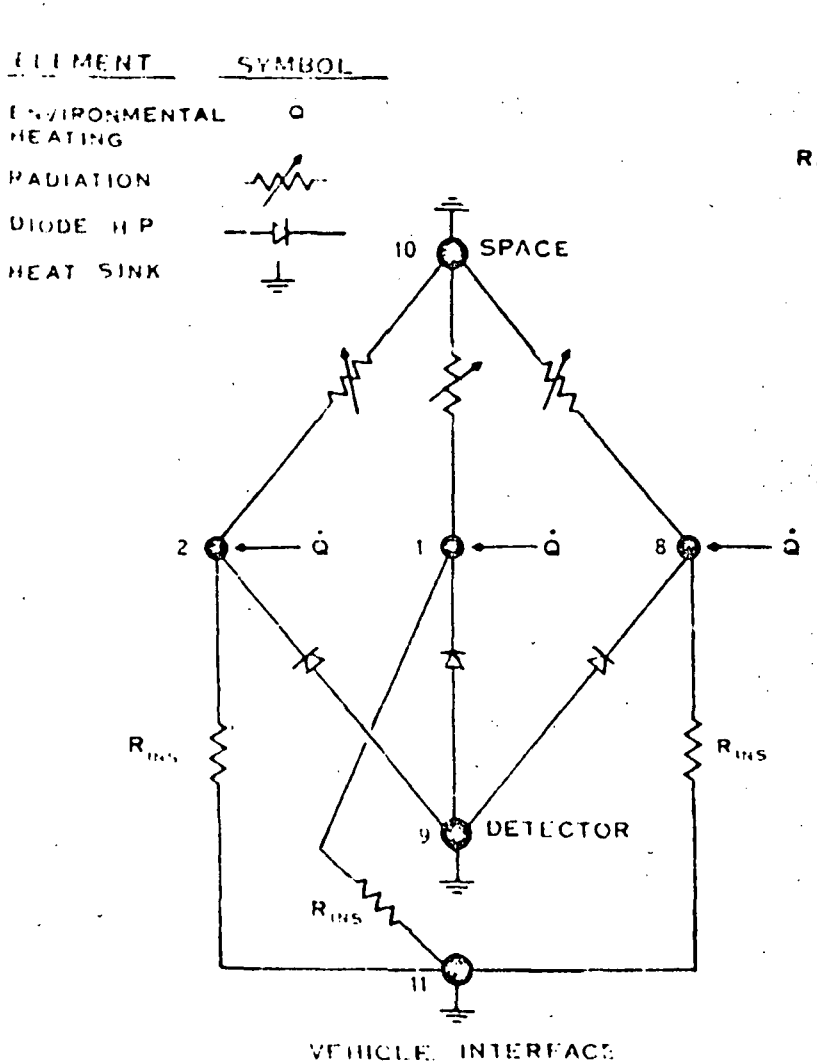

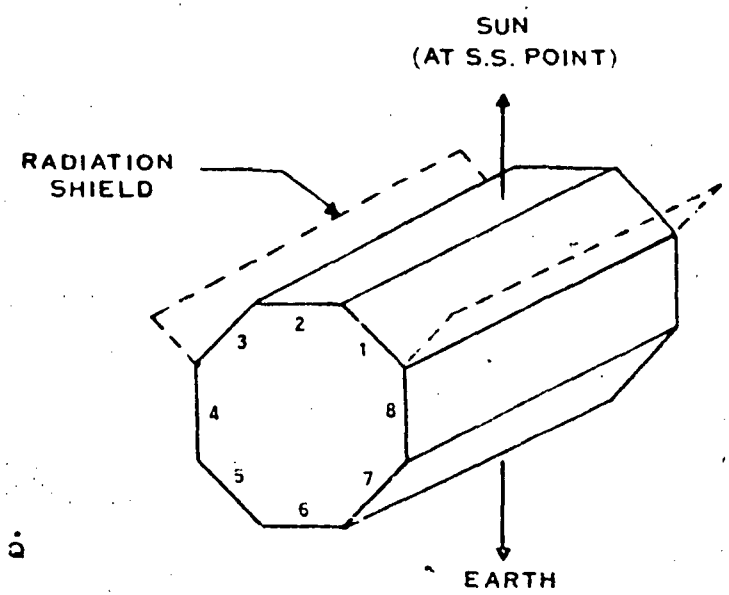

RADIATOR PROPERTIES

α_S		0.15
ϵ_T	-	0.85
η	=	0.90
W A	-	1.0 LB_M/FT^2 (4.89 KG M^2)
C_p	=	0.2 BTU LB_M ^oR (0.84 JOULE G-^oK)

Figure 3-2 Thermal Math Model of Diode Heat Pipe Radiator System

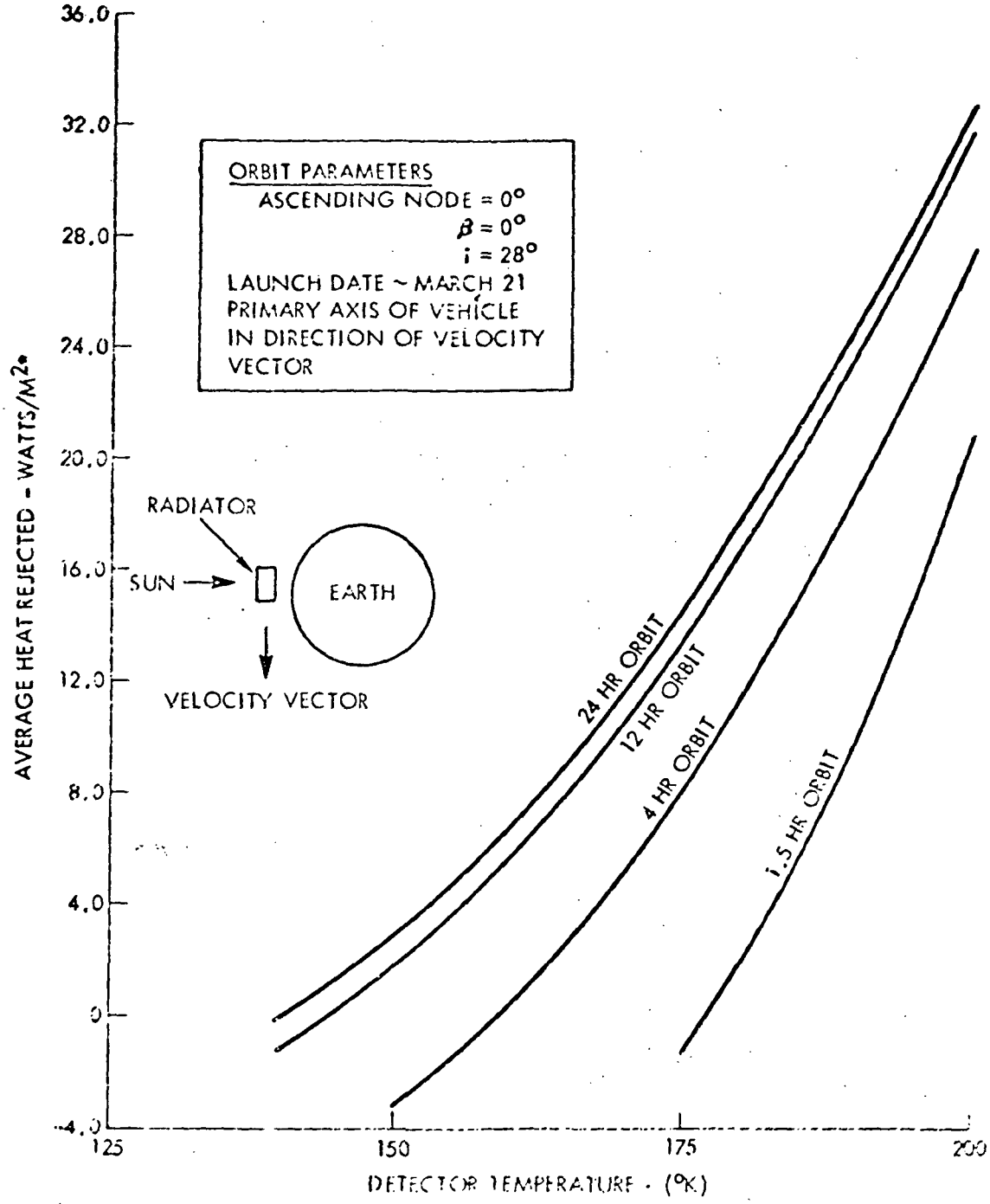

*TOTAL RADIATOR AREA = 0.279 M^2

Figure 3-3 Average Orbital Heat Rejection vs. Detector Temperature - Worst Case Orbit (Subsolar)

Figure 3-4 Diode Heat Pipe Thermal Model for Transient Parametric Analyses

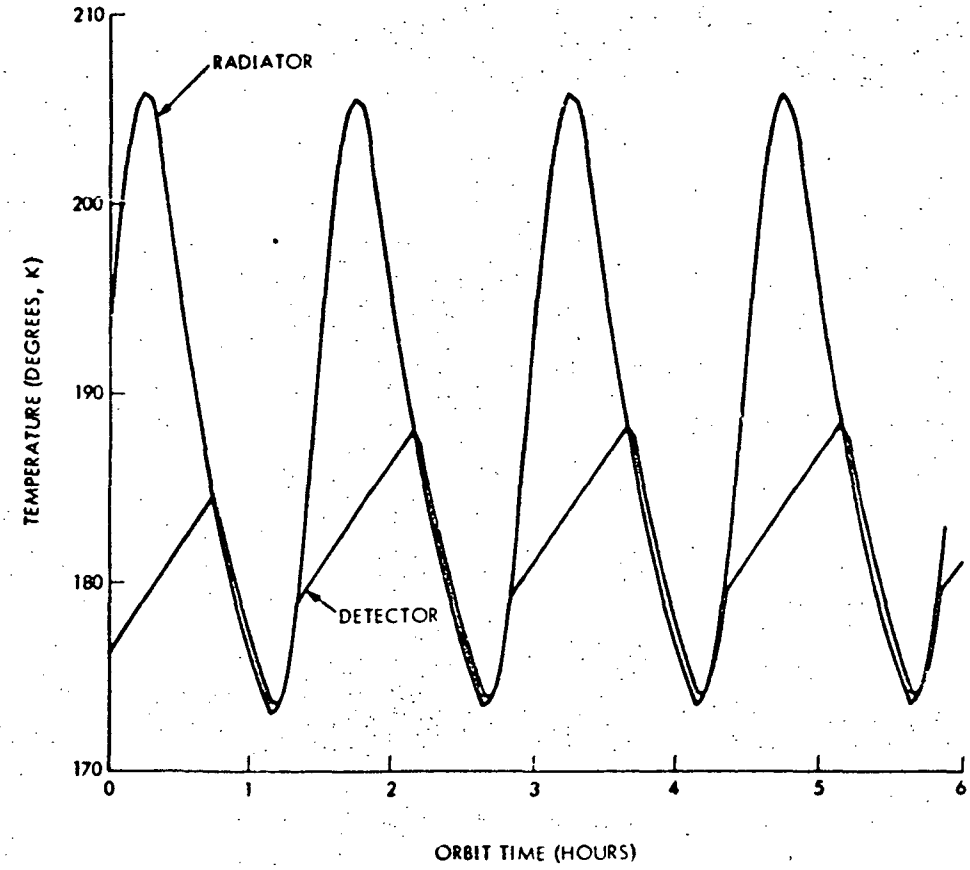

Figure 3-5 Transient Diode System Temperature Response with Floating Detector Temperature ($A = 5.0\ ft^2$, $\dot{q} = 0.33\ w$)

fusion (36 Cal/g) which is a prime requisite for a PCM device.

The PCM container was aluminum with heat conduction fins to increase the heat transfer through the container and thereby reduce the temperature difference between the diode heat pipe evaporator and the detector. The model was run with a 0.5 lbm PCM device and a 0.95-watt heat load. The resulting detector temperature history is shown in Figure 3-6. The total detector temperature excursion was reduced to approximately 3°K by addition of the PCM package. The aluminum heat sink concept consisted of adding a thermal capacitance to simulate an aluminum block in contact with the detector node. A 3-pound mass was selected for the block based on a total system weight goal of 10 pounds for a 5.0-square-foot system. The model was run with the aluminum heat sink; the detector temperature history is shown in Figure 3-7. These

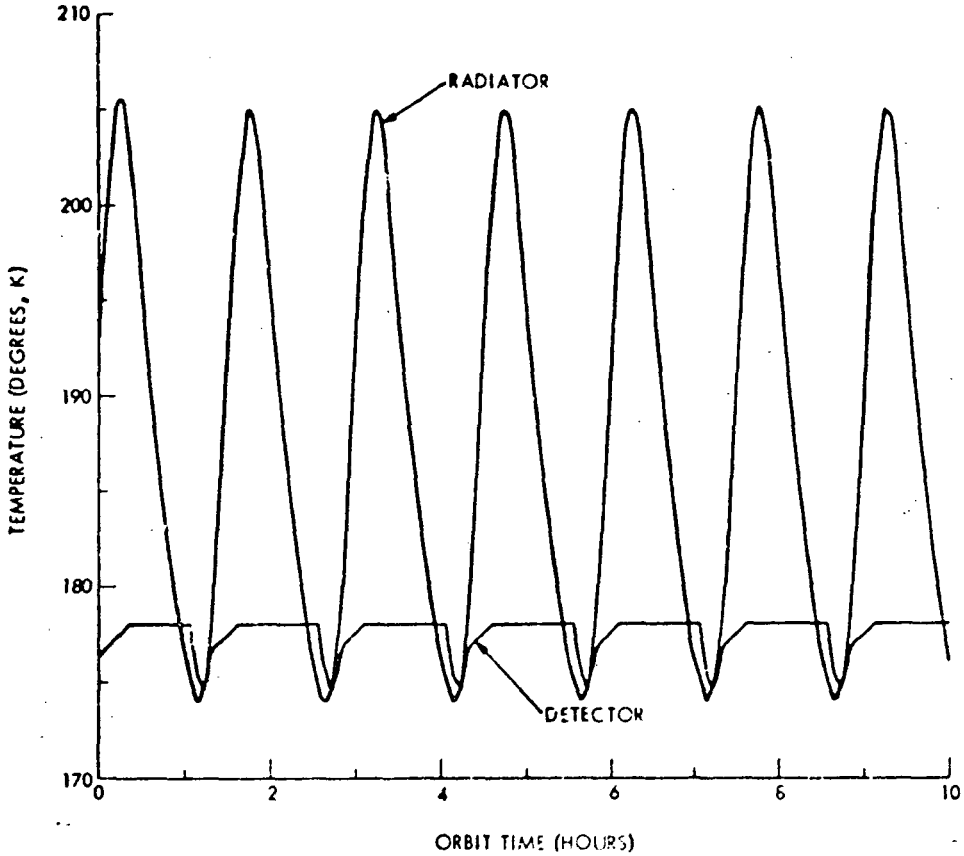

Figure 3-6 Transient Diode System Thermal Response with PCM Heat Sink ($A = 5.0\ ft^2$, $\dot{q} = 0.95$ w)

results show a detector temperature excursion of approximately 6.5°K. Based on the results of the two computer runs with the heat storage devices, the aluminum heat sink was selected over the PCM device because of its simplicity. The PCM has inherent uncertainties due to unknown wetted areas and voids that develop in a zero-g environment which results in a nonrepeatable performance from one melt to another. The extensive development and testing that would be required to employ a PCM package for this system would not justified by the somewhat better control range over the aluminum block.

Variable Conductance Heat Pipe

Temperature data generated in the analysis decribed are based on a worst-case subsolar earth orbit. This orbit constitutes the worst design case upon which the required radiator area is determined for a given maximum heat load requirement. As the orbit precesses, however, the external thermal

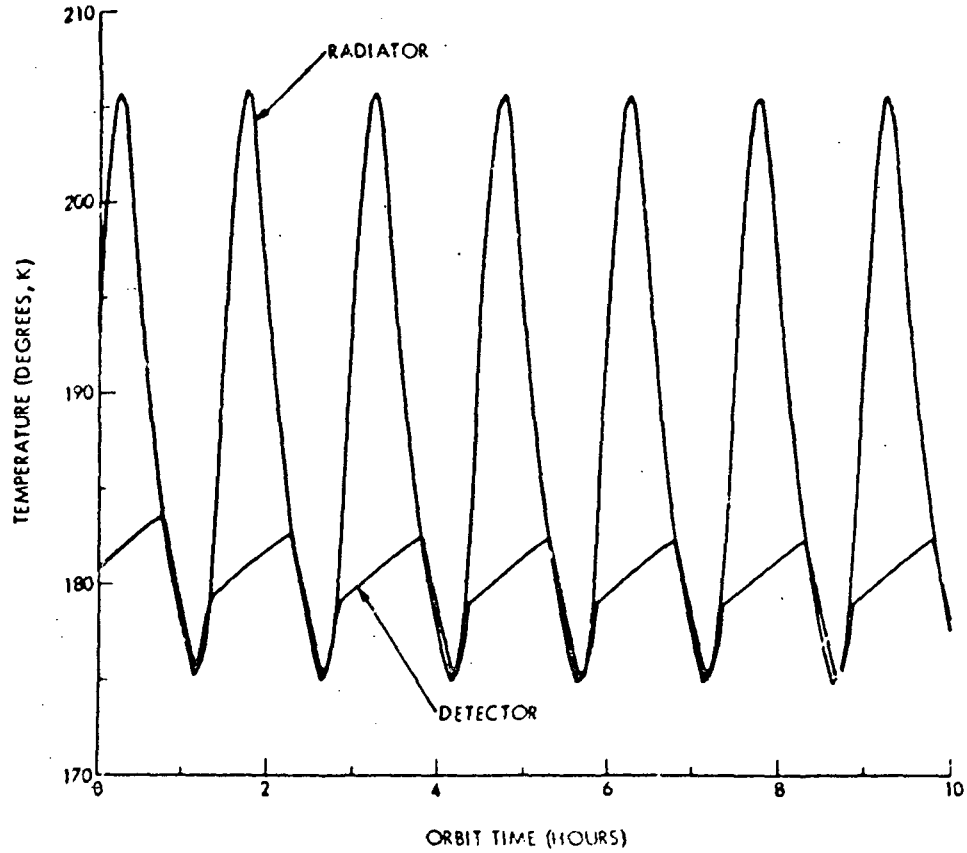

Figure 3-7 Transient Diode System Temperature Response with 3.0 lb Aluminum Heat Sink (A = 5.0 ft^2, $\dot{q}$ = 0.33 w)

environment seen by the radiator will change and hence the average orbital temperature will change. For a terminator orbit, the average orbital temperature for the same radiator would be approximately 100°K rather than 175°K. The average temperature also would change if the heat load generated at the detector were to change.

To accommodate these fluctuations, a variable conductance heat pipe (VCHP) would be required. A variable conductance heat pipe utilizes a noncondensible gas reservoir to provide temperature control. The gas volume responds to small fluctuations in the vapor temperature, thereby modulating the effective condenser area on the radiator. This modulation tends to provide a relatively constant temperature at the evaporator as the heat load and the external thermal environment vary. The detailed operational theory of a VCHP is well documented and will not repeated here.

SELECTED DESIGN CONFIGURATION

A detailed 1-g test configuration for a diode heat pipe radiator system was designed based on the results of the parametric analysis. The system was designed for a simulated detector heat load of 1 watt and a required operating temperature of 175°K. Environmental heat loads to the radiator were computed for a 100-n.mi. subsolar earth orbit as in the previous cases.

The 1-g system design configuration is shown in Figure 3-8. The system consists of a simulated detector which is attached to a 3 lbm aluminum heat sink block, a diode heat pipe, a variable conductance heat pipe and reservoir, and the radiator. The system is supported off a mounting structure which simulates the spacecraft interface (300°K boundary) by low-conductance supports.

The diode heat pipe is a 1/4-inch outside diameter stainless steel pipe with ethane as the working fluid. The small diameter was selected to minimize the reverse conductance and shutdown energy and because the heat transport requirement is only 1 watt. The diode uses a 3/8-inch-diameter liquid trap reservoir shown in Figure 3-8. It has a forward conductance of 4.1 watts/°C and a reverse conductance of 0.002 watt/°C. These values were calculated based on test data for an ethane liquid trap diode heat pipe which was developed and tested under the Space Division's independent research and development program (Reference 6). The shutdown energy of the diode heat pipe is estimated to be 0.36 watt-hour.

The variable conductance heat pipe also uses ethane as the working fluid. The pipe is made from a 6063 aluminum heat pipe extrusion which was developed for the Applications Technology Satellite program (Reference 7) and for the RM-20B sensor program (Reference 3). The VCHP is thermally connected to the diode heat pipe with an aluminum coupling block secured with tension straps. The VCHP reservoir is designed for a reservoir-to-condenser volume ratio of 10:1. Argon is used as the control gas.

The radiator consists of two 10-mil-thick sheets of 6061 aluminum and is supported by lateral and longitudinal fiberglass stiffeners. The 10-mil thickness was sized for fin efficiency of 0.90 based on the results of the parametric fin studies (Section 2). The VCHP is bonded to the radiator as

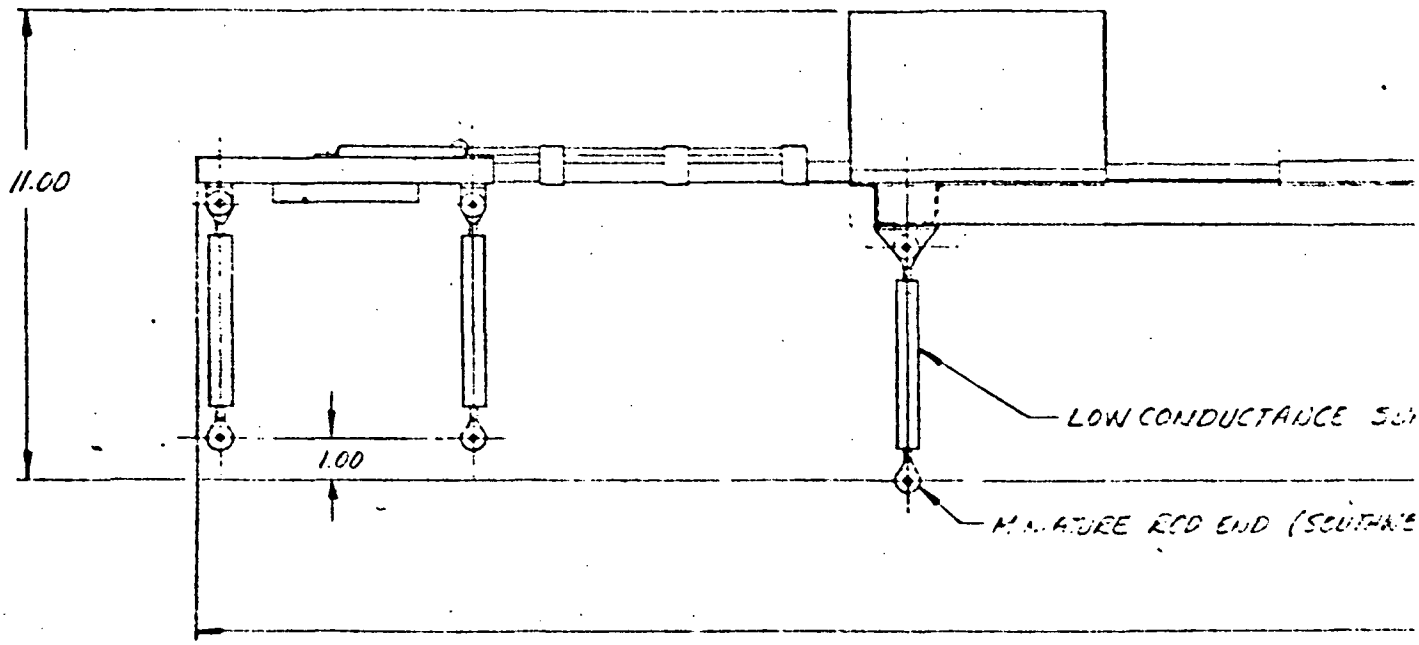

LDOUT FRAME

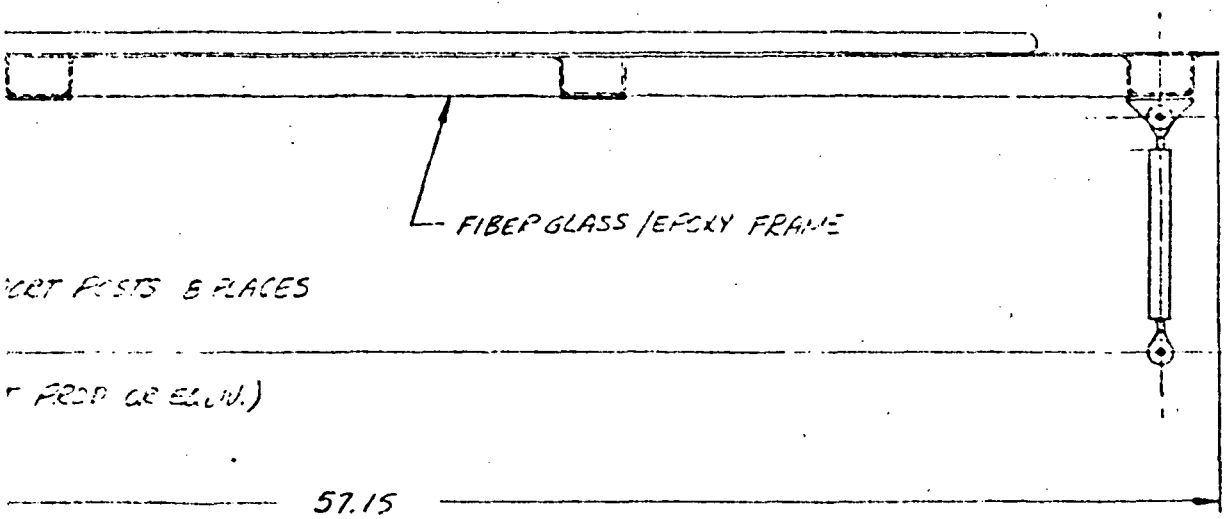

VIEW C-C
SCALE 1/2

WEIGHT FRAME

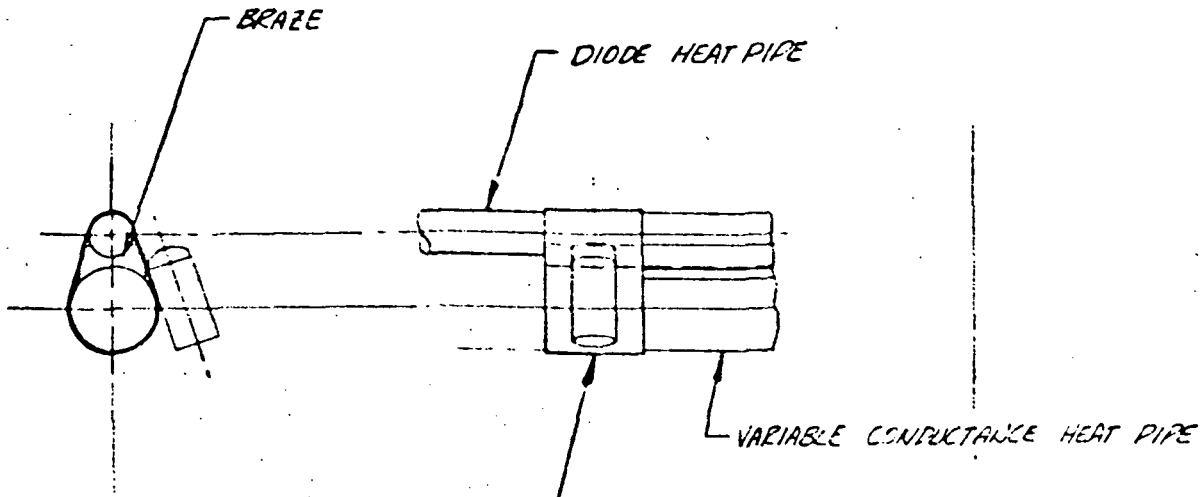

SECTION D-D
SCALE 2/1
ROTATED 30°CCW

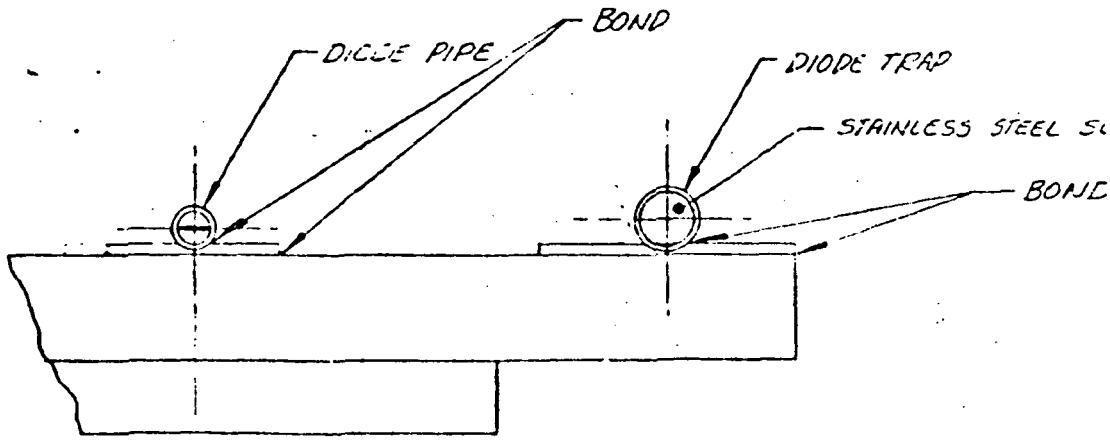

SECTION E-E
SCALE 2/1

OUT FRAME 3

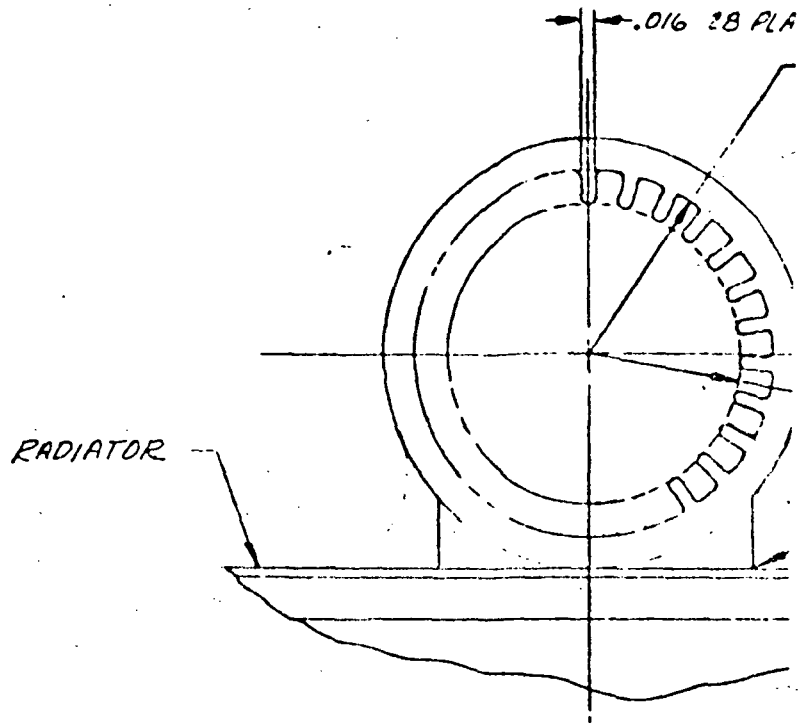

SECTION A-A
SCALE 10/1
ROTATED 90° CCW

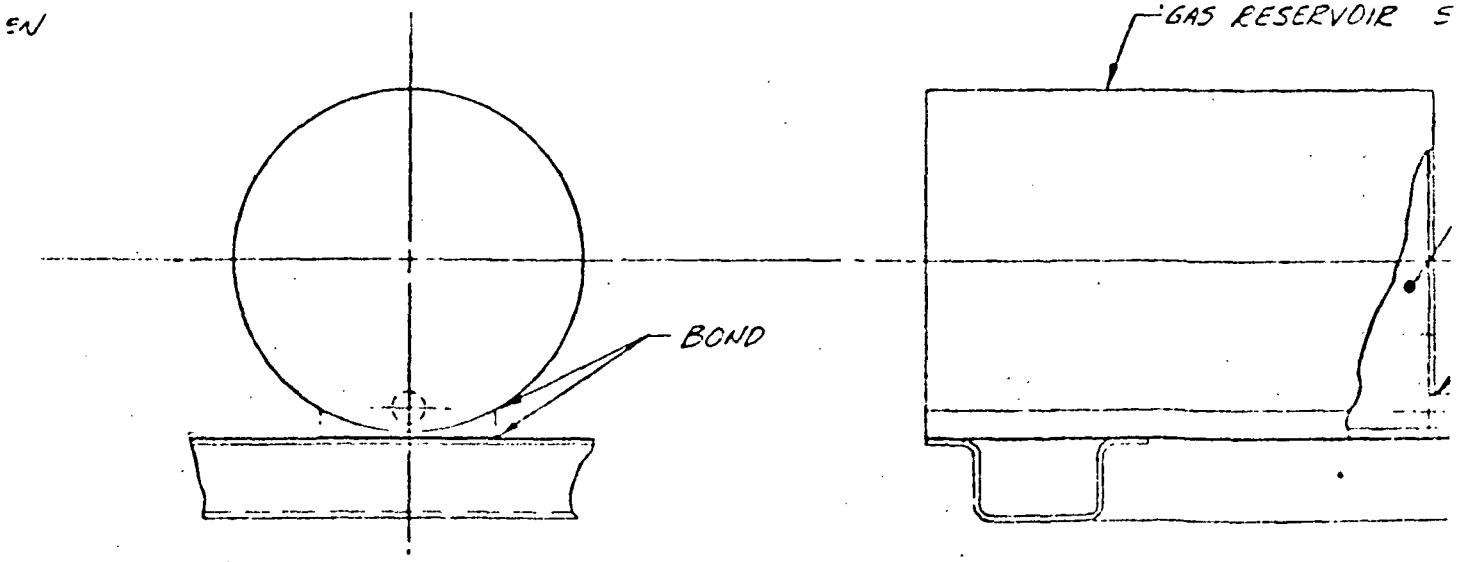

SECTION B-B
SCALE 1/1

'5
215 R

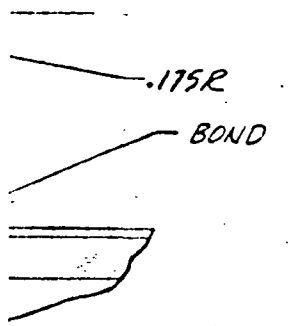

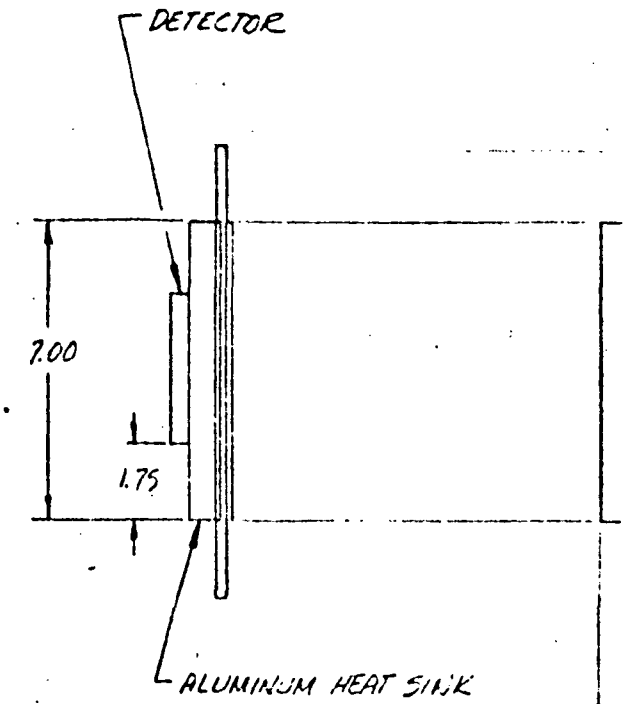

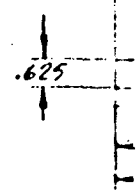

VLESS STEEL

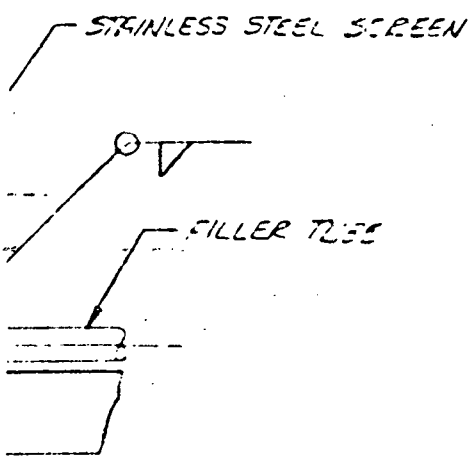

OUT FRAME

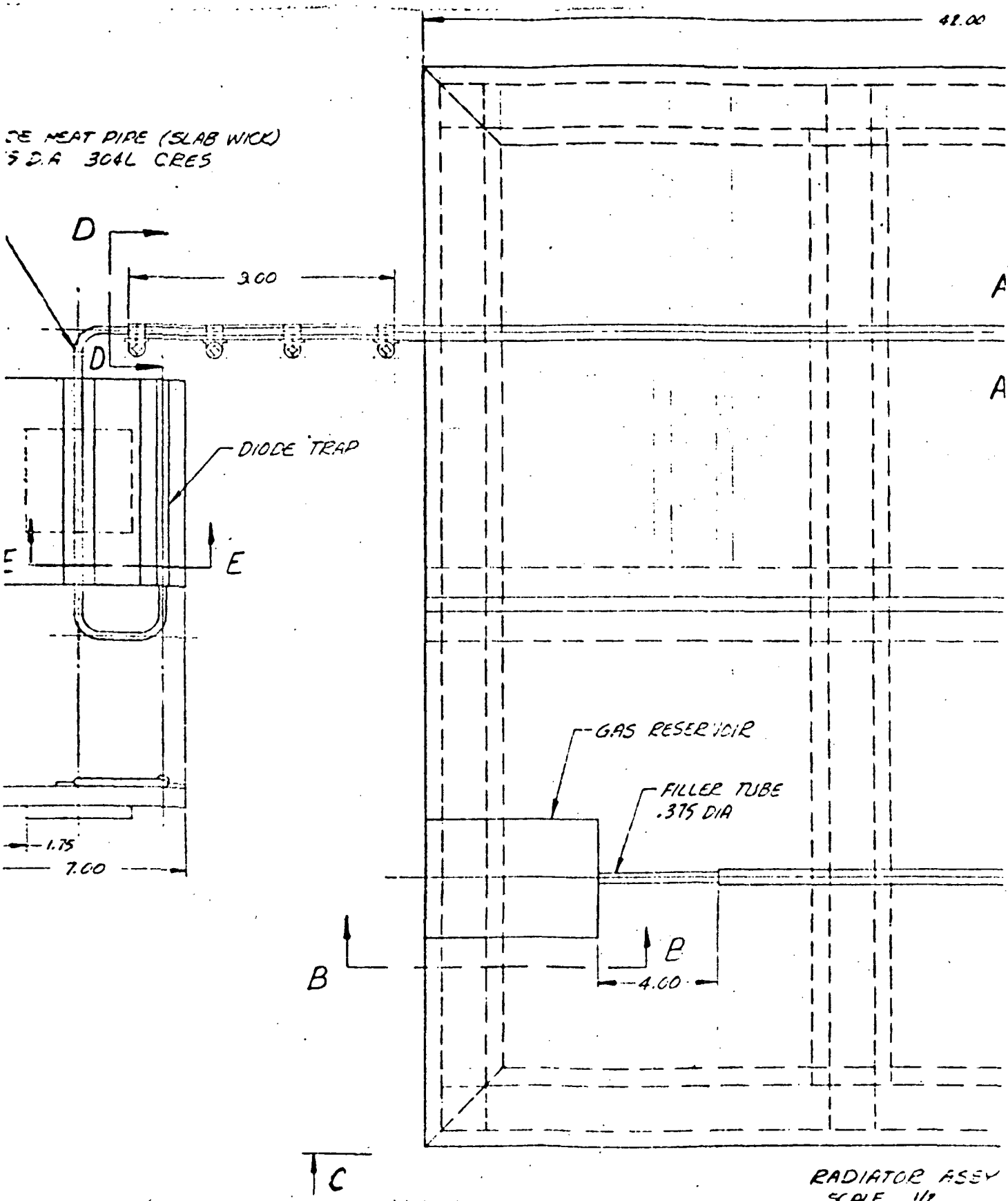

RADIATOR ASSY
SCALE 1/2

UNIT FRAME

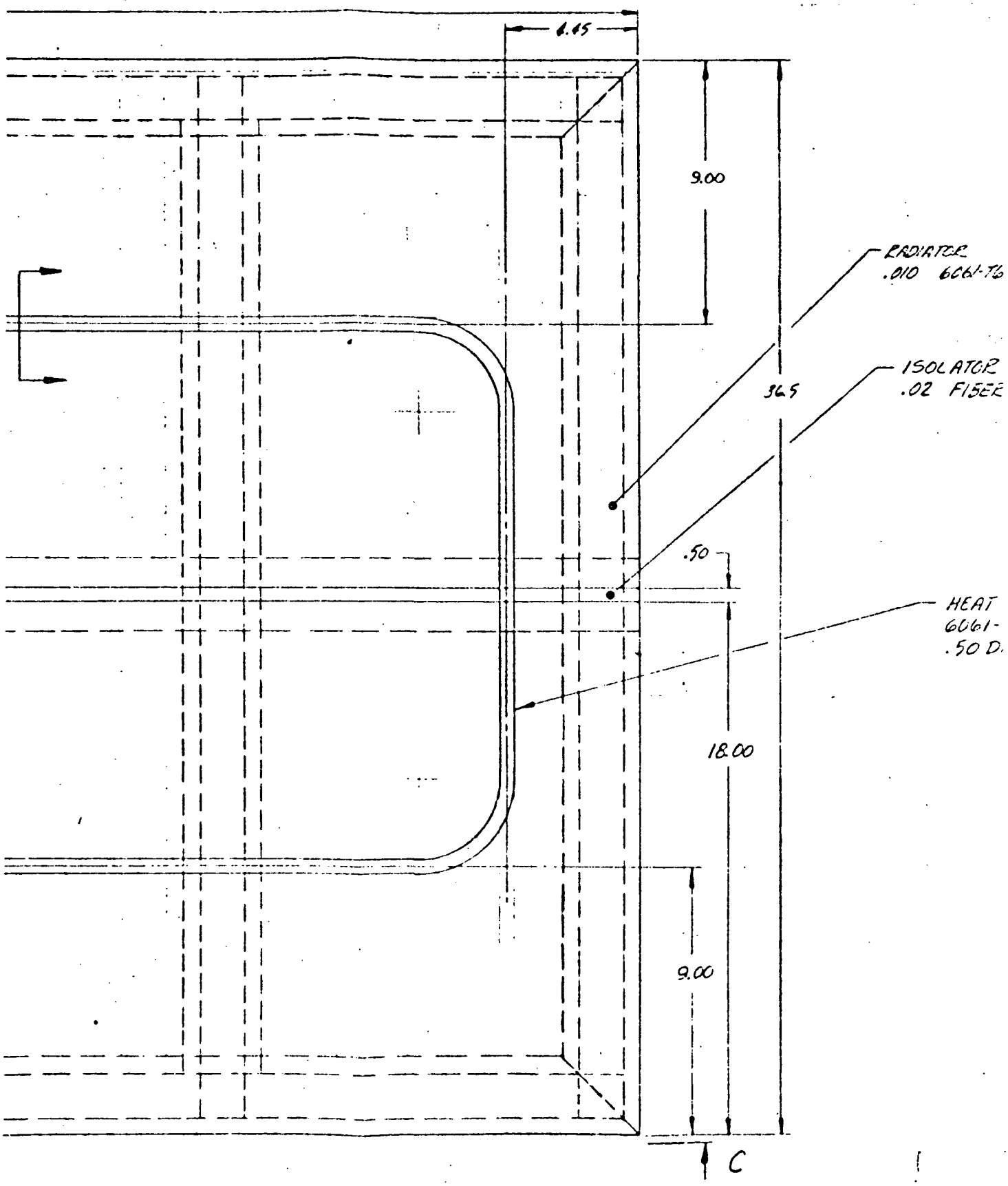
6.15
9.00
36.5
RADIATOR
.010 6061-T6
ISOLATOR
.02 FISER
.50
HEAT
6061-
.50 D.
18.00
9.00
C

'L ALLOY

LASS

?IPE
; AL ALLOY

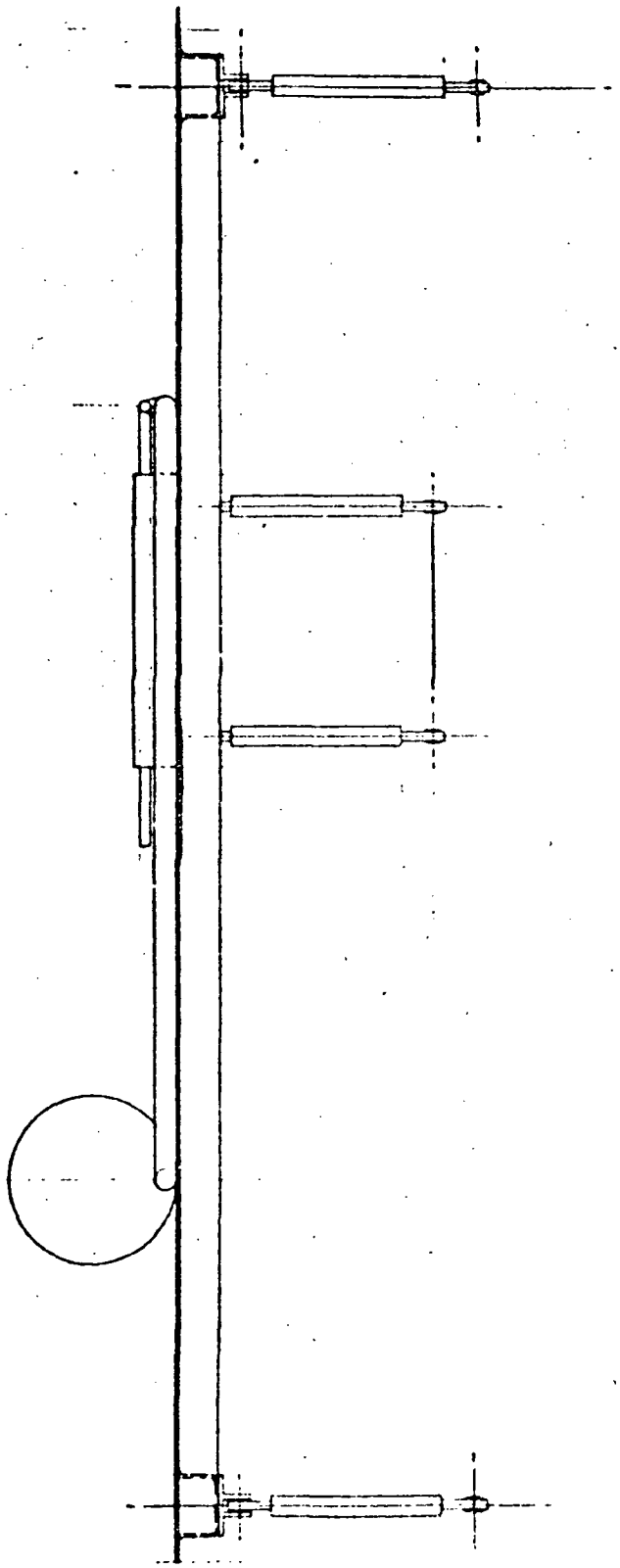

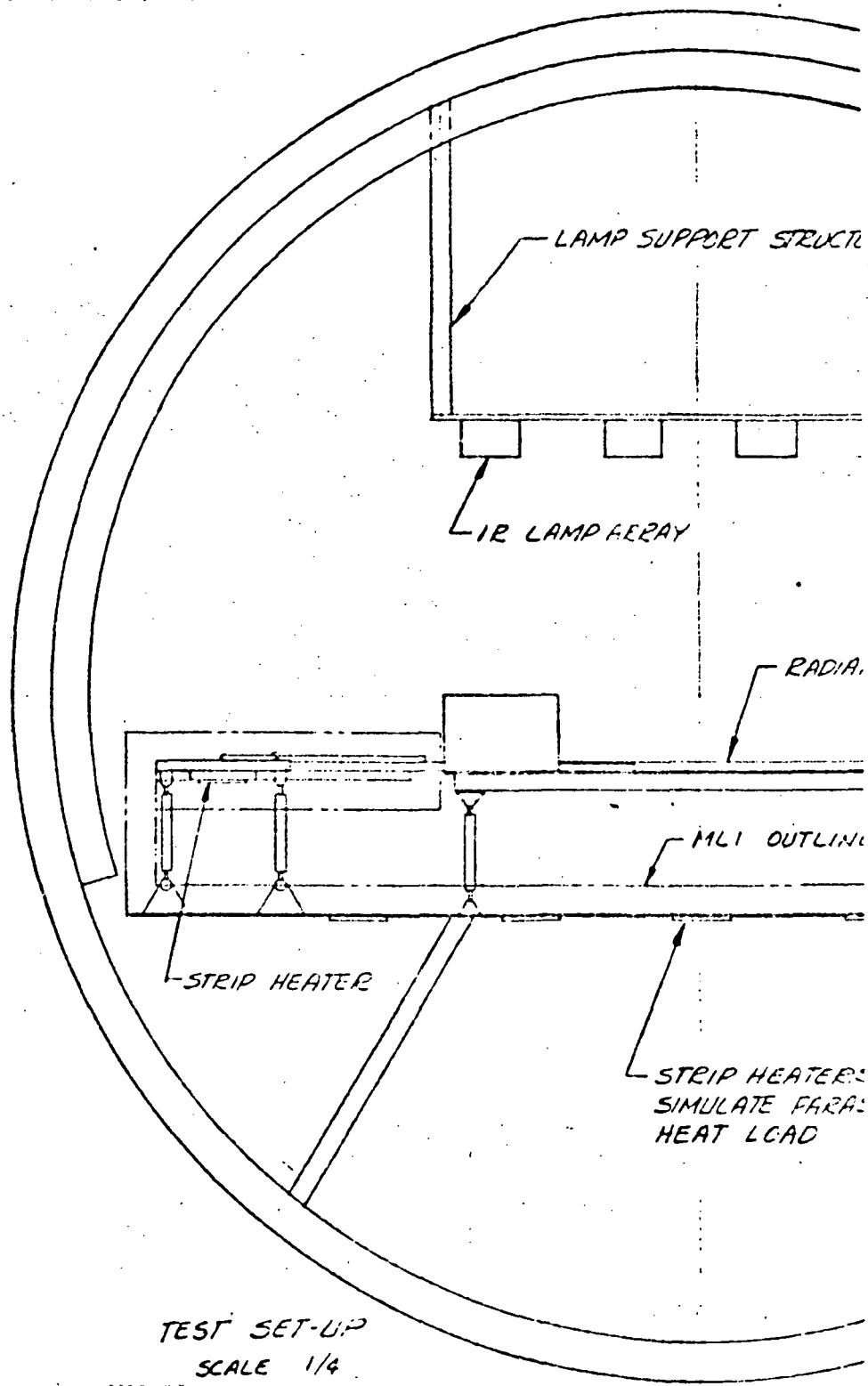

TEST SET-UP
SCALE 1/4

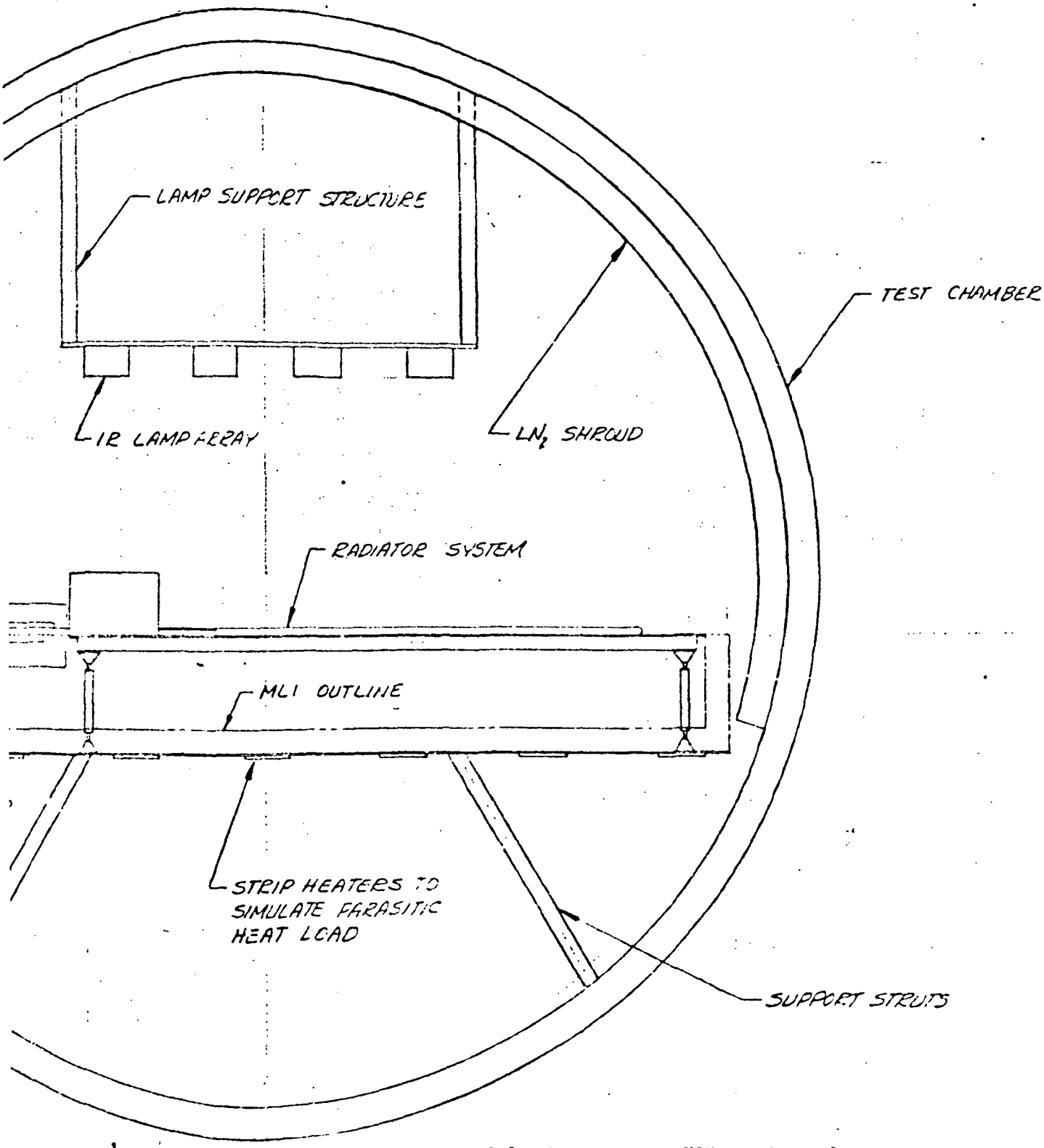

Figure 3-8. Layout-Diode VCHP Radiator System

shown in Figure 3-8. The saddle area is minimized to reduce the transient response time of the radiator assembly. The VCHP is bent into a "U" shape to provide a long condenser length for gas modulation control and to distribute the heat over the radiator in the full-on mode to provide a high radiator efficiency with a minimum skin thickness. The two sections of the radiator are thermally isolated from each other by a fiberglass doubler. The radiator is coated with a white thermal control paint to provide a solar absorptance of 0.3 and an infrared emittance of 0.9.

Test Setup

The proposed test setup for the diode radiator assembly also is depicted in Figure 3-8. The radiator and heat pipe are mounted off the support structure by the low-conductance standoffs with one inch of multilayer insulation in between. The entire assembly is shown mounted in a 5-foot vacuum chamber. The system is oriented so that both the diode and the variable conductance heat pipes are level to within 0.1 inch end to end.

The orbital thermal environment is simulated by the LN_2 shroud and the IR lamp array. The shroud simulates deep space; the temperature of the lamp array is monitored from outside the chamber to simulate solar, earth, and albedo heating. The IR array structure is mounted off the chamber wall and the lamp array is designed to minimize blockage of the view from the radiator to the shroud.

During test, the detector heating would be simulated by varing power to a heater which is bonded to the aluminum block. The lamp array temperature would be controlled to provide a flux history equivalent to a subsolar low earth orbit; temperatures on the heat pipes and radiators would be monitored to evaluate the system performance and the control tolerance range at the detector interface.

Predicted System Performance

The thermal network from the radiator and heat pipe assembly is shown in Figure 3-9. The predicted performance for the subsolar low earth orbit case is shown in Figure 3-10. Response data are shown for five orbits to allow the system to reach cyclic steady-state. As shown in Figure 3-10, the detector is maintained within a range of 175 $\pm$ 3°K over the 6-hour period while the

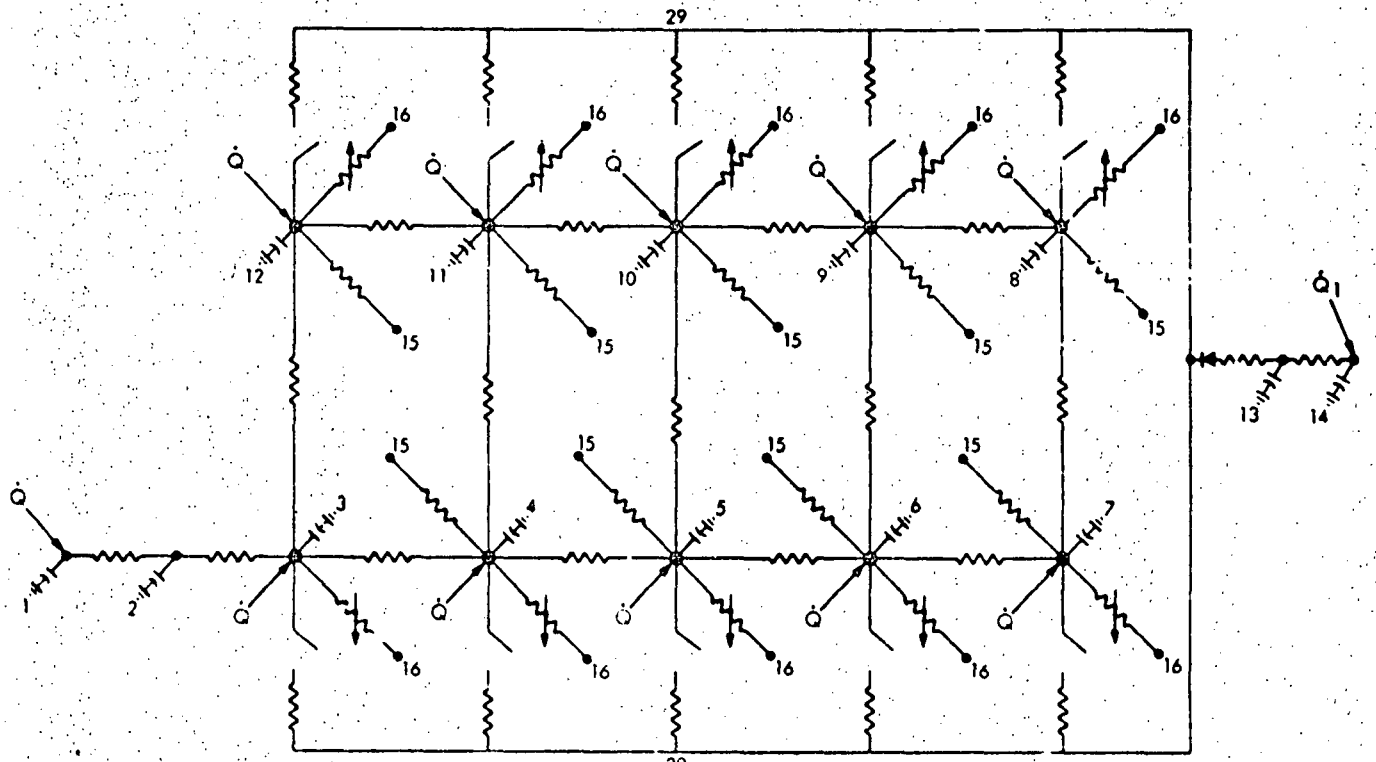

NODE NO.	LOCATION
1	GAS RESERVOIR
2	FILL TUBE
3-12	CONDENSER RADIATOR
13	AL. HEAT SINK
14	DETECTOR EVAPORATOR
15	SPACECRAFT INTERIOR
16	SPACE NODE
29	VAPOR

SYMBOL	DEFINITION
	DIODE PIPE
	CONDUCTORS
	CAPACITORS
	RADIATION CONDUCTOR
$\dot{Q}_1$	DISSIPATED HEAT LOAD
$\dot{Q}$	ENVIRONMENTAL HEAT LOAD
	GAS FRONT SIMULATOR

Figure 3-9 Thermal Network for Diode/VCHP Radiator Assembly

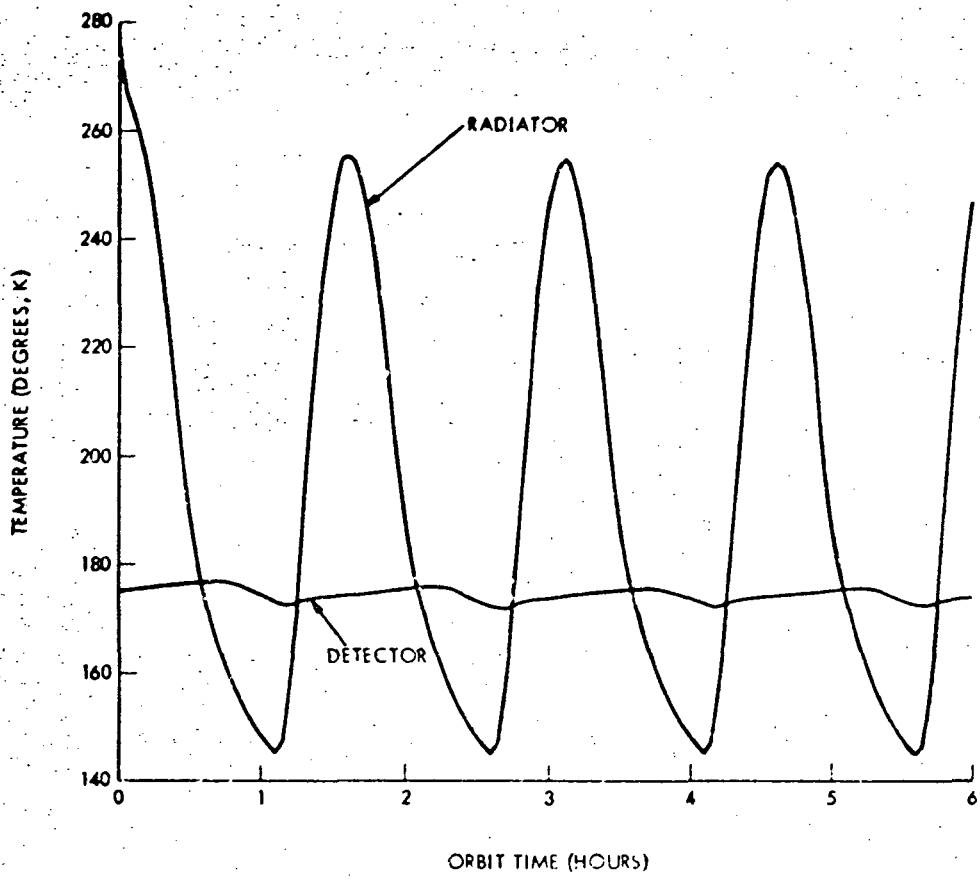

Figure 3-10 Predicted System Response for Diode/VCHP Radiator Assembly

radiator varies between 145°K and 255°K.

One additional computer run was made with the aluminum heat sink removed in an attempt to minimize the weight of the system; however, the results shown in Figure 3-11 indicate that the system without the heat sink is unsatisfactory, having a total temperature excursion of 17°K.

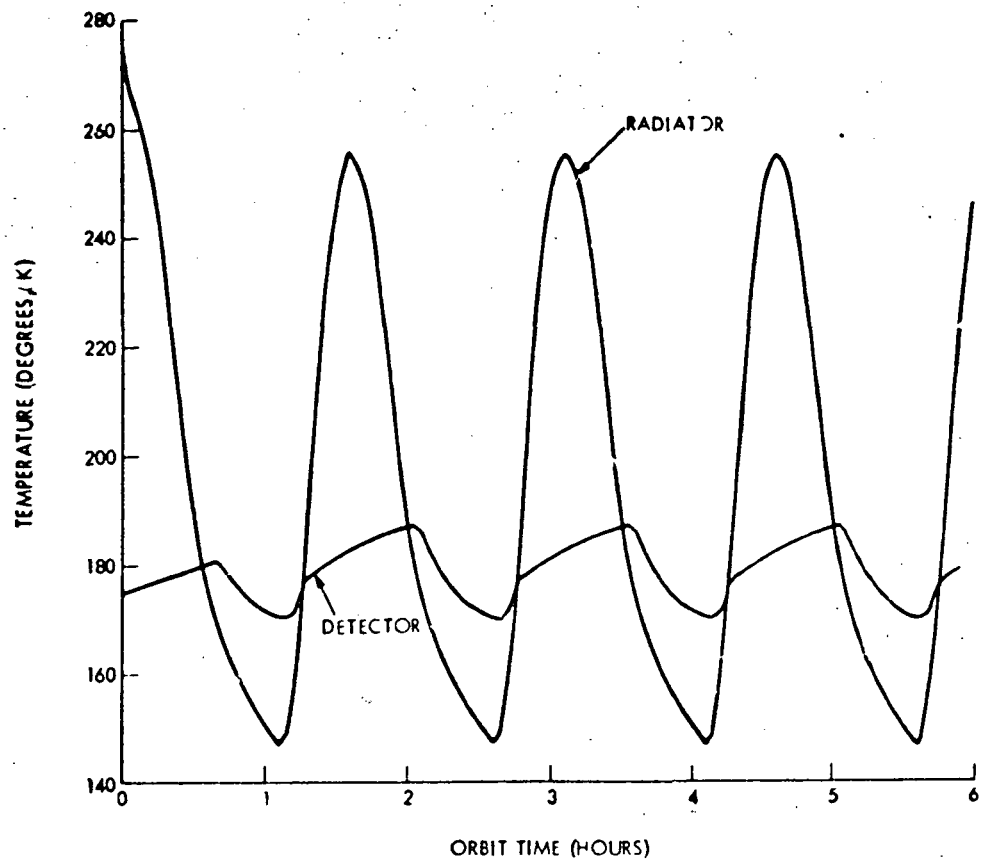

Figure 3-11 Predicted Diode/VCHP Radiator System Response with Aluminum Heat Sink Removed

4. CONCLUSIONS AND RECOMMENDATIONS

Results of the analyses and design efforts completed during this study point to significant improvements in passive low-temperature cooling technology. Recent advances in cryogenic, diode, and variable conductance heat pipe technology have made this possible. Conclusions from the multistage and diode radiator analyses and recommendations for future development and test efforts are summarized in the following paragraphs.

The parametric analysis of multistage radiators resulted in the following conclusions about their design and optimization sensitivity:

1. On a weight basis, one-, two-, and three-stage radiators have distinct temperature ranges in which they are optimum. A cold stage COP parameter was defined which relates to the cold stage heat rejection capability per square foot of projected (first-stage) area to the theoretical emissive power of a surface at the cold stage temperature. Results show that the crossover points between the optimum temperature regimes of one-, two-, and three-stage radiators decrease with the decreasing values of the effective emittance of the insulation beneath the radiator stages.

2. At temperatures approaching the lower theoretical limit for two- and three-stage radiators, the cold stage heat rejection is a strong function of insulation emittance in the analyzed range of 0.005 to 0.020.

3. Temperatures as low as 15°K are theoretically possible for a three-stage radiator, assuming an insulation emittance of 0.01. At temperatures below about 30°K, however, the coefficient of performance drops drastically with temperature.

4. Intermediate stage heat loads of five or even ten times the cold stage heat load do not appreciably affect the optimum areas nor the cold stage COP. The ability to reject large heat loads at the intermediate stage temperature is significant for IR sensor systems which have intermediate temperature cooling requirements for optics, shields, and baffles.

5. The required area for the detailed design configuration at 35°K was approximately twice the theoretical area requirement, based on the parametric analysis. The increase was due to additional parasitic heat loads from the shields, heat pipes, supports, insulation edges, and penetrations. The baseline design has a projected area of approximately 10 square feet for heat load requirements of 10 mw at 35°K and 100 mw at the second stage.

6. From the parametric radiator fin optimization analysis, it is clear that optimum fin geometries for low-temperature radiators are significantly different from those for ambient temperature radiator systems with which most thermal design engineers are accustomed to working. Optimum thicknesses at temperatures below 75°K may be as low as 1 mil or less. The optimum efficiency on a weight basis is independent of temperature and is equal to 0.565 for a deep-space sink temperature. For most design applications, however, higher efficiencies are generally desirable even at the expense of a slightly greater weight because of available radiator area restrictions on a spacecraft.

The following conclusions are evident from the results of the diode heat pipe radiator system analysis:

1. Heat rejection at temperatures as low as 175°K in worst-case (hot) low earth orbits are possible with the diode radiator system concept. The lower temperature limit in low earth orbit is due to the large view factor angles to the earth and the relatively short orbital period, which does not provide sufficient time for the radiator to cool down.

2. The total temperature excursion of the low-temperature heat source (e.g., detector) can be reduced significantly by adding a thermal capacitor to the system. The optimum location for the capacitance is nearest the detector. For a fixed radiator area and design temperature tolerance, the addition of a thermal capacitance can increase the average heat load capacity of the system.

3. For the same weight, the reduction in the temperature excursion of the detector for a phase change material device is greater than for a fixed aluminum block. However, for low earth orbits where the orbital period is on the order of 1.5 hours, very little of the PCM material has a chance to melt. For orbits with longer periods such as geosynchronous, PCM devices could significantly increase the heat load handling capability of the system.

4. To maintain precise temperature control over a wide range of orbital environments and detector heat loads, a variable conductance heat pipe must be added to the system. The VCHP would be connected between the diode heat pipe and the radiator. The detailed system design configuration incorporated a VCHP as well as a liquid trap diode heat pipe; the temperature control band was 175 $\pm$ 3°K for a simulated subsolar low earth orbit.

Based on the detailed analysis results for the selected multistage and diode heat pipe radiator design configurations, it can be concluded that significant improvements in low-temperature cooling technology can be realized with current thermal control elements. Both of these systems are applicable to many classes of proposed future Shuttle payloads, and offer perhaps the only solution for long-life (> 2 years), low-temperature cooling for space systems.

A ground test program, in which breadboard systems would be fabricated and tested based on the designs presented, is strongly recommended. Following the ground test program, flight qualified versions of these systems should be flown and tested on early Shuttle test flights. The system would then be qualified for use on NASA as well as DOD payloads.

REFERENCES

1. Wright, J. P., and D. E. Wilson, Development of Thermal Control Methods for Specialized Components and Scientific Instruments at Very Low Temperatures. Rockwell International, Space Division, SD 76-SA-0077 (May 1976).

2. Liebleim, S., Analysis of Temperature Distribution and Radiant Heat Transfer Along a Rectangular Fin of Constant Thickness. NASA TN D-196 (November 1969).

3. RM-20B Program Development and Qualification Test Report, Vol. 1. Rockwell Space Division, SD 75-SA-0068-1, USAF Contract F04701-72-C-0052, CDRC Item A007 (July 15, 1974).

4. General Thermal Analyzer Program, User's Guide (Program No. XF0014). Rockwell Space Division, SD 73-CE-0005 (November 1973).

5. Thermal Radiation Analysis System (TRASYS), User's Manual. Martin Marietta Corp., NASA Contract NAS9-13033 (May 1973).

6. Wright, J. P., Heat Pipe Technology. Rockwell International, Space Division, SD 75-SA-0200 (December 1975).

7. Kroliczek, E. J., and P. J. Brennan, "Axially Grooved Heat Pipes - Cryogenic Through Ambient," ASME Papaer No. 73-ENA's-48.